# UNIVERSIDAD DE JAÉN

**ESCUELA POLITÉCNICA SUPERIOR DE JAÉN**

**CENTRO DE ESTUDIOS AVANZADOS EN CIENCIAS DE LA TIERRA, ENERGÍA Y MEDIO AMBIENTE**


## TESIS DOCTORAL

# ESTUDIO Y MODELADO DEL IMPACTO DEL ESPECTRO SOLAR, EL POLVO Y LA SUCIEDAD SOBRE EL COMPORTAMIENTO EN EXTERIOR DE LOS MATERIALES FOTOVOLTAICOS


**PRESENTADA POR:**
**JOSE ANTONIO CABALLERO CUERVA**

**DIRIGIDA POR:**
**DR. D. EDUARDO FERNÁNDEZ FERNÁNDEZ**
**DR. D. GUSTAVO EDUARDO NOFUENTES GARRIDO**



**JAÉN, JUNIO DE 2021**


Universidad de Jaén

Escuela de Doctorado

# TESIS DOCTORAL

## ESTUDIO Y MODELADO DEL IMPACTO DEL ESPECTRO SOLAR, EL POLVO Y LA SUCIEDAD SOBRE EL COMPORTAMIENTO EN EXTERIOR DE LOS MATERIALES FOTOVOLTAICOS

**PRESENTADA POR:**
**JOSE ANTONIO CABALLERO CUERVA**

**DIRIGIDA POR:**
**DR. D. EDUARDO FERNÁNDEZ FERNÁNDEZ**
**DR. D. GUSTAVO EDUARDO NOFUENTES GARRIDO**

**JAÉN, JUNIO 2021**

Universidad de Jaén
Escuela de Doctorado

# UNIVERSIDAD DE JAÉN
# ESCUELA POLITÉCNICA SUPERIOR DE JAÉN

# TESIS DOCTORAL

La memoria titulada “ESTUDIO Y MODELADO DEL IMPACTO DEL ESPECTRO SOLAR, EL POLVO Y LA SUCIEDAD SOBRE EL COMPORTAMIENTO EN EXTERIOR DE LOS MATERIALES FOTOVOLTAICOS”, ha sido desarrollada dentro del Centro de Estudios Avanzados en Ciencias de la Tierra, Energía y Medio Ambiente (CEACTEMA) de la Universidad de Jaén y presentada por D. José Antonio Caballero Cuerva, aspirante al grado de Doctor en “Energías Renovables”, bajo la dirección de los doctores D. Eduardo Fernández Fernández y D. Gustavo Eduardo Nofuentes Garrido.

Jaén, junio 2021

**El doctorando**

CABALLERO CUERVA JOSE ANTONIO - 75712061V

Firmado digitalmente por CABALLERO CUERVA JOSE ANTONIO - 75712061V
Fecha: 2021.06.05 12:29:24 +02'00'

Fdo. Jose Antonio Caballero Cuerva

**Los directores de Tesis**

FERNANDEZ FERNANDEZ EDUARDO - 71766586P

Firmado digitalmente por FERNANDEZ FERNANDEZ EDUARDO - 71766586P
Fecha: 2021.06.08 10:49:33 +02'00'

Fdo. Dr. D. Eduardo Fernández Fernández

NOFUENTES GARRIDO GUSTAVO EDUARDO - 25998627W

Firmado digitalmente por NOFUENTES GARRIDO GUSTAVO EDUARDO - 25998627W
Fecha: 2021.06.05 13:52:21 +02'00'

Fdo. Dr. D. Gustavo Eduardo Nofuentes Garrido

Universidad de Jaén

Escuela de Doctorado

# TESIS DOCTORAL

## ESTUDIO Y MODELADO DEL IMPACTO DEL ESPECTRO SOLAR, EL POLVO Y LA SUCIEDAD SOBRE EL COMPORTAMIENTO EN EXTERIOR DE LOS MATERIALES FOTOVOLTAICOS

**TRIBUNAL EVALUADOR:**

**Presidente:**

**Secretario:**

**Vocal:**

**Suplente:**

**Suplente:**

**JAÉN, JUNIO 2021**

"Ya no importa cuán estrecho haya sido el camino,
ni cuántos castigos lleve a la espalda:
Soy el amo de mi destino,
soy el capitán de mi alma."

***WILLIAM ERNEST HENLEY***

# AGRADECIMIENTOS

El objeto de las presentes líneas no es otro que el de expresar mi gratitud a todas aquellas personas importantes para mí, las cuales me han ayudado de alguna forma para poder culminar la presente Tesis doctoral.

En el ámbito familiar, agradezco a mis abuelos por transmitir la importancia de la humildad, la unidad de la familia y la cultura del esfuerzo, así como a mis padres y hermanos, por su apoyo incondicional, educarme en valores y por ayudarme a luchar ante cualquier adversidad. A María, por su apoyo diario, confianza y ser un gran ejemplo de esfuerzo y superación.

En el ámbito laboral, agradecer a Guada, Lourdes, Fani, Carmen, Fernando y Azahara por su gran acogida en CTAER, así como por todos aquellos momentos vividos. Fue en aquella etapa cuando despertó mi curiosidad por el aprendizaje ligado a la investigación en energías renovables. Asimismo, agradezco a mis actuales amigos y compañeros de trabajo de PVH su apoyo y confianza, juntos formamos una pequeña familia, superamos los retos que se nos plantean y luchamos por aprender y mejorar cada día.

En el ámbito investigador, agradezco con especial interés a mi tutor y codirector de Tesis, Gustavo, al cual considero un gran amigo, todo lo que ha demostrado desde que nos conocimos cuando comencé mi beca de iniciación a la investigación en la Universidad de Jaén hasta el día de hoy. Sin duda, ha sido un pilar básico para que este trabajo se haya podido finalizar. Igualmente, agradezco enormemente a mi otro codirector de Tesis, Eduardo, por ser otra pieza fundamental en la culminación del presente trabajo, por ser ejemplo de gran persona, además de un investigador incansable, de mente brillante que merece triunfar. Finalmente, agradezco a Juan, al cual considero otro amigo y gran persona, por su apoyo y recibimiento durante mi estancia en la Universidad de Jaén.

A todos os digo, que este mundo necesita más personas como vosotros.

# RESUMEN

La tecnología solar fotovoltaica desempeñará un papel crucial en la lucha contra el cambio climático, esperándose que para el año 2050 represente un 46% de la capacidad total mundial eléctrica instalada.

A pesar de que la tecnología fotovoltaica ya ha alcanzado un grado de madurez avanzado, existen algunos aspectos mejorables en el modelado del comportamiento de los sistemas fotovoltaicos. A fin de lograr esa mejora, en la presente Tesis se han realizado las siguientes aportaciones:

Primeramente, se ha comprobado si es posible caracterizar biunívocamente las formas que adopta la distribución espectral de la irradiancia solar directa mediante un parámetro escalar denominado energía media del fotón. Para ello, se ha realizado un análisis estadístico de 78.772 espectros medidos entre 350 y 1050 nm. Tales espectros han sido registrados en la Universidad de Jaén (Jaén, España, latitud 37º49' N, longitud 3°47'O) mediante un espectrorradiómetro EKO® MS700 con tubo colimador montado sobre un seguidor solar a dos ejes. Los resultados obtenidos indican que únicamente se puede considerar —a efectos prácticos tan solo— que existe dicha relación biunívoca entre las formas de la distribución espectral de la irradiancia solar directa y la energía media del fotón en la banda de longitudes de onda comprendidas entre 450 y 900 nm.

La segunda contribución ha consistido en modelar la influencia de la distribución espectral de la irradiancia incidente en la electricidad producida por los dispositivos fotovoltaicos de simple unión a partir de la masa del aire (AM, por las siglas del inglés *air mass*), el espesor óptico del aerosol (AOD, por las siglas del inglés *aerosol optical depth*) y el agua precipitable (PW, por las siglas del inglés *precipitable water*). Estos dos últimos parámetros atmosféricos cada vez son más ampliamente disponibles para el diseñador de sistemas fotovoltaicos. Para ello, se han registrado cada 5 minutos medidas simultáneas de la irradiancia solar inclinada de banda ancha y de su distribución espectral entre 350 y 1050 nm en la Universidad de Jaén. La campaña experimental se ha extendido durante un año empleándose un piranómetro Kipp & Zonnen® CMP21 y un espectroradiómetro EKO® MS-700. Los valores de los parámetros AOD y PW fueron registrados de forma síncrona a las referidas medidas de irradiancia, en la misma Universidad de Jaén a través de un medidor de irradiancia espectral Spectrafy Inc. ® modelo SolarSIM-D2, instalado sobre un seguidor solar de dos ejes. Los resultados confirman que es posible modelar con un alto grado de exactitud las correcciones espectrales de la irradiancia de banda ancha en función de la tecnología fotovoltaica considerada. Dentro de los buenos resultados obtenidos globalmente para todas las tecnologías de simple unión estudiadas, la tecnología en la que se logró un mejor ajuste fue la de silicio amorfo, mientras que la que obtuvo un ajuste menos preciso fue la de silicio monocristalino. Así, al comparar los valores del factor espectral modelados con los empíricos, se obtienen valores porcentuales de la raíz cuadrada del error cuadrático medio por debajo de 0,85% para todos los materiales bajo estudio. Esta cifra mejora el ajuste del método de referencia actual, propuesto por el Laboratorio Nacional de Sandia y en el que únicamente se considera AM como parámetro de entrada.

Finalmente, se ha estimado el impacto de la suciedad y el polvo —*soiling*, en inglés— a lo largo de la banda de absorción de distintos materiales fotovoltaicos y su relación con la distribución espectral de la irradiancia incidente sobre los mismos. Para ello, se ha llevado a cabo una campaña experimental de 48 semanas de duración en la Universidad de Jaén consistente en exponer a la intemperie una muestra de vidrio fotovoltaico cuadrada de 4 x 4 $cm^2$ con un espesor de 3 mm anclada y dispuesta horizontalmente, de forma que la muestra en cuestión se vio afectada por el polvo y la suciedad que se depositaba sobre ella de forma natural. A lo largo de toda la campaña experimental se han realizado con periodicidad semanal medidas de transmitancia óptica hemisférica de la muestra expuesta en el exterior y de otra que permaneció limpia y custodiada en interior. Dichas medidas se practicaron mediante un espectrofotómetro Lambda® 950, con una esfera integradora de 60 mm de diámetro. Finalmente, con los datos registrados semanalmente, se calcularon las pérdidas totales derivadas de la deposición de polvo y suciedad. Tras realizar un análisis de los resultados, se detectó que existía una estrecha relación entre dichas pérdidas y la transmitancia óptica promedio calculada en intervalos determinados del espectro (visible, ultravioleta o infrarrojo). Una dependencia similar se identificó entre las pérdidas causadas por el *soiling* y la transmitancia óptica asociada a luz prácticamente monocromática (1 nm de anchura de banda) . Las bandas más apropiadas para estimar las pérdidas totales producidas por polvo y suciedad a partir de la transmitancia óptica promedio se localizan en la región del espectro visible. Para inferir dichas pérdidas a partir de este último parámetro se puede emplear, o bien toda esta región, o luz monocromática (1 nm de anchura de banda) comprendida entre 500 y 600 nm en función de la tecnología FV empleada. Debido a los hallazgos logrados, se pueden proponer enfoques innovadores para estimar las pérdidas producidas por el polvo y la suciedad mediante el desarrollo de dispositivos novedosos y de bajo coste que permitan registrar la pérdida de transmitancia óptica en regiones limitadas del espectro.

# ABSTRACT

Solar photovoltaic technology is expected to become a key player in fighting climate change, accounting for 46% of the world's total installed capacity by 2050.

Despite the fact that photovoltaic technology has already achieved an advanced degree of development, there are certain issues that can be improved in the energy modeling associated with photovoltaic systems. In order to ensure this goal, the following contributions have been made in this Thesis:

First, it has been checked whether it is possible to biunivocally characterize the shapes adopted by the spectral distribution of direct solar irradiance by using a scalar parameter denominated average photon energy. For such purpose, a statistical analysis of 78,772 spectra collected from 350 to 1050 nm has been performed. Such spectral data were recorded at the University of Jaén (Jaén, Spain, latitude 37º49' N, longitude 3°47' W) using an EKO® MS700 spectroradiometer with a collimating tube mounted on a two-axis solar tracker. The findings suggest that only in practical terms it is possible to consider that a bijective relationship exists between the shapes of the spectral distribution of the direct solar irradiance and the average photon energy within the 450–900-nm waveband.

The second contribution has consisted of modelling the influence of the spectral distribution of incident irradiance on the electricity produced by single-junction photovoltaic devices from air mass (AM), aerosol optical depth (AOD) and precipitable water (PW). The latter two atmospheric parameters are becoming more widely available to the PV system designer. To this end, 5-minute measurements of the global tilted irradiance in conjunction with its spectral distribution from 350 to 1050 nm were recorded simultaneously at the University of Jaén. The experimental campaign has been extended for one year using a Kipp & Zonnen® CMP21 pyranometer and an EKO® MS-700 spectroradiometer. The measurements of both AOD and PW parameters were recorded synchronously with the irradiance measurements at the University of Jaén using a Spectrafy Inc. ® model SolarSIM-D2 spectral irradiance meter, installed on a two-axis solar tracker. The overall results confirm that it is possible to model with a high degree of accuracy the spectral corrections of the broadband irradiance in accordance with the PV technology considered. Among the overall good results obtained for all the single-junction technologies studied, the technology with the best fit was amorphous silicon, while the technology with the worst fit was monocrystalline silicon. Hence, by comparing the modelled spectral factor values with the empirical ones, we obtain that the root mean square error percentage values stay below 0.85% for all PV materials under scrutiny. Therefore, the model proposed here outperforms the reference method proposed by the Sandia National Laboratories, which only considers AM as a single input parameter.

Finally, the impact of soiling along the absorption band of different photovoltaic materials and its relationship with the spectral distribution of the incident irradiance on them has been estimated. For this purpose, a 48-week

experimental campaign has been carried out at the University of Jaen consisting of exposing a 4 x 4 $cm^2$ square photovoltaic glass sample with a thickness of 3 mm fixed and arranged horizontally outdoors, so that such sample was affected by the dust and dirt that was naturally accumulated over it. Throughout the experimental campaign, hemispheric optical transmittance measurements were recorded weekly on the sample exposed outdoors and on another one that was kept clean indoors. Such measurements were carried out using a Lambda® 950 spectrophotometer with a 60 mm diameter integrating sphere. After analysing the results, it was found that there was a close relationship between the average optical transmittance associated with certain ranges of the spectrum (visible, ultraviolet or infrared) and the losses caused by soiling. A similar dependence was identified between the optical transmittance associated with certain regions of the spectrum of just 1-nm width and the aforementioned losses caused by natural deposition of soiling exposed to the outdoors. The most appropriate band for assessing total soiling losses lie within the visible region of the spectrum, where either the entire visible region or a monochromatic light (1-nm-width waveband) between 500 and 600 nm can be used, depending on the PV technology employed. The findings suggest that innovative approaches to estimate dust and dirt losses can be proposed by developing novel, low-cost devices to measure optical transmittance loss in constrained regions of the spectrum.

# ÍNDICE GENERAL

# ESTRUCTURA DEL DOCUMENTO

La presente Tesis se encuentra dividida en dos bloques, a saber:

## BLOQUE I. MEMORIA.

El primer bloque se compone de una breve introducción sobre el panorama energético mundial actual y esperado durante las próximas décadas, la problemática del cambio climático y cómo la tecnología fotovoltaica puede desempeñar un papel crucial para combatirlo. Posteriormente, se exponen los objetivos específicos con los que se puede contribuir con este trabajo a la mejora de la ingeniería fotovoltaica, explicando la metodología utilizada para tal fin. A continuación, se muestran los resultados obtenidos y las conclusiones alcanzadas a partir de los mismos. Finalmente se indican futuras líneas de investigación.

## BLOQUE II. PUBLICACIONES REALIZADAS EN EL MARCO DE LA TESIS DOCTORAL.

La segunda parte del presente documento consiste en un compendio de tres artículos publicados en revistas indexadas realizados en el marco de la presente Tesis Doctoral. Cada artículo se corresponde con cada uno de los tres objetivos específicos planteados en el marco de la presente Tesis Doctoral.

# BLOQUE I. MEMORIA

# 1. INTRODUCCIÓN

El dióxido de carbono ($CO_2$), junto con el metano, óxido de nitrógeno, ozono troposférico y algunos compuestos halogenados conforman el grupo de gases comúnmente denominado como gases de efecto invernadero (GEI). Estos son originados en mayor medida en países industrializados como consecuencia de la quema de combustibles fósiles con la finalidad de cubrir las necesidades de la población tales como el transporte, la climatización o la actividad industrial, entre las que es preciso destacar las emisiones generadas por la industria cementera. No obstante, este tipo de gases también son generados por otras actividades primarias como son la ganadería y la agricultura, destacando especialmente, tanto las emisiones provocadas por los cultivos de arroz en campos inundados, como las generadas por fertilizantes nitrogenados o estiércol en el abono de los campos de agricultura.

El aumento de emisiones de GEI a la atmósfera terrestre como consecuencia de la actividad humana propicia que tales gases absorban parte de la radiación solar infrarroja que es emitida por la tierra en forma de calor, aumentando así la temperatura del planeta, es decir, que se produzca el llamado "efecto invernadero" [1], desencadenando el correspondiente calentamiento global de la Tierra. La falta de acciones contundentes a nivel global para mitigar y frenar el citado calentamiento global tendría consecuencias desastrosas para el planeta y para los seres vivos que lo habitan. En este sentido, se aceleraría el cambio climático de la tierra, que, a su vez, aumentaría la sucesión de eventos atmosféricos extremos. Además de lo anterior, sería especialmente relevante el efecto de la fusión de parte de la masa de hielo en los polos, con el consiguiente aumento del nivel del mar que produciría inundaciones en localizaciones costeras actualmente habitadas, e incluso, la desaparición de pequeños estados insulares.

Según datos de Grupo Banco Mundial [2], en el año 1960, las emisiones mundiales de $CO_2$ fueron de 9.213.447,532 kt. En 1990 dichas emisiones se incrementaron un 243%, alcanzando las 22.421.693,577 kt Más recientemente, en 2016 dichas emisiones ascendieron a 33.819.401,161 kt, lo que a su vez supone un incremento de emisiones mundiales de $CO_2$ de un 50% con respecto a las contabilizadas en el año 1.990.

Con el objetivo de limitar el calentamiento global muy por debajo de 2 grados centígrados por encima de los niveles de temperatura preindustriales, se adoptó por 196 gobiernos un tratado internacional sobre el cambio climático en la 21 conferencia de las partes de París (COP21) celebrada el 12 de diciembre de 2015. Dicho tratado es jurídicamente vinculante y entró en vigor el pasado 4 de noviembre de 2016.

La consecución de los objetivos a largo plazo del Acuerdo de París tiene su esencia en las contribuciones determinadas a nivel nacional (NDC, por las siglas del inglés *Nationally Determined Contribution*). En las NDC, cada país preparará, comunicará y mantendrá las medidas nacionales de mitigación de emisión de GEI para la lucha contra el cambio climático, las cuales serán desarrolladas para

alcanzar los objetivos específicos que se han propuesto lograr. Dichas medidas serán revisadas en periodos de 5 años y pueden ser afrontadas mediante recursos financieros propios o a través de mecanismos financieros de apoyo internacional.

De acuerdo con un informe de la Agencia Internacional de las Energías Renovables (IRENA, por las siglas del inglés *International Renewable Energy Agency*) [3], las medidas propuestas en las citadas NDC en materia de energía no son lo suficientemente ambiciosas para cumplir los objetivos establecidos en el Acuerdo de París. En este sentido, se afirma que los objetivos planteados para la generación de electricidad mediante energías renovables se encuentran incluso por debajo de los objetivos ya establecidos en las estrategias y planes nacionales de los diferentes países. Por ende, las NDC, hasta el momento, no pueden ser consideradas como el principal elemento motriz en el avance de la generación eléctrica mediante fuentes de energías renovables.

Las energías renovables han experimentado un gran despliegue durante los últimos años, y entre ellas, cabe destacar el rápido avance de la tecnología fotovoltaica (FV) [4]. En efecto, esta es una de las técnicas limpias de producción de electricidad más prometedoras en la actualidad. En este sentido, el mercado FV mundial rondó los 131 GWp durante el año 2019, para alcanzar 708 GWp de potencia acumulada a finales de 2020 [5]. Además, el 8,7% del consumo eléctrico de Alemania durante el año 2018 fue cubierto exclusivamente mediante la tecnología FV, a pesar de ser un país que no destaca por su recurso solar, lo que pone de manifiesto la importancia que tiene adoptar políticas ambiciosas en materia energética basadas en energías renovables. Como contrapartida, a nivel mundial, durante el año 2018 solamente un 2,2% de la energía consumida se originó mediante tecnología FV, lo cual justifica la necesidad de continuar investigando en la generación de electricidad de origen solar fotovoltaico.

A día de hoy, la generación eléctrica distribuida mediante la tecnología FV continúa en crecimiento, incluso a pesar de la pandemia de la COVID-19 [6]. Este crecimiento se debe al incesante incremento de su competitividad, a su modularidad, rápida escalabilidad y potencial de creación de empleo. Los costos de la energía solar FV se han reducido casi un 80% en la última década, y la tendencia no tiene visos de remitir, a la luz de los recientes contratos de compraventa de energía (PPA, por las siglas del inglés *Power Purchase Agreement*) en los que el precio medio de la electricidad FV podría alcanzar los 0,039 USD/kWh para los proyectos que se pongan en marcha en 2021 —lo que supone un descenso de un 42% con respecto a 2019— y más de un 20% menos que el coste asociado a las centrales eléctricas de carbón [4]. En abril de 2021, se ha publicado la firma de un acuerdo PPA de 0,0104 USD/kWh para un proyecto de 600 MWp ubicado en el reino de Arabia Saudí [7]. No obstante, este dato hay que tomarlo con cautela al tratarse de un proyecto subvencionado mediante un programa nacional del reino de este país. Por otro lado, debido a las continuas mejoras tecnológicas y a la competitividad en la cadena de suministro, se estima que la electricidad procedente de los sistemas de concentración fotovoltaica (CFV) se sitúen en precios medios de subasta de 0,075 USD/kWh para el año 2021 [8].

Algunas previsiones apuntan a que la demanda de energía eléctrica mundial del año 2018 (26.380 TWh) prácticamente se triplique para el año 2050 [8]. En efecto, para dicho año la demanda eléctrica se ha previsto que alcance los 78.800 TWh, considerando que se mantenga el escenario en que la movilidad en las próximas décadas se base en el vehículo eléctrico [5]. Del mismo modo, se estima que la capacidad de potencia FV instalada en la mitad del presente siglo represente el 46% de la potencia total mundial, la cual se prevé que sea de algo más de 30.000 GW [9].

Resulta evidente el gran reto al que se enfrenta la humanidad y el papel crucial que desempeñará la tecnología FV para lograr superarlo. En ese sentido, se ha de hacer especial hincapié en que el coste nivelado de la electricidad (LCOE, por las siglas del inglés *Levelized Cost Of Energy*, en $€\cdot MWh^{-1}$]) es el parámetro del que dependerá la competitividad de esta técnica de generación de energía limpia frente a las convencionales. Entre otros factores que determinan el valor de LCOE cabe destacar los siguientes:

- Ubicación del proyecto (código de red aplicable, normativa de cálculo estructural aplicable, latitud, irradiación solar anual, temperatura ambiente, precipitación anual e intensidad de lluvia, velocidad de viento, carga de nieve, sismo, corrosión ambiental, ensuciamiento natural por polvo y la suciedad — *soiling*, en inglés—, etc.).
- Topografía del terreno (analizando pendientes en dirección este-oeste o norte-sur en función del tipo de estructura, necesidad de extender la longitud de las cimentaciones o de realizar movimientos de tierra para lograr la adaptabilidad de la estructura al terreno con objeto de mantener la estabilidad estructural con la que ha sido diseñada, determinar la separación entre estructuras para disminuir el efecto de sombreado de los módulos FV).
- Eficiencia de los módulos FV. En efecto, a mayor eficiencia, se requiere menor área de captación y menor gasto en elementos del resto del sistema (BOS, por las siglas de inglés *balance of system*).
- Coste del BOS.
- Degradación que los módulos FV empleados sufrirán a lo largo del tiempo.
- Mecanismos financieros disponibles (préstamo, *leasing* y financiación estructurada).
- Características y composición química del terreno que determinarán, junto con el tipo de estructura, el tipo de cimentación necesaria y protección a la corrosión necesaria.
- Tipo de inversor elegido (central u orientado a *string*) y su ubicación, lo que influirá en el número de filas en que se distribuye el generador FV y en el dimensionado del cableado.
- Coste de la operación y mantenimiento de componentes eléctricos y mecánicos en función de la durabilidad de los componentes instalados.
- Origen de los componentes de la planta y precio de transporte hasta el destino.
- Coste de la mano de obra tanto en el lugar de origen de los materiales como en el lugar donde se ha de ejecutar la instalación FV.

- Existencia de políticas y programas para promover la generación de energía mediante técnicas no convencionales en un marco de seguridad jurídica.

Resulta ocioso destacar la importancia de mejorar tanto la comprensión teórica como el ejercicio de la ingeniería de los sistemas FV, bien sean basados en panel plano —los cuales hacen uso de dispositivos de simple unión— o basados en luz concentrada. Dichas mejoras pasan por estimar con mayor finura el comportamiento de los referidos sistemas en el exterior. Así, la presente Tesis trata de solventar problemas pendientes en el diseño de los sistemas fotovoltaicos, derivados de un modelado insuficiente de la electricidad que estos producen. De este modo se permitirá a los proyectistas fotovoltaicos aumentar la exactitud tanto del cálculo de la energía estimada como del cómputo de la energía esperada de un sistema fotovoltaico en un determinado enclave, a través de las siguientes aportaciones:

**1) Arrojar luz acerca de la posible relación biyectiva entre la energía media del fotón y la distribución espectral de la irradiancia normal directa.**

La posibilidad de encontrar un parámetro escalar que caracterice de forma biunívoca las formas que adoptan las distribuciones espectrales de la DNI supondría lograr una variable mucho más fácil de manejar desde el punto de vista ingenieril que la distribución espectral en sí, representada por un conjunto de puntos, a menudo, extenso. Tras una revisión del estado del arte exhaustiva, se considera que — sin estar exento aún de controversia— el índice más apropiado para estudiar si puede ser utilizado como un parámetro escalar que represente de forma única a una distribución espectral completa es la energía media del fotón (EMF, en eV) [10-14]. En la literatura científica existen estudios que sugieren que la relación entre la EMF y la forma de los espectros individuales de irradiancia global inclinada (GTI, por las siglas del inglés *global tilted irradiance*, en $W \cdot m^{-2}$), irradiancia global horizontal (GHI, por las siglas del inglés *global horizontal irradiance*, en $W \cdot m^{-2}$,) o la irradiancia directa normal (DNI, por las siglas del inglés *direct normal irradiance*, en $W \cdot m^{-2}$) es biyectiva [15-19]. Merece ser destacado que, hasta donde sabemos, esta presunta biyectividad entre la EMF y la DNI espectral ha sido escrutada en una única contribución en la literatura [17], siendo nuestra investigación la segunda que analiza la posible existencia de tal relación.

**2) Modelar la influencia de la distribución espectral de la irradiancia incidente en la electricidad producida por los dispositivos fotovoltaicos de simple unión a partir de la masa del aire, el espesor óptico del aerosol, y el agua precipitable.**

Las especificaciones eléctricas de los módulos FV son facilitadas por sus fabricantes, como mínimo, en las denominadas condiciones estándares de medida (CEM), las cuales se definen por una irradiancia incidente —o de banda ancha— de 1.000 $W/m^2$ con una distribución espectral AM1.5G [20] y una temperatura de la célula de 25ºC. En tales condiciones, al menos se

proporcionan la potencia máxima que puede entregar el módulo FV, la corriente de cortocircuito y la tensión de circuito abierto. No obstante, en la práctica, la irradiancia incidente, su distribución espectral y la temperatura de la célula difieren la mayor parte del tiempo de las establecidas en las mencionadas CEM [21-49]. Es tarea del proyectista estimar cuál será la tecnología FV idónea y su comportamiento en función de las condiciones reales asociadas al enclave en el que se ubicará cada instalación concreta. Los parámetros de irradiancia incidente integrada y temperatura ambiente se encuentran ampliamente accesibles en recursos tales como Meteonorm, SoDa o PVGIS (por las siglas del inglés *Photovoltaic Geographical Information System*). Sin embargo, la distribución espectral de la irradiancia rara vez coincide con la de referencia. En este sentido, un mismo valor de irradiancia de banda ancha se traduce en distintas irradiancias efectivas para un determinado dispositivo FV dependiendo de las distribuciones espectrales de aquellas y de la respuesta espectral de la tecnología FV bajo estudio. Por otro lado, se ha demostrado que existe una estrecha dependencia entre la variación espectral de la irradiancia y los parámetros atmosféricos siguientes: masa del aire (AM, por las siglas del inglés *air mass*), el espesor óptico del aerosol (AOD, por las siglas del inglés *aerosol optical depth*), y el agua precipitable (PW, por las siglas del inglés *precipitable water,* en cm) [50-56]. Así, el parámetro AM se puede calcular matemáticamente en cualquier enclave de forma exacta para cada momento del día, y con respecto a los parámetros AOD y PW, ambos se encuentran ampliamente disponibles en bases de datos como AERONET[1] [57]. En este trabajo se investiga, por vez primera, la posibilidad de proponer ecuaciones que permitan estimar con gran exactitud los efectos espectrales asociados al comportamiento de diferentes tecnologías FV de simple unión a partir de los mencionados parámetros AM, AOD y PW. Este modelado del impacto del espectro supondría una contribución importante a la ingeniería de los sistemas FV. En efecto, las medidas de las distribuciones espectrales de irradiancia no suelen estar disponibles y, en el caso de que lo estuviesen para un enclave dado, su adecuado tratamiento e incorporación al diseño de sistemas FV resultaría ciertamente complicado, al tratarse de medidas bidimensionales (tiempo y longitud de onda).

### 3) Estimar el impacto de la suciedad y el polvo a lo largo de la banda de absorción de distintos materiales fotovoltaicos y su relación con la distribución espectral de la irradiancia incidente sobre los mismos.

La acumulación de polvo y suciedad sobre la superficie de captación de las instalaciones FV es inevitable, y al mismo tiempo, un fenómeno poco estudiado que puede provocar caídas en la generación eléctrica de hasta un 70% [58]. Tales perdidas pueden explicarse debido a la disminución de la transmitancia óptica del vidrio FV por la suciedad como consecuencia de la absorción de parte de la radiación incidente y al incremento de la radiación solar reflejada [59-61].

[1] El proyecto AERONET consiste en una federación de redes de aerosoles de teledetección terrestre establecida por la NASA y PHOTONS (por las siglas del francés de *Photométrie pour Le Traitement Opérationnel de Normalisation Satellitaire*), siendo ampliada en gran medida por otras redes y colaboradores de agencias nacionales, institutos, universidades, científicos individuales y socios de todo el mundo.

Asimismo, cabe resaltar que la presencia del *soiling* no solamente disminuye la irradiancia integrada que incide sobre la superficie de captación, sino que también puede modificar su distribución espectral, alterando así la irradiancia efectiva asociada a las diferentes tecnologías FV. Los dispositivos existentes en el mercado para cuantificar las pérdidas producidas por *soiling* para un determinado espécimen FV, se basan principalmente en la comparación del comportamiento en exterior de una muestra que ha quedado limpia con otra que se ha ensuciado. Sin embargo, de esta forma no se puede conocer la correlación existente entre la naturaleza espectral del *soiling*, el espectro de la irradiancia y las pérdidas totales producidas. Es por ello, que en este trabajo se investigará la dependencia de las pérdidas atribuidas al *soiling* respecto de la transmitancia —tanto en distintas bandas de longitudes de onda como monocromática— del vidrio fotovoltaico expuesto en exteriores. Una comprensión superior acerca de la naturaleza espectral del *soiling* y su relación con el comportamiento en exterior de los sistemas FV puede contribuir a desarrollar dispositivos innovadores de bajo coste y de mayor versatilidad orientados a cuantificar las pérdidas causadas por este fenómeno en diferentes tecnologías FV. El desarrollo de tales dispositivos podría disminuir el coste asociado a la monitorización de dichas pérdidas, lo que se traduciría en una menor inversión para obtener información fiable que determine cuándo resulta económicamente viable realizar las tareas de limpieza de una planta FV.

# 2. OBJETIVOS

El objetivo principal de la presente Tesis Doctoral consiste en contribuir a aumentar la exactitud en la estimación del comportamiento eléctrico en exterior de sistemas FV —tanto aquellos basados en panel plano como los que emplean luz concentrada— a través del refinamiento del modelado de los efectos espectrales que estos experimentan, por un lado, y del análisis del impacto que el *soiling* ejerce sobre los mismos, por otro.

El logro del mencionado objetivo principal se basa, a su vez, en la consecución de los siguientes objetivos específicos:

**1) Determinación de un parámetro escalar que caracterice de forma biunívoca las formas que adoptan las distribuciones espectrales de la irradiancia directa normal.**

A la hora de modelar el impacto espectral sobre el fotovoltaico bajo luz concentrada, un índice unidimensional (tiempo) es más fácil de manejar desde el punto de vista ingenieril que una variable bidimensional (longitud de onda, tiempo), tal como la distribución espectral en sí. Se da la circunstancia que un índice popular en la comunidad científica resulta ser aquel sobre el que más se ha debatido la posibilidad de que posea una relación biyectiva con la forma de la distribución espectral de la DNI es la EMF. De hecho, aún existe controversia al respecto. Así, la investigación desarrollada en esta Tesis pretende esclarecer esta cuestión, determinando bajo qué supuestos la relación entre la forma del espectro de la DNI y el referido índice podrá considerarse una biyección.

**2) Modelado de los efectos espectrales en dispositivos de una sola unión en función de la masa de aire, el espesor óptico del aerosol y el agua precipitable.**

Los parámetros atmosféricos AM, AOD y PW condicionan la distribución espectral de la irradiancia. El primero de ellos —el más influyente en el modelado— se puede obtener matemáticamente de forma inmediata en función de las coordenadas geográficas del enclave, el día del mes y la hora, mientras que los dos últimos han empezado a estar ampliamente documentados en bases de datos. La mejora del modelado del impacto del espectro en dispositivos de una sola unión en función de los referidos parámetros aumentará la finura con la que se estime la energía producida por los sistemas fotovoltaicos.

**3) Análisis del impacto del polvo y la suciedad a lo largo de la banda de absorción de distintos materiales fotovoltaicos y su relación con la distribución espectral de la irradiancia incidente sobre los mismos.**

El polvo y la suciedad son factores a los que hasta hace relativamente poco se les había prestado escasa atención. Sin embargo, recientes estudios han señalado que el *soiling* podría ser el parámetro que más influye en el rendimiento energético de un sistema FV después de la irradiancia incidente. Hasta el

momento, los estudios realizados con objeto de entender el impacto espectral que ejerce dicho parámetro han sido realizados con *soiling* artificial. El objetivo de esta investigación consiste en analizar el efecto producido por el polvo y la suciedad —depositados de forma natural en exteriores— sobre la transmitancia óptica de diferentes muestras de vidrios fotovoltaicos expuestos en el exterior y las consecuentes pérdidas causadas por este fenómeno. De este modo, se comprenderá mejor la influencia del *soiling* tanto sobre la irradiancia integrada que incide en la banda de absorción de diferentes tecnologías fotovoltaicas de una unión, como sobre el modo en que la citada irradiancia incidente se distribuye espectralmente.

# 3. RESULTADOS Y DISCUSIÓN

Los objetivos específicos planteados en el marco de la presente Tesis Doctoral han sido alcanzados satisfactoriamente. Así, el logro de dichos objetivos ha dado lugar a resultados merecedores de ser publicados en revistas especializadas recogidas en el *ISI Science JCR*. A continuación, se expone con mayor detalle cómo se ha logrado cada uno de los objetivos específicos establecidos:

1) El primer objetivo —**determinación de un parámetro escalar que caracterice de forma biunívoca las formas que adoptan las distribuciones espectrales de la irradiancia directa normal**— ha sido abordado con éxito, difundiéndose los resultados y conclusiones obtenidos en la siguiente publicación:
Nofuentes, G.; Gueymard, C.; Caballero, J.; Marques-Neves, G.; Aguilera, J. Experimental Evaluation of a Spectral Index to Characterize Temporal Variations in the Direct Normal Irradiance Spectrum. Applied Sciences 2021, 11(3), 897; https://doi.org/10.3390/app11030897

En la investigación que se presenta en esta primera publicación se analiza la posibilidad de que cada valor de EMF se encuentre biunívocamente asociado a una única forma de las que adoptan las distribuciones espectrales de la DNI en un enclave soleado como Jaén. A este fin, se propone un análisis estadístico más completo que el utilizado en el único estudio anterior sobre este tema del que se tiene conocimiento [8]. Para realizar el estudio, se recolectaron valores de DNI espectral entre 350 y 1050 nm, durante un periodo de 12 meses en la ciudad de Jaén (latitud 37º49’ N, longitud 3°47'O). A este fin se utilizó un espectrorradiómetro EKO® MS700 con tubo colimador montado sobre un seguidor solar a dos ejes para aplicaciones CFV, concretamente el BSQ® D1506. Tras el control de calidad y el filtrado de datos, se obtuvieron 78.772 espectros válidos. La metodología de cálculo se basa en un análisis estadístico de las distribuciones espectrales agrupadas en 8 intervalos de EMF de 0,02 eV de anchura, con valores centrales de los referidos intervalos que se extienden desde 1,74 hasta 1,90 eV. La banda de longitud de onda comprendida entre 350-1050 nm, es dividida en 14 intervalos de 50 nm cada uno. Para cada uno de dichos intervalos, se calcula la contribución porcentual de cada medida espectral ($R_c$) a la irradiancia integrada, a lo largo de toda la banda de longitudes de onda en el que se registran medidas espectrorradiométricas (350-1050 nm). A continuación, se determinan tanto la desviación estándar (SD, por las siglas del inglés *standard deviation*) como el coeficiente de variación (CV) de $R_c$ para cada agrupación de medidas espectrales de acuerdo con su valor de EMF, a lo largo de los referidos intervalos de 50 nm. Los valores de CV se mantienen por debajo del 3,5% dentro del intervalo de 450-900 nm, pero estos aumentan hasta el 13% fuera del este rango de longitudes de onda. La conclusión final es que se puede considerar que la EMF caracteriza de forma única la distribución espectral de la DNI para Jaén (y presumiblemente para lugares con climas similares) solamente —y a efectos prácticos— en el margen de longitud de onda comprendido entre 450-900 nm. Por último, merece la pena ser destacado que los valores medios de $R$c para todas las medidas espectrales agrupadas en los 8 intervalos de EMF considerados son prácticamente iguales en la banda de 600-650 nm, lo cual

indica que el valor de la DNI integrada en dicha banda y el valor de la DNI integrada para todo el rango espectral considerado (350-1050 nm) son muy aproximadamente proporcionales.

2) El segundo objetivo —**modelado de los efectos espectrales en dispositivos FV de una sola unión en función de la masa de aire, el espesor óptico del aerosol y el agua precipitable**— ha sido abordado con éxito, difundiéndose los resultados y conclusiones obtenidos en la siguiente publicación:

Caballero, J.A.; Fernández, E.F.; Theristis, M.; Almonacid, F; Nofuentes, G. *Spectral Corrections Based on Air Mass, Aerosol Optical Depth, and Precipitable Water for PV Performance Modeling. IEEE Journal of Photovoltaics 2018, 8(2), 552-558;*

https://doi.org/10.1109/jphotov.2017.2787019

En el artículo se proponen seis ecuaciones para modelar los efectos espectrales de varias tecnologías FV de una unión. La metodología para la obtención de las ecuaciones en cuestión siguió un procedimiento muy similar al descrito en [62], de modo que los coeficientes de cada monomio de dichas ecuaciones se estimaron llevando a cabo un análisis de regresión lineal múltiple sobre medidas obtenidas en exterior. Cada una de dichas ecuaciones se aplica a un material FV concreto, a saber: a-Si, perovskita, CdTe, mc-Si, sc-Si y CIGS. Dichas ecuaciones emplean los parámetros atmosféricos más influyentes sobre la forma de la distribución espectral: AM, AOD y PW, de los cuales se ha de destacar que los dos últimos se hallan cada vez más documentados a través de bases de datos tales como AERONET. La campaña experimental para validar las ecuaciones propuestas se extendió desde marzo de 2016 hasta febrero de 2017, registrándose datos en intervalos 5-minutales, mediante la instrumentación existente en la cubierta del Edificio A3 y C6 de la Universidad de Jaén. En concreto, se dispuso de un piranómetro para la medida de la GTI de banda ancha y un espectrorradiómetro EKO® MS-700 para registrar la GTI espectral desde 350 a 1050 nm. Fuera de dicho intervalo de longitud de onda se extrapoló la referida irradiancia espectral escalando la distribución del espectro de referencia AM1.5G según la razón existente entre la integral de cada espectro de irradiancia global medido y la integral del espectro de referencia en el rango de 700 a 1050 nm, tal y como se describe en el método de Martin y Ruiz [63]. Asimismo, se utilizó un medidor de irradiancia solar espectral Spectrafy Inc. ® modelo SolarSIM-D2, instalado sobre un seguidor solar de dos ejes BSQ®, situado en la azotea del edificio C6 de la Universidad de Jaén. Mediante dicho instrumento se registraron los valores de AOD y PW, igualmente a intervalos de cinco minutos de forma síncrona con las medidas espectrales. Las medidas de las sucesivas distribuciones del espectro solar en combinación con las respuestas espectrales de cada material FV considerado, permitieron calcular los valores experimentales del factor de desacoplo espectral (MM, por las siglas del inglés *mismatch factor*). Los valores de este último parámetro se modelaron introduciendo los valores calculados de AM y registrados de AOD y PW en las ecuaciones propuestas. Al representar los valores experimentales de MM frente a los modelados, se obtienen coeficientes de determinación en un margen que va desde 0,87 para el mc-Si hasta 0,92 para el a-Si. Además, para todos los

materiales FV estudiados los valores porcentuales del sesgo obtenido entre los valores modelados y empíricos de MM son prácticamente nulos, mientras que los valores porcentuales de la raíz cuadrada del error cuadrático medio permanecen por debajo de 0,85%. Habida cuenta de estos resultados, se puede afirmar que se ha logrado el objetivo propuesto cuando se planificó la investigación. En efecto, las ecuaciones propuestas mejoran sustancialmente el ajuste de los datos empíricos de MM frente a los modelados que se consigue empleando el popular método propuesto por los Laboratorios Sandia (EE.UU.), orientado al mismo propósito y únicamente basado en el parámetro AM.

3) El tercero de los objetivos planteados —**analizar el impacto de la suciedad y el polvo a lo largo de la banda de absorción de distintos materiales fotovoltaicos y su relación con la distribución espectral de la irradiancia incidente sobre los mismos**— se ha abordado con éxito, difundiéndose los resultados y conclusiones obtenidos mediante la siguiente publicación:

Micheli, L.; Caballero, J.A.; Fernández, E.F.; Smestad, G.P.; Nofuentes, G.; Mallik, T.K.; *Correllating Photovoltaic Soiling Losses to Waveband and Single-Value Transmittance Measurements. Energy 2019, 180, 376-386;*

https://doi.org/10.1016/j.energy.2019.05.097

En esta publicación se identifican las regiones del espectro (ultravioleta, visible e infrarrojo cercano) que pueden utilizarse para estimar con gran exactitud las pérdidas por polvo y suciedad que experimentan las diferentes tecnologías fotovoltaicas de una sola unión, a partir del análisis de la transmitancia espectral media (AST, por las siglas del inglés *average spectral transmittance*) obtenida en cada una de las anteriores bandas para el vidrio FV expuesto en exteriores. Para los materiales FV en cuestión también se identifican en el antedicho artículo los valores individuales de longitud de onda a partir de los cuales pueden estimarse con finura las referidas pérdidas a través del estudio de la transmitancia óptica simple del vidrio FV dejado a la intemperie. A este fin, se llevó a cabo una campaña experimental de 48 semanas de duración en la terraza del Edificio A3 de la Universidad de Jaén, la cual se extendió desde enero de 2017 hasta enero de 2018. En dicha ubicación se habilitó una zona restringida para exponer a la intemperie una muestra de vidrio fotovoltaico cuadrada de 4 x 4 $cm^2$ con un espesor de 3 mm anclada y dispuesta horizontalmente. De este modo, el vidrio fotovoltaico podría ensuciarse o limpiarse de forma natural. Al mismo tiempo, una muestra idéntica a la dispuesta en el exterior se almacenó en un lugar seguro y limpio, con objeto de servir como referencia. Ambas muestras fueron analizadas semanalmente en el Centro de Instrumentación Científico Técnica (CICT) de la Universidad de Jaén, con el fin de utilizar un espectrofotómetro Lambda® 950, con una esfera integradora de 60 mm de diámetro, para registrar medidas de transmitancia hemisférica del vidrio limpio y del que se encontraba a la intemperie. Cabe destacar que durante todo el experimento únicamente se limpió de forma manual la muestra expuesta en el exterior durante la semana 24, con objeto de verificar si se había producido algún tipo de degradación óptica permanente en dicha muestra.

Con los datos recopilados semanalmente, se calcularon las pérdidas totales de transmitancia óptica producidas por el polvo y la suciedad mediante el índice SR (por las siglas del inglés *soiling ratio*). A continuación, se representó gráficamente dicho coeficiente frente al valor de AST asociado a las regiones espectrales de ultravioleta (UV), visible (VIS) o infrarrojo cercano (NIR por las siglas del inglés *near infrared*). En el caso de estimar las pérdidas totales producidas por polvo y suciedad a través de la AST asociada a la región del espectro VIS, se obtuvieron valores de coeficientes de determinación excelentes —desde 0,94 para el mc-Si hasta el 1,00 para el a-Si—, evidenciándose así la posibilidad de generar nuevos dispositivos que permitan estimar las pérdidas totales producidas por polvo y suciedad en las tecnologías FV disponibles actualmente, a través de la AST asociada a una región limitada del espectro. Asimismo, de manera análoga, se graficó el índice SR con respecto a la transmitancia óptica correspondiente a bandas de 1 nm de anchura —considerándose dichas bandas en la práctica como longitudes de onda individuales, correspondientes a luz monocromática—, mejorándose en algunos casos las estimaciones obtenidas de SR a partir de un valor de AST calculado a lo largo del espectro visible. En este segundo análisis, los mejores ajustes de correlación lineal entre SR y la transmitancia óptica se observan para longitudes de onda individuales comprendidas en el intervalo de 500 y 600 nm. Así, y para el peor de los casos (perovskita) se obtiene un coeficiente de determinación de 0,99, mientras que, para el mejor de los casos (CdTe) el referido coeficiente toma un valor de 1,00, siendo realizadas ambas estimaciones a partir de la transmitancia óptica simple medida en la longitud de onda de 550 nm. Los resultados de este artículo pueden conducir a enfoques innovadores conducentes al desarrollo de dispositivos novedosos orientados a la medida del impacto de la suciedad en la operación de plantas FV que ya estén en funcionamiento. En concreto, este estudio abre la posibilidad de estimar las pérdidas de sistemas FV utilizando elementos de bajo coste tales como diodos LED.

# 4. CONCLUSIONES Y LINEAS FUTURAS DE INVESTIGACIÓN

Mediante la realización de la presente Tesis doctoral se ha alcanzado un nivel superior de conocimiento sobre el comportamiento en exterior que experimentan diferentes tecnologías fotovoltaicas, tanto basadas en panel plano como de concentración. Así, se ha arrojado luz sobre la posible biyección existente entre la forma de la distribución espectral de la DNI y la EMF. Adicionalmente, se ha modelado la influencia que los parámetros atmosféricos AM, AOD y PW ejercen sobre la irradiancia efectiva que incide sobre los dispositivos de simple unión. Por último, se ha analizado el efecto de la deposición natural de polvo y suciedad sobre vidrios fotovoltaicos. Dicho análisis ha permitido detectar la dependencia de las pérdidas producidas por *soiling* en varios materiales FV de simple unión, a partir de la atenuación de la transmitancia óptica en bandas limitadas del espectro solar.

A continuación, se detallan las principales conclusiones alcanzadas:

- La relación biunívoca entre la EMF y la distribución espectral de la DNI solamente puede ser asumida, en la banda de longitudes de onda comprendida entre 450 y 900 nm, en términos prácticos. Fuera de dicha banda, las distribuciones espectrales con el mismo valor de la EMF no guardan una semejanza que permita considerarlas aproximadamente iguales desde un punto de vista pragmático. En consecuencia, la utilidad real del empleo de la EMF en la ingeniería de los sistemas fotovoltaicos bajo luz concentrada resulta ser escasa.

- Se ha logrado modelar con un alto grado de exactitud, mediante las primeras ecuaciones analíticas existentes en la literatura fotovoltaica, las correcciones espectrales de la irradiancia de banda ancha dependiendo de la tecnología fotovoltaica plana de unión simple considerada. Dichas ecuaciones involucran los parámetros atmosféricos AM, AOD y PW. Así, se han obtenido al comparar valores experimentales del factor de desacoplo frente a valores modelados de dicho factor coeficientes de determinación $R^2$ que van desde 0,87 en el peor de los casos (mc-Si) hasta 0,92 en el mejor de ellos (a-Si). Los modelos de correcciones espectrales propuestos en la presente Tesis mejoran sustancialmente otros ya existentes. En este sentido, se han conseguido mejores resultados con las ecuaciones aquí propuestas que con el modelado de los efectos espectrales propuesto por los Laboratorios Sandia, el cual únicamente involucra al parámetro AM en el cálculo de la irradiancia efectiva a partir de la irradiancia de banda ancha. Así, y como ejemplo en el caso de la tecnología sc-Si, los valores de RMSE y MBE que se obtienen con las ecuaciones propuestas son de 0,280% y 3,16E-14% respectivamente, mientras que con el método de los Laboratorios Sandia se obtienen valores de 0,345% y 0,017% para los referidos estadísticos.

- Existe una estrecha relación entre la medida de AST limitada en una región del espectro determinada (UV, VIS, NIR), e incluso, entre la transmitancia óptica en una banda de tan solo 1 nm de anchura —asumida como una longitud

de onda única— y el valor de SR integrado en la banda de absorción de cada una de las diferentes tecnologías fotovoltaicas planas de una unión sobre las que se depone polvo y suciedad de forma natural, en exteriores. Así pues, la mejor región del espectro para estimar las pérdidas producidas por *soiling* es la región del espectro visible, obteniéndose en el caso del mc-Si, un coeficiente de determinación de 0,98. En cambio, las mejores longitudes de onda individuales para estimar los valores de SR son la de 550 nm para materiales cuya respuesta espectral es mayor en longitudes de onda cortas (a-Si, CdTe y perovskita) y la de 600 nm para materiales cuya respuesta espectral es más alta en longitudes de onda largas (sc-Si y mc-Si). Como muestra de este último hecho cabe ser destacado que el coeficiente de determinación obtenido en el caso del mc-Si al graficar SR frente a la transmitancia óptica simple obtenida en 600 nm es del 1,00.

A partir de las conclusiones expuestas con anterioridad, se proponen las siguientes líneas de investigación futuras:

- Hasta el momento y hasta donde sabemos solamente se han dado a conocer dos investigaciones que han tratado de verificar si existe una relación biunívoca entre la EMF y la distribución espectral de la DNI, habiéndose desarrollado ambas en localizaciones con climas templados —Kusatsu (Japón, latitud 36°12' N, longitud 138°15' E) y Jaén. Por tanto, es preciso realizar otros estudios experimentales similares en lugares con climatología diferente, con el objetivo de poder generalizar las conclusiones obtenidas, si procede.

- Es preciso validar las ecuaciones propuestas para el modelado de efectos espectrales mediante parámetros atmosféricos (AM, AOD y PW) en localizaciones con condiciones atmosféricas extremas. Para ello, se debería profundizar en dicha cuestión realizando incluso mediciones reales en módulos fotovoltaicos, lo que permitirá obtener un método general y universal.

- Es necesario realizar estudios similares al propuesto para estimar la influencia espectral del polvo y la suciedad sobre la transmitancia óptica de los vidrios fotovoltaicos en otras ubicaciones y durante periodos más prolongados de tiempo. Asimismo, se debe analizar la variación de la transmitancia óptica de un vidrio fotovoltaico con polvo y suciedad acumulada bajo diferentes ángulos de incidencia. Esto será fundamental para verificar si se confirman los hallazgos realizados en la investigación desarrollada durante la presente Tesis y/o para introducir nuevas correcciones que permitan el desarrollo de un método general y universal.

# 5. NOMENCLATURA

| | |
|---|---|
| AEMET: | Agencia Estatal de Meteorología |
| AERONET: | Red Robótica de Aerosoles (del inglés *Aerosol Robotic Network*) |
| AM: | Masa de aire (del inglés *air mass*) |
| AOD: | Espesor óptico del aerosol (del inglés *aerosol optical depth*) |
| AST: | Transmitancia espectral media (del inglés *average spectral transmittance*) |
| BOS: | Balance de sistema (del inglés *balance of system*) |
| CEM: | Condiciones estándares de medida |
| CFV: | Concentración fotovoltaica |
| CICT: | Centro de Instrumentación Científico Técnico |
| COP21: | Conferencia de las Partes de París |
| CV: | Coeficiente de variación |
| DNI: | Irradiancia normal directa (del inglés *direct normal irradiance*) [$W \cdot m^{-2}$] |
| EMF: | Energía media del fotón [eV] |
| FV: | Fotovoltaica/o |
| GEI: | Gases de Efecto Invernadero |
| GHI: | Irradiancia global horizontal (del inglés *global horizontal irradiance*) [$W \cdot m^{-2}$] |
| GTI: | Irradiancia global inclinada (del inglés *global tilted irradiance*) [$W \cdot m^{-2}$] |
| IRENA: | Agencia Internacional de las Energías Renovables (del inglés *International Renewable Energy Agency*) |
| LCOE: | Coste normalizado de la energía (del inglés *Levelized Cost Of Energy*) [$€ \cdot MWh^{-1}$] |
| MM: | Factor de ajuste espectral (del inglés *mismatch spectral factor*) |
| NASA: | Administración Nacional Aeronáutica y del Espacio (del inglés *National Aeronautics* and *Space Administration*) |
| NDC: | Contribución Determinada a nivel Nacional (del inglés *Nationally Determined Contribution*) |
| NIR: | Infrarrojo cercano (del inglés *near infrared*) |
| PHOTONS: | Fotometría para el Tratamiento Operacional de Normalización Satelital (del francés *Photométrie pour le Traitement Opérationnel de Normalisation Satellitaire*) |
| PPA: | Contrato de Compraventa de Energía (del inglés *Power Purchase Agreement*) |
| PVGIS: | Sistema de Información Geográfica Fotovoltaico (del inglés *Photovoltaic Geographical Information System*) |
| PW: | Agua precipitable (del inglés *precipitable water*) [cm] |
| SD: | Desviación estándar (del inglés *standard deviation*) |
| SR: | *Soiling ratio* |
| UV: | Ultravioleta |
| VIS: | Visible |

# 6. REFERENCIAS

[1] Darkwah WK, Odum B, Addae M, Koomson D, Kwakye Danso B, Oti-Mensah E et al. Greenhouse Effect: Greenhouse Gases and Their Impact on Global Warming. Journal of Scientific Research and Reports 2018;17:1-9.

[2] Grupo Banco Mundial. Emisiones de CO2 (kt) 19/03/2021. ["https://datos.bancomundial.org/indicator/EN.ATM.CO2E.KT"] (último acceso 01/04/2021).

[3] IRENA. NDCs in 2020: Advancing renewables in the power sector and beyond. International Renewable Energy Agency 2019. ["https://www.irena.org/-/media/Files/IRENA/Agency/Publication/2019/Dec/IRENA_NDCs_in_2020.pdf"] (último acceso 01/04/2021).

[4] Fraunhofer ISE. Photovoltaics Report 16/09/2020. [https:// https://www.ise.fraunhofer.de/content/dam/ise/de/documents/publications/studies/Photovoltaics-Report.pdf ] (último acceso 12/05/2021).

[5] IRENA. Solar energy. ["https://www.irena.org/solar"] (último acceso 13/05/2021).

[6] Micheli L, Solas ÁF, Soria-Moya A, Almonacid F, Fernández EF. Short-term impact of the COVID-19 lockdown on the energy and economic performance of photovoltaics in the Spanish electricity sector. J Clean Prod 2021;308:127045.

[7] PV magazine. Saudi Arabia's second PV tender draws world record low bid of $0.0104/kWh 08/04/2021. ["https://www.pv-magazine.com/2021/04/08/saudi-arabias-second-pv-tender-draws-world-record-low-bid-of-0104-kwh"] (último acceso 09/04/2021).

[8] IRENA. Renewable Power Generation Costs in 2019. International Renewable Energy Agency 2020. ["https://www.irena.org/publications/2020/Jun/Renewable-Power-Costs-in-2019"] (último acceso 01/04/2021).

[9] IRENA. World Energy Transitions Outlook: 1.5°C Pathway. International Renewable Energy Agency 2021. ["https://www.irena.org/-/media/Files/IRENA/Agency/Publication/2021/March/IRENA_World_Energy_Transitions_Outlook_2021.pdf"] (último acceso 01/04/2021).

[10] Hofmann M, Vanicek P, Haselhuhn. Is the average photon energy (APE) a suitable measure to describe the uniqueness of solar spectra? 29th European Photovoltaic Solar Energy Conference and Exhibition: 2014; 3461-66.

[11] Sutterlueti J, Ransome S, Kravets R, S. L. Characterising PV modules under outdoor conditions: What's most important for energy yield. 26th European Photovoltaic Solar Energy Conference and Exhibition:2011;5–11.

[12] Louwen A, de Waal AC, van Sark, W. G. J. H. M. Evaluation of different indicators for representing solar spectral variation. 2016 IEEE 43rd Photovoltaic Specialists Conference (PVSC) 2016:133.

[13] Paudyal BR, Imenes AG. Analysis of spectral irradiance distribution for PV applications at high latitude. 2020 47th IEEE Photovoltaic Specialists Conference (PVSC) 2020:1834-41.

[14] Rodrigo P, Fernández E, Almonacid F, Perez-Higueras P. Quantification of the spectral coupling of atmosphere and photovoltaic system performance: Indexes, methods and impact on energy harvesting. Solar Energy Mater Solar Cells 2017;163:73–90.

[15] Minemoto T, Nakada Y, Takahashi H, Takakura H. Uniqueness verification of solar spectrum index of average photon energy for evaluating outdoor performance of photovoltaic modules. Solar Energy 2009;83:1294-9.

[16] Norton M, Amillo AG, Galleano R. Comparison of solar spectral irradiance measurements using the average photon energy parameter. Solar Energy 2015;120:337-44.

[17] Chantana J, Ueno S, Ota Y, Nishioka K, Minemoto T. Uniqueness verification of direct solar spectral index for estimating outdoor performance of concentrator photovoltaic systems. Renewable Energy 2015;75:762-6.

[18] Nofuentes G, Gueymard CA, Aguilera J, Pérez-Godoy MD, Charte F. Is the average photon energy a unique characteristic of the spectral distribution of global irradiance? Solar Energy 2017;149:32-43.

[19] Tsuji M, Rahman MM, Hishikawa Y, Nishioka K, Minemoto T. Uniqueness verification of solar spectrum obtained from three sites in Japan based on similar index of average photon energy. Solar Energy 2018;173:89-96.

[20] IEC 60904-3, ed. 4. Photovoltaic devices - Part 3: Measurement principles for terrestrial photovoltaic (PV) solar devices with reference spectral irradiance data. International Electrotechnical Commission, 2019.

[21] Gottschalg R, Betts T, Infield D, Kearney M. On the importance of considering the incident spectrum when measuring the outdoor performance of amorphous silicon photovoltaic devices. Measurement Science and Technology 2004;15:460-6.

[22] Duck BC, Fell CJ. Comparison of methods for estimating the impact of spectrum on PV output. 2015 IEEE 42nd Photovoltaic Specialist Conference (PVSC) 2015:1-6.

[23] Duck BC, Fell CJ. Improving the spectral correction function. 2016 IEEE 43rd Photovoltaic Specialists Conference (PVSC) 2016:2647-52.

[24] Marion B, Deceglie MG, Silverman TJ. Analysis of measured photovoltaic module performance for Florida, Oregon, and Colorado locations. Solar Energy 2014;110:736-44.

[25] Senthilarasu S, Fernández EF, Almonacid F, Mallick TK. Effects of spectral coupling on perovskite solar cells under diverse climatic conditions. Solar Energy Mater Solar Cells 2015;133:92-8.

[26] Nofuentes G, García-Domingo B, Muñoz JV, Chenlo F. Analysis of the dependence of the spectral factor of some PV technologies on the solar spectrum distribution. Appl Energy 2014;113:302-9.

[27] Nofuentes G, Fuentes M, Aguilera J, Diez JV. An Assessment on Simple Modeling Approaches to the Electric Behavior of Two CIS PV Modules in a Sunny Climate. Journal of Solar Energy Engineering-transactions of The Asme - J SOL ENERGY ENG 2009;131.

[28] Ishii T, Otani K, Takashima T, Xue Y. Solar spectral influence on the performance of photovoltaic (PV) modules under fine weather and cloudy weather conditions. Prog Photovoltaics Res Appl 2011;21.

[29] Ye JY, Reindl T, Aberle AG, Walsh TM. Effect of Solar Spectrum on the Performance of Various Thin-Film PV Module Technologies in Tropical Singapore. IEEE Journal of Photovoltaics 2014;4:1268-74.

[30] Gottschalg R, Betts TR, Infield DG, Kearney MJ. The effect of spectral variations on the performance parameters of single and double junction amorphous silicon solar cells. Solar Energy Mater Solar Cells 2005;85:415-28.

[31] Alonso-Abella M, Chenlo F, Nofuentes G, Torres-Ramírez M. Analysis of spectral effects on the energy yield of different PV (photovoltaic) technologies: The case of four specific sites. Energy 2014;67:435-43.

[32] Dirnberger D, Blackburn G, Müller B, Reise C. On the impact of solar spectral irradiance on the yield of different PV technologies. Solar Energy Mater Solar Cells 2015;132:431-42.

[33] Fernández EF, Cruz FA, Mallick TK, Sundaram S. Effect of Spectral Irradiance Variations on the Performance of Highly Efficient Environment-Friendly Solar Cells. IEEE Journal of Photovoltaics 2015;5:1150-7.

[34] Jardine CN, Gottschalg R, Betts T, Infield D. Influence of Spectral Effects on the Performance of Multijunction Amorphous Silicon Cells. Proceedings Photovoltaic in Europe Conference, 2002.

[35] Betts T, Gottschalg R, Infield D. Spectral Irradiance Correction for PV System Yield Calculations. Proceedings of the 19th Photovoltaic Solar Energy Conference, 2004.

[36] Peharz G, Siefer G, Bett AW. A simple method for quantifying spectral impacts on multi-junction solar cells. Solar Energy 2009;83:1588-98.

[37] Gottschalg R, Betts TR, Infield DG, Kearney MJ. Experimental investigation of spectral effects on amorphous silicon solar cells in outdoor operation. Conference Record of the Twenty-Ninth IEEE Photovoltaic Specialists Conference, 2002. 2002:1138-41.

[38] Takahashi H, Fukushige S, Minemoto T, Takakura H. Output estimation of Si-based photovoltaic modules with outdoor environment and output map. J Cryst Growth 2009;311:749-52.

[39] Minemoto T, Takahashi H, Nakada Y, Takakura H. Outdoor performance evaluation of photovoltaic modules using contour plots. Current Applied Physics; The Proceeding of the International Renewable Energy Conference and Exhibition 2008 (RE2008) 2010;10:S257-60.

[40] Nofuentes G, Casa J, Ramirez M, Alonso Abella M. Solar Spectral and Module Temperature Influence on the Outdoor Performance of Thin Film PV Modules Deployed on a Sunny Inland Site. International Journal of Photoenergy 2013.

[41] García-Domingo B, Aguilera J, de la Casa J, Fuentes M. Modelling the influence of atmospheric conditions on the outdoor real performance of a CPV (Concentrated Photovoltaic) module. Energy 2014;70:239-50.

[42] Nofuentes G, de la Casa J, Solís-Alemán EM, Fernández EF. Spectral impact on PV performance in mid-latitude sunny inland sites: Experimental vs. modelled results. Energy 2017;141:1857-68.

[43] Neves G, Vilela W, Pereira E, Yamasoe M, Nofuentes G. Spectral impact on PV in low-latitude sites: The case of southeastern Brazil. Renewable Energy 2021;164:1306-19.

[44] Braga M, do Nascimento LR, Rüther R. Spectral modeling and spectral impacts on the performance of mc-Si and new generation CdTe photovoltaics in warm and sunny climates. Solar Energy 2019;188:976-88.

[45] Fernández-Solas Á, Micheli L, Almonacid F, Fernández EF. Optical degradation impact on the spectral performance of photovoltaic technology. Renewable and Sustainable Energy Reviews 2021;141:110782.

[46] Banerjee A, Bora B, Singh R, Sastry OS. Initial outdoor performance analysis of different PV module technology. 2016 7th India International Conference on Power Electronics (IICPE) 2016:1-6.

[47] Hüttl B, Gottschalk L, Schneider S, Pflaum D, Schulze A. Accurate performance rating of photovoltaic modules under outdoor test conditions. Solar Energy 2019;177:737-45.

[48] Park H, Chang S, Park S, Kim WK. Outdoor Performance Test of Bifacial n-Type Silicon Photovoltaic Modules. Sustainability 2019;11.

[49] Sharma V, Kumar A, Sastry O, Chandel S. Performance assessment of different solar photovoltaic technologies under similar outdoor conditions. Energy 2013;58:511-8.

[50] Muller M, Marion B, Kurtz S, Rodriguez J. An Investigation into Spectral Parameters as they Impact CPV Module Performance. AIP Conference Proceedings 2010;1277:307-11.

[51] Marion B. Influence of atmospheric variations on photovoltaic performance and modeling their effects for days with clear skies. 2012 38th IEEE Photovoltaic Specialists Conference 2012:3402.

[52] Polo J, Alonso-Abella M, Ruiz-Arias J, Balenzategui JL. Worldwide analysis of spectral factors for seven photovoltaic technologies. Solar Energy 2017;142:194-203.

[53] Osterwald C, Emery K, Muller M. Photovoltaic module calibration value versus optical air mass: The air mass function. Progress in Photovoltaics Research and Applications 2014;22.

[54] King D, Kratochvil J, Boyson W. Photovoltaic Array Performance Model. 2004;8.

[55] Lee M, Panchula AF. Variation in spectral correction of PV module performance based on different precipitable water estimates. 2016 IEEE 43rd Photovoltaic Specialists Conference (PVSC) 2016:2692-7.

[56] Gueymard C. SMARTS2, a simple model of the atmospheric radiative transfer of sunshine: algorithms and performance assessment. Florida Solar Energy Center, 1995.

[57] Holben B, Eck T, Slutsker I, Tanré D, Buis J, Setzer A, Vermote E, Reagan J, Kaufman Y, Nakajima T, Lavenu F, Jankowiak I, Smirnov A. AERONET-A federated instrument network and data archive for aerosol characterization, Remote Sens Environ 1998;66(1):1–16.

[58] Sarver T, Al-Qaraghuli A, Kazmerski LL. A comprehensive review of the impact of dust on the use of solar energy: History, investigations, results, literature, and mitigation approaches. Renewable and Sustainable Energy Reviews 2013;22:698-733.

[59] Qasem H, Betts T, Müllejans H, AlBusairi H, Gottschalg R. Dust Induced Shading on Photovoltaic Modules. Progress in Photovoltaics 2014;22.

[60] Kalogirou S, Agathokleous R, Panayiotou G. On-site PV characterization and the effect of soiling on their performance. Energy 2013;51:439–446.

[61] Kaldellis JK, Kokala A. Quantifying the decrease of the photovoltaic panels' energy yield due to phenomena of natural air pollution disposal. Energy; The 3rd International Conference on Sustainable Energy and Environmental Protection, SEEP 2009 2010;35:4862-9.

[62] Theristis M, Fernández EF, Almonacid F, Pérez-Higueras P. Spectral Corrections Based on Air Mass, Aerosol Optical Depth, and Precipitable Water for CPV Performance Modeling. IEEE Journal of Photovoltaics 2016;6:1598-604.

[63] Martin N, Ruiz JM. A new method for the spectral characterisation of PV modules. Prog Photovoltaics Res Appl 1999;7:299-310.

# BLOQUE II. PUBLICACIONES REALIZADAS EN EL MARCO DE LA TESIS DOCTORAL.

En este bloque se anexan las contribuciones realizadas en el marco de la presente Tesis Doctoral. Dichas contribuciones son un compendio de tres artículos publicados en revistas indexadas en el ISI *Journal Citation Reports Science Edition* de la Web of Science (WoS). En adelante se hace referencia a dichos artículos, al factor de impacto de las revistas donde fueron publicados y a la posición que estas ocupan dentro de las categorías científicas a las que pertenecen.

Nofuentes, G.; Gueymard, C.; Caballero, J.; Marques-Neves, G.; Aguilera, J. Experimental Evaluation of a Spectral Index to Characterize Temporal Variations in the Direct Normal Irradiance Spectrum. Applied Sciences 2021, 11(3), 897; https://doi.org/10.3390/app11030897

**Estado:** Publicado

**Factor de Impacto (JCR Science Edition 2019)**: 2.474

**Categorías científicas y posición dentro de las mismas (JCR Science Edition 2019):** 88/177 (Q2) en “Chemistry, Multidisciplinary”; 62/154 (Q2) en “Physics, Applied”; 32/91 (Q2) en “Engineering, Multidisciplinary” y 161/314 (Q3) en “Materials Science, Multidisciplinary'

applied sciences

MDPI

*Article*

# Experimental Evaluation of a Spectral Index to Characterize Temporal Variations in the Direct Normal Irradiance Spectrum

**Gustavo Nofuentes [1,2,*], Christian A. Gueymard [3], José A. Caballero [4], Guilherme Marques-Neves [5,6] and Jorge Aguilera [1]**

1 IDEA Research Group, University of Jaén, Campus de Las Lagunillas, 23071-Jaén, Spain; aguilera@ujaen.es
2 Center for Advanced Studies in Earth Science, Energy and Environment (CEACTEMA), University of Jaén, Campus Las Lagunillas, 23071 Jaén, Spain
3 Solar Consulting Services, Colebrook, NH 03576, USA; chris@solarconsultingservices.com
4 PVhardware Solutions S.L. Polígono Industrial Castilla, Vial I, 13. 46380 Cheste, Spain; chipi.c19@gmail.com
5 GDF Research Group, Brazilian National Institute for Space Research, Av. Dos Astronautas, 1758 São José dos Campos, Brazil; gmnevess@gmail.com
6 Labren Research Group, Brazilian National Institute for Space Research, Av. Dos Astronautas, 1758 São José dos Campos, Brazil
* Correspondence: gnofuen@ujaen.es

**Featured Application: The conclusions of this work may prove highly useful in developing easier models to capture the spectral impact on CPV devices.**

**Abstract:** A simple index is desirable to assess the effects on both flat-plate and concentrating photovoltaics of natural changes in the solar spectrum. Some studies have suggested that the relationship between the Average Photon Energy (APE) and the shape of individual global tilted irradiance, global horizontal irradiance, or direct normal irradiance (DNI) spectra is bijective and can therefore be used as a single number to unequivocally replace a complete spectral distribution. This paper reevaluates these studies with a modified methodology to assess whether a one-to-one relationship really exists between APE and spectral DNI. A 12-month dataset collected in Jaén (Spain) using a sun-tracking spectroradiometer provides the necessary spectral DNI data between 350 and 1050 nm. After quality control and filtering, 78,772 valid spectra were analyzed. The methodology is based on a statistical analysis of the spectral distributions binned in 0.02-eV APE intervals, from 1.74 to 1.90 eV. For each interval, both the standard deviation and coefficient of variation (CV) are determined across all 50-nm bands into which the 350–1050-nm waveband is divided. CV stays below 3.5% within the 450–900-nm interval but rises up to 13% outside of it. It is concluded that APE may be approximately assumed to uniquely characterize the DNI spectrum distribution for Jaén (and presumably for locations with similar climates) only over the limited 450–900-nm waveband.

**Keywords:** spectral irradiance; direct solar spectrum; spectroradiometer; average photon energy; effective wavelength



**Citation:** Nofuentes, G.; Gueymard, C.A.; Caballero, J.A.; Marques-Neves, G.; Aguilera, J. Experimental Evaluation of a Spectral Index to Characterize Temporal Variations in the Direct Normal Irradiance Spectrum. *Appl. Sci.* **2021**, *11*, 897. https://doi.org/10.3390/app11030897

Academic Editor: Alejandro Pérez-Rodróhiez
Received: 23 December 2020
Accepted: 18 January 2021
Published: 20 January 2021



## 1. Introduction

The accurate estimation of both the expected and predicted electricity yields of photovoltaic (PV) systems is normally carried out by following a standard procedure [1]. This step is crucial to ascertain the production of electricity that such systems may deliver, thus enabling both the bankability of PV projects [2] and the quality assurance for PV plants [3], among other desirable outcomes. After the two quantities (incident broadband irradiance and temperature) that have the most impact on power output, the spectral distribution of the irradiance (spectral irradiance, in short) is generally considered the largest influence to natural variations in the output of clean PV devices [4,5]. It is worth noting that conventional flat-plate PV are less sensitive to varying spectral irradiance than Concentrating

Photovoltaics (CPV). Such a higher sensitivity of the latter technology to spectral effects is especially noticeable when concentrated sunlight of 1000 suns or more is used in High Concentrating Photovoltaics (HCPV) [6], where multi-junction solar cells based on series-connected subcells with different bands of absorption are used in conjunction with optical elements [7,8]. The present contribution is mostly related to the latter type of application.

Spectral effects may be quantified using two methods aimed at estimating a spectral mismatch (MM) factor [9]. The first is based on measurements of the outdoor short-circuit current of the PV device under investigation. The second is based on combining its spectral response with spectra recorded with spectroradiometers—although synthetic or modeled spectra may also be used. One hindrance in the first method is that spectral effects might be difficult to isolate the impacts of device temperature, soiling, or degradation and, in the case of flat-plate PV, angular losses. Hence, the second method is often preferred but requires knowledge of (i) the actual spectrum under the atmospheric conditions at any specific moment (in the case of outdoor exposure) and (ii) the actual spectral response of the PV device under test. The procedure also implies numerical integrations in a 2D domain (wavelength and time). This can become cumbersome if this needs to be repeated at high frequency and can be inexact if the spectral response of the PV device is not known precisely, which is often the case.

To overcome the above difficulties, a simplifying approach—recourse to 1D (time only) spectral indexes that would be independent of the cell's spectral response—has been proposed in the literature. Indeed, such kinds of indexes are often preferred to the integrated useful fraction [10], the spectrally weighted ratio [11], the spectrally corrected global irradiance [12], or other metrics used in non-concentrating PV that depend on the specific device under scrutiny. The same preference holds for some other PV device-dependent indexes used in CPV characterization, such as the Z-parameter [13], the spectrally corrected direct normal irradiance [14], etc. A comprehensive review of spectral indexes has been recently presented [8].

In view of the above, finding a PV device-independent spectral index that could uniquely characterize individual spectra would be most useful for both PV science and engineering. A review of the literature shows that only two such indexes have been investigated and proposed as possible candidates to meet this requirement: the *blue fraction* (BF) and the *average photon energy* (APE). BF has been introduced to assess the ratio of spectral irradiance integrated below 650 nm to the total irradiance [15], whereas APE is the mean energy of all the photons that impinge on a given surface [16].

Despite some early promising results presented by Louwen et al. [17] and later limited results reported by Paudyal and Imenes [18], the possible one-to-one relationship between BF and spectral irradiance still remains highly unexplored. Indeed, this issue has been scarcely addressed thus far [8,18], therefore justifying further investigation. In contrast, APE is an older and more popular index amongst the PV community. It has been widely used to provide a readily qualitative assessment on whether a specific spectrum is shifted to shorter or longer wavelengths relative to the standard spectrum. Thus, a more in-depth analysis of this parameter, including its physical significance, is provided hereafter.

Minemoto et al. [19] first analyzed the relationship between APE and the spectrum shape of global tilted irradiance (GTI). Their experimental campaign was conducted in Kusatsu City, Japan (latitude 34°58′ N) over a period of three years. Spectral irradiance was monitored on a 15.3°-tilted surface facing the equator and led the authors to the conclusion that the relationship between APE and the GTI spectrum was bijective. Their methodology was based on an International Electrotechnical Commission (IEC) standard [20], which states by how much the output of a solar simulator can deviate from the AM1.5G reference spectrum. Their reasoning was basically that, if spectral distributions grouped in very narrow APE intervals have a very small standard deviation (SD) in all considered 50-nm bands, such distributions may be considered equal. A closer insight to that methodology is provided in what follows. Subsequent work assumed this one-to-one relationship between

APE and GTI [21–30], although further investigation at other sites was encouraged to confirm the possible universality of such a relationship.

Norton et al. [31] carried out a statistical analysis very similar to that of Minemoto et al. [19], using measurements of spectral global horizontal irradiance (GHI) collected at two sites with different climates: Ispra, Italy (latitude 45°49′ N, longitude 8°36′ E) and Golden, CO, USA (latitude 39°45′ N, longitude 105°13′ W). Measurements were recorded for 16 months at the latter location and over two years at the former, using dissimilar instruments and experimental protocols at each site. Norton and coworkers concluded that the relationship between APE and the GHI spectrum shape was bijective. However, these authors also raised the need for further collection and analysis of spectral irradiance data at other sites because firm conclusions could not be drawn from measurements at only two sites.

In contrast, the relationship between the spectral distribution of GTI and APE was found *not* bijective by Dirnberger et al. [12]. They noted that spectral distributions with the same value of APE might yield different values of MM for the same PV material. Their conclusion was based on the analysis of spectral GTI data collected on a 35°-tilt equator-facing surface over a 3.5-year experimental campaign conducted in Freiburg im Breisgau, Germany (latitude 47°59′ N).

A later study presented by Nofuentes et al. [32] applied the same methodology as proposed by Minemoto et al. [19] to two spectral datasets collected on a 30°-tilt equator-facing surface during a two-year experimental campaign conducted in two Spanish cities with nearly the same Mediterranean-Continental climate: Jaén (latitude 37°49′ N) and Madrid (latitude 40°24′ N). These authors underlined that the coefficient of variation (CV) was more appropriate in evaluating the dispersion around the mean than SD alone. Hence, they postulated that spectral distributions with nearly the same APE value should have a small value of CV across all considered 50-nm bands to be considered equivalent. The results obtained for the two Spanish sites under scrutiny showed that bijectivity between APE and GTI spectrum shape could be assumed only from a pragmatic point of view and only over the 450–900-nm waveband, where CV stays below 3.3%. The reasons why noticeable dispersion occurred below 450 nm or above 900 nm were deeply analyzed from both an instrumental standpoint and atmospheric physics principles.

Tsuji et al. [33] carried out a similar statistical analysis to that of Minemoto et al. [19] with spectral GTI data collected on equator-facing surfaces at three Japanese sites for one or two years: Kusatsu (15.3° tilt, as in the study discussed above [19]), Tsukuba (latitude 36°04′ N, 20° tilt), and Miyazaki (latitude 31°49′ N, 35° tilt). They concluded that APE uniquely represented the spectral distribution of GTI, even though CV values in excess of 30% were found within the 900–950 nm waveband for the three sites under scrutiny.

The literature reviewed above targets flat-plate PV applications only and thus focuses on the *global* spectrum (on either horizontal or tilted surfaces). The bijectivity between APE and spectral direct normal irradiance (DNI) has not received much attention so far, which is a justification for the present investigation. Apparently, Chantana et al. [34] are the only authors who have explored the APE–DNI relationship experimentally and only at a single site. They applied the same general methodology as Minemoto et al. [19] to spectral DNI measurements collected over a one-year experimental campaign conducted in Kusatsu. Chantana and coworkers concluded that a one-to-one relationship did exist between APE and the DNI spectral shape. Unfortunately, they did not analyze the variation of CV across all the studied 10-nm wavebands. It is worth mentioning, though, that a previous theoretical study presented by Gueymard [35] and based on simulations of the cloudless direct spectrum by means of the Simple Model of the Atmospheric Radiative Transfer of Sunshine (SMARTS) 1 [36] had disproved the bijectivity between APE and the DNI spectral shape. That study showed that different combinations of air mass (AM), aerosol optical depth (AOD), and precipitable water (PW) could result in significantly different DNI spectral distributions with however the same resulting APE value.

The present work aims at exploring whether the APE uniquely characterizes the varying DNI spectrum—at least in practical terms—from an experimental standpoint. In view of the above literature review, this study is the second known attempt to elucidate such an issue by analyzing measured DNI spectra. The present 12-month experimental study is based on spectroradiometric measurements at Jaén, Spain. The general methodology of Nofuentes et al. [32] is followed to perform an appropriate statistical analysis of the spectral data.

## 2. Materials and Methods

### *2.1. Experimental Setup*

The experimental campaign was conducted at the University of Jaén (Spain, with a Mediterranean-Continental climate), a small-size city (113,000 inhabitants) where periodic Saharan dust episodes occur in summer, together with high levels of olive-tree pollen during May. A comprehensive description of this site in atmospheric terms was carried out in a previous work [32].

The empirical data used in this paper was collected at the outdoor research facilities located on the flat roof of one of the buildings of the High Technical School of the Engineering and Technology campus, located within the city. These facilities were described in detail in previous studies [37,38].

The direct spectrum was measured by an EKO$^{TM}$ MS700 spectroradiometer equipped with a collimator tube and fixed to a two-axis BSQ$^{TM}$ D1506 solar tracker for concentrating PV applications, as shown in Figure 1. The collimator tube was made of black PVC and was devised according to the values of the slope angle (1°) and aperture angle (5°) specified in the MS700 spectroradiometer datasheet. This experimental setup has been successfully used in earlier work [39].

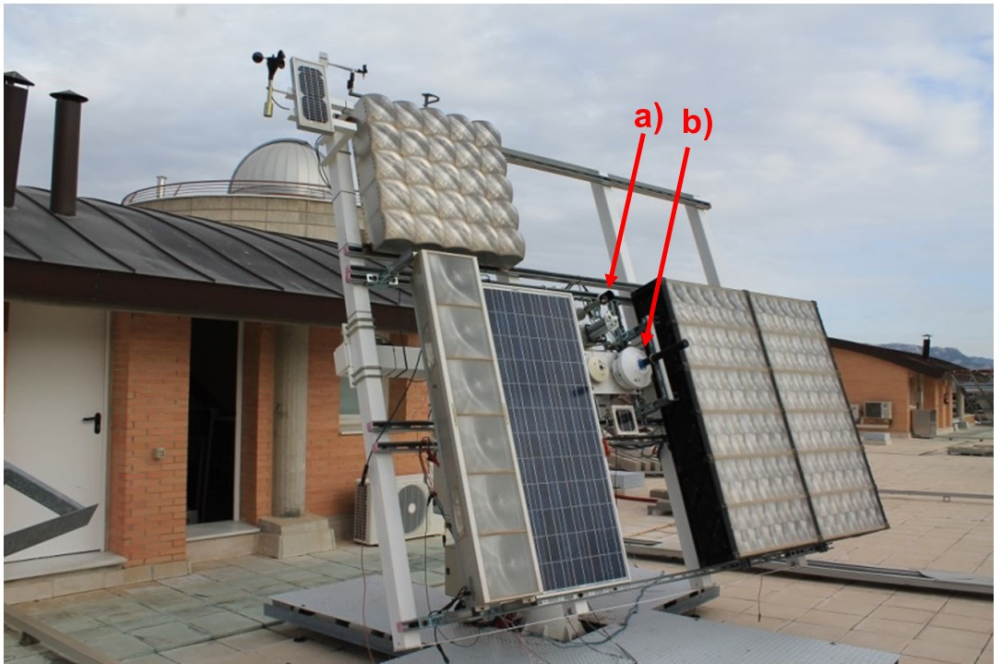


**Figure 1.** Pyrheliometer (**a**) and spectroradiometer with collimator tube (**b**) used in this work.

The specifications of the above instrumentation include a 10-nm spectral resolution, a wavelength interval of ≈3.3 nm between 350 and 1050 nm, and a temperature dependency of ±1% between −20 and +50 °C. The 12-month monitoring period extended from March 2013 to February 2014 at different time intervals. Observations were normally done every 20 s, but the interval had to be relaxed to 5 min during a few periods; this did not influence the results, as discussed in Section 2. The instruments were calibrated by the manufacturer

just before the experimental campaign and after it, in October 2014, with no significant change in sensitivity. Additionally, the broadband DNI was measured with a first-class Kipp & Zonen CHP 1 pyrheliometer. Spectral instances recorded while the broadband DNI was below 50 $W \cdot m^{-2}$ were excluded to avoid the noise introduced by a low signal. Neglecting these measured spectra does not affect the calculations to be presented in what follows because the annual DNI fraction collected below this threshold only accounts for ≈1% in Jaén [38]. After filtering of the data, 78,772 valid DNI spectra were available for further analysis.

As discussed earlier, the possible bijectivity between APE and spectral DNI for a given site was apparently investigated in only one study so far [34]. Thus, it is worth mentioning that the same spectroradiometer brand and model that was used in their work is also used here, thus making any comparison of results impervious to experimental differences. Their data filtering and its subsequent processing do not differ substantially from that presented in this paper either, except in a few aspects that will be described hereafter.

### 2.2. Average Photon Energy

Originally proposed by Jardine et al. [16] to qualitatively assess the shape of the spectral irradiance, APE is the average energy of the photons over a specific spectrum distribution. It may be expressed as follows:

$$\mathrm{APE} = \frac{\int_a^b E(\lambda)\mathrm{d}\lambda}{\int_a^b \Phi_{\mathrm{ph}}(\lambda)\mathrm{d}\lambda} \tag{1}$$

where $E(\lambda)$ in $W \cdot m^{-2} \cdot nm^{-1}$ is the spectral irradiance, $\Phi_{\mathrm{ph}}(\lambda)$ in $m^{-2} \cdot nm^{-1} \cdot s^{-1}$ is the spectral photon flux density, and $a$ in nm and $b$ in nm are the lower and upper limits, respectively, of the considered waveband of the solar spectrum. Solar spectra rich in photons with shorter wavelengths yield higher values of APE, whereas solar spectra rich in photons with longer wavelengths yield lower values of APE.

An equivalent definition was proposed later [35]:

$$\mathrm{APE} = hc(kq\lambda_{\mathrm{eff}})^{-1}, \tag{2}$$

where

$$\lambda_{\mathrm{eff}} = \frac{\int_a^b \lambda E(\lambda)\mathrm{d}\lambda}{\int_a^b E(\lambda)\mathrm{d}\lambda} \tag{3}$$

and where $\lambda_{\mathrm{eff}}$ is the "effective wavelength" in nm, $h$ is the Planck constant, $c$ is the speed of light in vacuum, $q$ is the electronic charge, and $k$ is a constant to reconcile units, equal here to $1 \times 10^{-9}$ for $\lambda_{\mathrm{eff}}$ expressed in nm. By using Equation (2), possible variations in APE are intuitively linked to varying incident irradiance spectral balances. Thus, blue-biased spectra are conducive to shorter effective wavelengths, which in turn lead to higher values of APE. Conversely, red-biased spectra—conducive to larger values of $\lambda_{\mathrm{eff}}$—lead to lower values of APE.

Obviously, the value of APE also depends on the considered spectral range. In this sense, the 350–1050 nm waveband (typically sensed by the silicon-based detectors used in many commercial spectroradiometers) has been used to calculate APE in many previous studies [16,19,32,34,40–44]. For that specific waveband, the values of APE for the AM1.5G and AM1.5D reference spectra equal 1.878 and 1.846 eV, respectively. The corresponding effective wavelengths are 662.6 and 671.7 nm, respectively. The slight red shift in the DNI spectrum compared to the GTI spectrum results from the latter's inclusion of diffuse irradiance, which is rich in blue wavelengths.

### 2.3. Methodology

As commented on in Section 1, the methodology initially proposed by Minemoto et al. [19] and followed by Chantana et al. [34], is applied as closely as possible in this investigation to assess whether a given APE value is *uniquely* linked to a specific DNI spectrum shape. However, as discussed in Section 1, such a methodology is improved here by adding a detailed analysis of variance, as argued by Nofuentes et al. [32]. In that study, the coefficient of variation (CV)—defined as the percentage ratio of the standard deviation (SD) to the mean—was shown to provide a better insight into the scatter around the mean than SD alone.

Based on previous experience, the design of the APE analysis procedure used in this work was articulated with the steps described below:

(1) The trapezoidal rule was used to calculate the broadband DNI between 350 and 1050 nm for each experimental direct spectrum. (That calculated DNI value was obviously smaller than the reading from the pyrheliometer, for which the spectral range was ≈290–4000 nm.)
(2) Equation (1) was used to calculate the APE for each DNI spectrum.
(3) The wavelength range was divided into fourteen 50-nm bands—from 350 to 1050 nm—for each spectral instance. The fractional contribution of each 50-nm spectral band to the broadband irradiance ($R_c$) calculated in step 1 was obtained.
(4) All the DNI spectral measurements were grouped into APE intervals of 0.02-eV width. More specifically, eight intervals ranging from 1.74–1.76 eV to 1.88–1.90 eV were considered. Spectral measurements having an APE within ±0.01 eV of the central value of each of these intervals were binned inside them.
(5) For every APE interval and within each 50-nm band, spectral measurements with $R_c$ values below the 10th percentile or above the 90th percentile were eliminated to minimize the influence of outliers.
(6) For every APE interval defined in step 4, mean values of $R_c$ (denoted $<R_c>$) were calculated in each 50-nm band. Values of SD and CV were also obtained for each of these bands to determine the dispersion of the values of $R_c$ around its mean value for every APE interval.

As mentioned in Section 1, it should be kept in mind that the analysis carried out by Chantana et al. [34] considered seventy-one 10-nm spectral bands into which the 350–1050 nm waveband was divided instead of the fourteen 50-nm bands considered here (step 3, above).

## 3. Results and Discussion

The recorded spectral instances that are outside the eight APE intervals stated in step 4 and removed according to step 5 of Section 2.2 account for less than 17% of the whole 12-month experimental database. After filtration, 65,881 spectral instances remained.

It is worth investigating to what extent the local spectral distribution for values of APE close to its standard value (1.846 eV) align with that of the standard spectrum when AM values are close to 1.5. Figure 2 shows the mean percentage contributions of every 50-nm band considered in this work relative to the integrated DNI for measured spectra in which APE and AM are within 1.84–1.86 eV and 1.45–1.55, respectively. The values of $R_c$ for each of the fourteen bands are shown for the reference spectrum as well. The latter seems to coincide reasonably well with local AM1.5D distributions. The fact that spectral DNI measurements with APE values in the vicinity of 1.85 eV closely resemble the distribution of the reference spectrum is according to expectations and confirms what was already noted by Chantana et al. [34] based on experimental measurements at Kusatsu, Japan. Nevertheless, a careful analysis shows that, despite being apparently small, the SD values obtained at both Jaén and Kusatsu are not negligible when compared to the $<R_c>$ values across the 50-nm band intervals used here—or 10-nm bands for the Japanese site—that lie outside the central wavelength range (450–900 nm). This dispersion of percentage contributions within the 350–450 nm and 900–1050 nm wavebands was also noted in local GTI spectral distributions for APE and AM around 1.88 eV and 1.5, respectively

(corresponding to the AM1.5G spectrum) for Jaén [32]. These two results are mutually consistent because the AM1.5G spectrum is essentially composed of direct irradiance (see, e.g., Figure 10 of [45]).

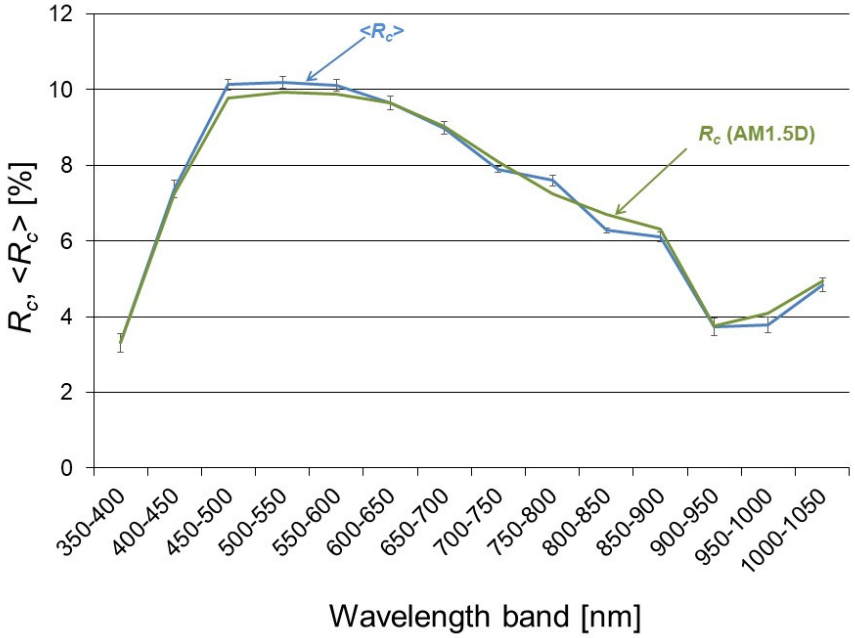


**Figure 2.** Mean percentage contributions to direct normal irradiance (DNI)—integrated from 350 to 1050 nm—across all 50-nm bands for spectral measurements with Average Photon Energy (APE) and air mass (AM) values of 1.85 ± 0.01 eV and 1.5 ± 0.05, respectively, recorded at Jaén (blue line): error bars indicate the standard deviation (SD) values related to each of these bands. The "reference" $R_c$ values calculated for each of these bands from the standard AM1.5D spectrum are also shown (green line).

The AM values corresponding to the spectral measurements recorded over the course of the 12-month experimental campaign spread over a large interval, 1.03–16.00; the calculated average AM is 2.19 and, hence, significantly above the standard 1.5 value. In parallel, the broadband DNI values obtained from the pyrheliometer range from 50 to 1047 W·m$^{-2}$ and average 715 W·m$^{-2}$, far lower than the 900 W·m$^{-2}$ standard value. This could be expected because DNI decreases rapidly when AM increases or when thin clouds partly obscure the sun's disc.

Figure 3 shows the values of <$R_c$> for every 50-nm band according to each APE bin into which the spectral measurements have been grouped. Higher values of APE imply shorter values of $\lambda_{eff}$ and, thus, higher relative contributions of shorter wavelengths relative to the integrated DNI within 50-nm bands. Conversely, values of <$R_c$> corresponding to 50-nm bands with longer wavelengths are enhanced as APE decreases (and $\lambda_{eff}$ increases). Interestingly, note that <$R_c$> tends to remain constant in the 600–650-nm spectral band, possibly because it corresponds to the "balance" wavelength for the 350–1050-nm spectrum, close to the effective wavelength of the AM1.5D standard spectrum. It is also worth noting that the results shown in Figure 3 are quite well aligned with those obtained by Chantana et al. [34] in their investigation of the purported one-to-one relationship between APE and the DNI spectrum in Kusatsu (see their Figure 5a).

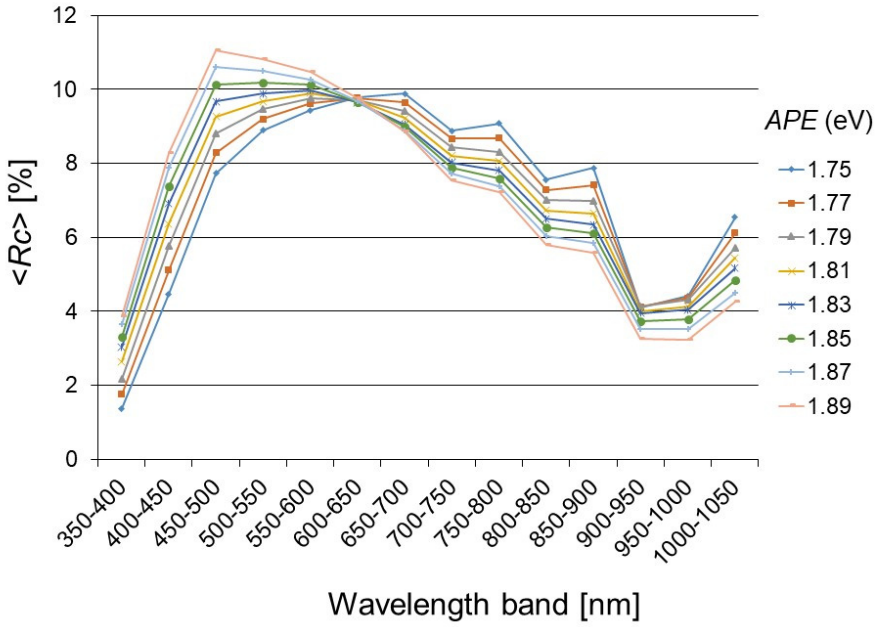


**Figure 3.** Mean values of relative contributions to DNI—integrated from 350 to 1050 nm—across all 50-nm bands for spectral measurements binned in 0.02-eV-width APE intervals over the range 1.75–1.89 eV (central values), using direct irradiance spectra recorded at Jaén.

Moreover, the results depicted in Figure 3 appear to be a good match for those obtained by Minemoto et al. [19] (also for Kusatsu), Norton et al. [31] (for Ispra and Golden, Colorado), Nofuentes et al. [32] (for Jaén and Madrid), and Tsuji et al. [33] for three Japanese cities: Kusatsu, Tsukuba, and Miyazaki. It should be kept in mind, though, that the work presented here is not strictly comparable with these studies, as they were carried out to elucidate the possible bijectivity between APE and either the GTI or GHI spectral distribution.

Table 1 provides details about the distribution of the spectral measurements binned by their corresponding APE interval. For each of these APE intervals, Table 1 also indicates the corresponding effective wavelength, in conjunction with the maximum, minimum, and mean SD values related to the relative contribution to the integrated 350–1050-nm DNI across the fourteen 50-nm bands under scrutiny. Note that only three APE bands ($1.79 \pm 0.01$ eV, $1.81 \pm 0.01$ eV, and $1.83 \pm 0.01$ eV) account for 80% of the spectral instances recorded. Moreover, only less than 1% of the spectral measurements are grouped in bins with APE greater than 1.85 eV, which indicates prevailing red-shifted spectra for the site under investigation. As expected from fundamentals of statistics, the scatter around the mean is larger in APE intervals with fewer samples. In spite of this, the maximum values of SD stay below 0.40%. In comparison, the SD values obtained by Chantana et al. [34] at Kusatsu across all the seventy-one 10-nm bands within the 350–1050 nm spectral range do not exceed 0.20%. Remarkably, SD peaks in the same wavebands (350–400 nm and 900–950 nm) at Kusatsu and Jaén, which deserves scrutiny.

As discussed before [32], SD alone is not enough to suitably assess the dispersion of $R_c$ around its mean for each APE interval across the 350–1050 nm range. Instead, CV is a more meaningful parameter intended for such purpose.

Figure 4 shows the CV values obtained for each 50-nm band grouping defined above. Within the 450–900-nm waveband, CV stays below ≈3.5% in contrast with the 900–1050-nm waveband, where CV is found to reach much larger values, close to 10%. Higher spikes even occur in the 350–450-nm waveband, where CV reaches up to 13%.

**Table 1.** Maximum, minimum, and mean values of SD of $R_c$ for every 50-nm band according to their APE interval and corresponding effective wavelength, $\lambda_{eff}$.

| Central Value of APE Interval (eV) | $\lambda_{eff}$ for the Central Value of APE Interval (nm) | $SD_{max}$ (%) | $SD_{min}$ (%) | $SD_{med}$ (%) | Number of Samples | Waveband where $SD_{max}$ Occurs (nm) | Waveband where $SD_{min}$ Occurs (nm) |
|---|---|---|---|---|---|---|---|
| 1.75 | 709 | 0.39 | 0.09 | 0.21 | 4123 | 900–950 | 800–850 |
| 1.77 | 701 | 0.38 | 0.09 | 0.20 | 7195 | 900–950 | 800–850 |
| 1.79 | 693 | 0.36 | 0.08 | 0.19 | 13,962 | 900–950 | 800–850 |
| 1.81 | 685 | 0.26 | 0.08 | 0.15 | 21,116 | 900–950 | 800–850 |
| 1.83 | 678 | 0.21 | 0.06 | 0.12 | 17,727 | 900–950 | 800–850 |
| 1.85 | 670 | 0.25 | 0.07 | 0.17 | 1317 | 350–400 | 800–850 |
| 1.87 | 663 | 0.35 | 0.07 | 0.19 | 338 | 350–400 | 800–850 |
| 1.89 | 656 | 0.31 | 0.09 | 0.19 | 103 | 350–400 | 800–850 |

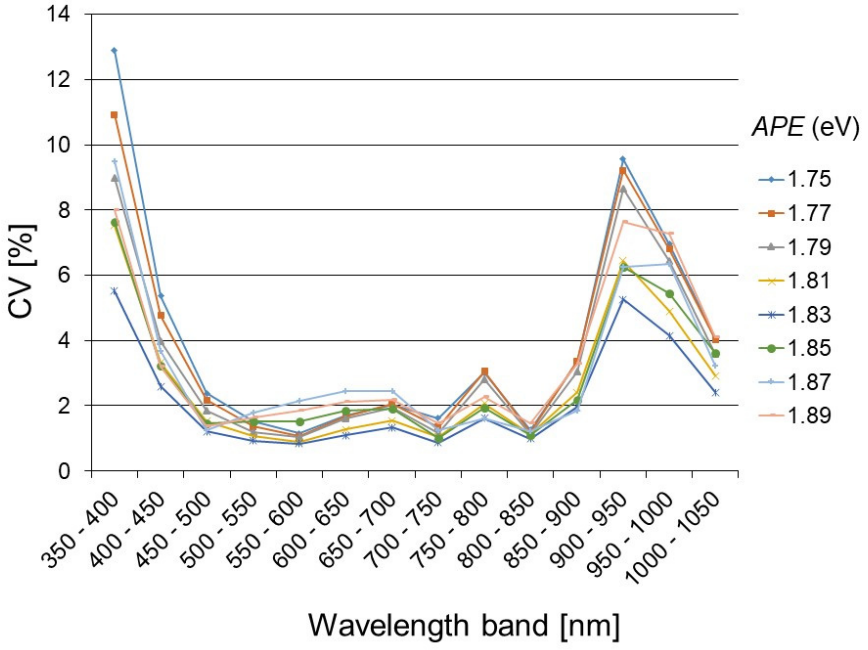


**Figure 4.** Coefficient of variation of $R_c$ across all 50-nm bands for spectral measurements binned in 0.02-eV width APE intervals over the range 1.75–1.89 eV (central values), using experimental spectral measurements at Jaén.

In practical terms, such results suggest that APE can be assumed to *uniquely* represent the shape of the direct spectrum within the central 450–900-nm wavelength range *only*. Following an identical procedure to that described in Section 2.2, Nofuentes et al. [32] came to the same conclusion for Jaén and Madrid regarding the purported one-to-one relationship between APE and spectral GTI. The present confirmation of the findings in [32] is likely related to the similarity between the GTI and DNI spectra under cloudless conditions, as mentioned above. Interestingly, CV values up to 6% and over 30% within the 350–400 nm and 900–1050 nm wavebands, respectively, were found in Japan [33]. However, despite the fact that such high CV values indicate a large scatter of $R_c$ around its mean, Tsuji et al. [33] claimed that APE is a unique characteristic of the GTI spectrum distribution. In any case, the results depicted in Figure 4 deserve some further discussion from both the experimental and theoretical standpoints.

The expanded uncertainties ($U_{95}$) for the spectral measurements obtained with the present spectroradiometer used are ±10.89%, ±4.13%, and ±4.06% for the 350–450 nm, 450–900 nm, and 900–1050 nm wavebands, respectively, according to the certificate of calibration issued by the manufacturer. No significant additional uncertainty resulting from actual outdoor laboratory measurement conditions is likely because the instrument was cleaned each working day. It was, however, not cleaned during a week in March 2013 and another week in August 2013. Given the relative short periods of time during which the instrument remained uncleaned, no significant differences were found between spectral data collected in such periods relative to those gleaned over the course of the entire experimental campaign.

The dispersion noticed for $R_c$ below 450 nm and the resulting higher values of CV may be explained in part by the higher values of $U_{95}$ at these shorter wavelengths. As discussed previously [32], however, another contribution is likely related to the substantial daily variance in AOD, which has a large impact on the direct spectrum at short wavelengths [46]. In contrast, the lowest $U_{95}$ values occur above 900 nm, where CV also peaks. This would seem paradoxical if $U_{95}$ was the only driver of CV variations along the spectrum, which thus requires scrutiny. As mentioned by Nofuentes et al. [32], it should be borne in mind that the instrument undergoes calibration indoors in a laboratory at a constant ambient temperature (25 °C), thus avoiding the potential impact of large temperature excursions

during sunny days. Those field conditions could influence the reading accuracy in the NIR part of the spectrum much more than at shorter wavelengths [47,48]. This temperature effect should be small here, however, because the detector core of this specific instrument is temperature controlled and has a specified temperature range of −10 to 50 °C. A more likely explanation for the high CV in the NIR is that the spectral irradiance is weak there due to water vapor absorption. Therefore, measurements in that band are more vulnerable to the influence of noise, which increases the actual measurement uncertainty. Moreover, water vapor conditions (characterized by PW) are variable on a daily basis over Jaén, which creates strong variance in the 900–950 nm waveband, where water vapor absorption is the strongest relative to the whole 350–1050 nm range.

The results shown in Figure 4 confirm previous theoretical findings obtained by means of synthetic spectra generated by the SMARTS radiation model for various ideal atmospheric conditions [35]. Both modeled and experimental spectra obtained under variable conditions show that AM and AOD influence APE in a way that longer wavelengths are enhanced when they increase (red shift). On the other hand, PW has a more limited but antagonistic effect (blue shift). Hence, different sets of conditions (AM, AOD, and PW) could lead to dissimilar spectral distributions of DNI that would exhibit the same value of APE. As a result, Gueymard [35] concluded that APE was not appropriate to characterize the DNI spectral shape with a single number. The present results tend to confirm that finding.

## 4. Conclusions

This study investigated whether the average photon energy (APE) uniquely represents the direct normal irradiance (DNI) spectrum over the 350–1050 nm band at Jaén, a Spanish sunny site with Mediterranean-Continental climate. No previous study focusing on the application of APE to the direct spectrum is known except at a Japanese location in a different climate.

The methodology used here is based on a procedure that was previously applied to assess the possible bijectivity between APE and the global tilted irradiance (GTI) spectrum at both Jaén and Madrid. This procedure centers on the analysis of the coefficient of variation (CV) of the relative importance of contributions of 50-nm bands compared to the integrated DNI (from 350 to 1050 nm) of the spectral distributions binned in specific APE intervals.

DNI spectra from 350 to 1050 nm were collected over the course of a 12-month experimental campaign. Over the range 450–900 nm, spectral distributions obtained for an APE of ≈1.85 eV and air mass (AM) of ≈1.5 match quite well that of the standard AM1.5D spectrum used as reference in concentrating photovoltaic applications. Nevertheless, some scatter is noticed outside of this central band. Likewise, spectral distributions corresponding to measurements binned in the same APE interval are well aligned within 450–900 nm, where CV remains below ≈3.5%. In contrast, this concordance does not hold outside of that spectral range, considering that CV reaches values of up to ≈10% and 13% within 350–450 nm and 900–1050 nm, respectively. This significant scatter at shorter wavelengths is only partially ascribed to the measurement uncertainty of the spectroradiometer reported by the manufacturer, which is relatively large below 450 nm. Theoretical considerations reveal that another explanation for the high CV there is related to the temporal variance in aerosol optical depth, which is significant at Jaen, and results in a more or less pronounced red shift in the spectrum. In contrast, the measuring uncertainty is far smaller beyond 900 nm, but steep temperature excursions during the day may influence measurements. Additionally, weak signal levels around the water vapor absorption band (940 nm) are especially vulnerable to noise, thus conducing an increased uncertainty related to the measurements in such band. Temporal variance in atmospheric precipitable water also induces a more or less significant blue shift of the spectrum.

From a theoretical standpoint, the results presented here confirm previous radiative transfer simulations that rejected the APE bijectivity by showing how a single APE value

could be obtained by combining different values of air mass, aerosol optical depth, and precipitable water, thus shaping significantly different DNI spectral distributions.

To summarize, the results presented in this study disprove the currently assumed one-to-one relationship between APE and the spectral DNI within the *whole* 350–1050 nm waveband. Rather, APE may only be assumed to uniquely characterize the DNI spectrum distribution *only* from ≈450 to 900 nm for Jaén in practical terms. Hence, this limited band is recommended when using APE to model the spectral impact on concentrating PV devices. The present findings confirm those from a previous work that focused rather on the GTI spectrum, which is the reference for flat-plate PV applications. The present conclusion that bijectivity is valid over only a part of the DNI spectrum presumably holds for sites with a similar climate as Jaén, although further verification is needed. Hence, further collection and analysis of spectrally resolved DNI data are desirable at more sites worldwide to better evaluate the impact of local climate, since this type of experimental methodology has been done so far at only two sites in relatively temperate climates, which do not allow drawing general conclusions on a worldwide basis.

**Author Contributions:** Conceptualization, methodology, and writing—review and editing, G.N.; conceptualization, methodology, supervision, and writing—review and editing, C.A.G.; software and data curation, J.A.C.; software, G.M.-N.; funding acquisition, project administration, and supervision, J.A. All authors have read and agreed to the published version of the manuscript.

**Funding:** This research was funded by the Spanish Science and Innovation Ministry (*Ministerio de Ciencia e Innovación de España*) and the ERDF, grant number ENE2009-08302, within the frame of the Project "Analysis and characterization of a concentrated PV system under natural sunlight. Comparison with other PV technologies" (*Análisis y caracterización de un sistema fotovoltaico de concentración a sol real. Comparativa con otras tecnologías fotovoltaicas*). This work was also funded by the Department of Science and Innovation of the Regional Government of Andalucía (*Consejería de Innovación, Ciencia y Empresa de la Junta de Andalucía*), grant number P09-TEP-5045, within the frame of the Project "Analysis and characterization of a concentrated PV system under natural sunlight. Comparison with other PV technologies" ("*Análisis y caracterización de un sistema fotovoltaico de concentración a sol real. Comparativa con otras tecnologías fotovoltaicas*").

**Institutional Review Board Statement:** Not applicable.

**Informed Consent Statement:** Not applicable.

**Data Availability Statement:** Not applicable.

**Acknowledgments:** Guilherme Marques-Neves acknowledges the Brazilian National Council for Scientific and Technological Development (CNPq) for granting a scholarship to support his stay at the University of Jaén. The authors greatly acknowledge the technical support of Beatriz García-Domingo and Miguel Torres Ramírez during the experimental campaign.

**Conflicts of Interest:** The authors declare no conflict of interest. The funders had no role in the design of the study; in the collection, analyses, or interpretation of data; in the writing of the manuscript; or in the decision to publish the results.

## Abbreviations

*Terminology*

| | |
|---|---|
| DNI | Direct normal irradiance |
| GHI | Global horizontal irradiance |
| GTI | Global tilted irradiance |
| IEC | International Electrotechnical Commission |
| PV | Photovoltaic(s) |
| SMARTS | Simple Model of the Atmospheric Radiative Transfer of Sunshine |

***Symbols***

| | |
|---|---|
| $a$ | Lower wavelength limit of an interval of the spectrum (nm) |
| AM | Air mass |
| APE | Average photon energy (eV) |
| AOD | Aerosol optical depth at any wavelength |
| $b$ | Upper wavelength limit of an interval of the spectrum (nm) |
| BF | Blue fraction |
| CV | Coefficient of variation (%) |
| $E(\lambda)$ | Spectral Irradiance of the actual solar spectrum ($W \cdot m^{-2} \cdot nm^{-1}$) |
| MM | Spectral mismatch factor |
| PW | Precipitable water (cm) |
| $R_c$ | Percentage contribution of a spectral band of a recorded spectral (%) measurement to the broadband irradiance |
| SD | Standard deviation of $R_c$ for every 50-nm band and the same APE interval (%) |
| $SD_{max}$ | Maximum value of standard deviation of $R_c$ for every 50-nm band and the same APE interval (%) |
| $SD_{mean}$ | Average value of standard deviation of $R_c$ for every 50-nm band and the same APE interval (%) |
| $SD_{min}$ | Minimum value of standard deviation of $R_c$ for every 50-nm band and (%) the same APE interval |
| $U_{95}$ | Expanded uncertainty related to spectral measurements (%) |
| UF | Useful fraction |
| $\Phi_{ph}(\lambda)$ | Spectral Photon Flux Density ($m^{-2} \cdot nm^{-1} \cdot s^{-1}$) |
| $\lambda_{eff}$ | Effective wavelength (nm) |

## References


1. IEC 61724-1. *Photovoltaic System Performance—Part 1: Monitoring*; International Electrotechnical Commission (IEC): Geneva, Switzerland, 2017.
2. Leloux, J.; Lorenzo, E.; García-Domingo, B.; Aguilera, J.; Gueymard, C.A. A Bankable Method of Assessing the Performance of a CPV Plant. *Appl. Energy* **2014**, *118*, 1–11. [CrossRef]
3. De la Parra, I.; Muñoz, M.; Lorenzo, E.; García, M.; Marcos, J.; Martínez-Moreno, F. PV Performance Modelling: A Review in the Light of Quality Assurance for Large PV Plants. *Renew. Sustain. Energy Rev.* **2017**, *78*, 780–797. [CrossRef]
4. Duck, B.C.; Fell, C.J. Improving the Spectral Correction Function. In Proceedings of the 43rd IEEE Photovoltaic Specialists Conference (PVSC), Portland, OR, USA, 5–10 June 2016; pp. 2647–2652. [CrossRef]
5. Pierro, M.; Bucci, F.; Cornaro, C. Full Characterization of Photovoltaic Modules in Real Operating Conditions: Theoretical Model, Measurement Method and Results. *Prog. Photovolt. Res. Appl.* **2015**, *23*, 443–461. [CrossRef]
6. Shanks, K.; Senthilarasu, S.; Mallick, T.K. High-Concentration Optics for Photovoltaic Applications. In *High Concentrator Photovoltaics. Fundamentals, Engineering and Power Plants*; Pérez-Higueras, P.J., Fernández, E.F., Eds.; Springer International Publishing: Geneva, Switzerland, 2015; pp. 85–114. [CrossRef]
7. Fernández, E.F.; Soria-Moya, A.; Almonacid, F.; Aguilera, J. Comparative Assessment of the Spectral Impact on the Energy Yield of High Concentrator and Conventional Photovoltaic Technology. *Sol. Energy Mater. Sol. Cells* **2016**, *147*, 185–197. [CrossRef]
8. Rodrigo, P.M.; Fernández, E.F.; Almonacid, F.M.; Pérez-Higueras, P.J. Quantification of the Spectral Coupling of Atmosphere and Photovoltaic System Performance: Indexes, Methods and Impact on Energy Harvesting. *Sol. Energy Mater. Sol. Cells* **2017**, *163*, 73–90. [CrossRef]
9. IEC 60904-7. *Photovoltaic Devices—Part 7: Computation of the Spectral Mismatch Correction for Measurements of Photovoltaic Devices*; International Electrotechnical Commission (IEC): Geneva, Switzerland, 2008.
10. Betts, T.R.; Infield, D.G.; Gottschalg, R. Spectral Irradiance Correction for PV System Yield Calculations. In Proceedings of the 19th European Photovoltaic Solar Energy Conference, Paris, France, 7–11 June 2004; pp. 2533–2536.
11. Hofmann, M.; Vanicek, P.; Haselbuhn, R. Is the Average Photon Energy (APE) a Suitable Measure to Describe the Uniqueness of Solar Spectra? In Proceedings of the 29th European Photovoltaic Solar Energy Conference and Exhibition, Paris, France, 22–26 September 2014; pp. 3461–3466.
12. Dirnberger, D.; Blackburn, G.; Müller, B.; Reise, C. On the Impact of Solar Spectral Irradiance on the Yield of Different PV Technologies. *Sol. Energy Mater. Sol. Cells* **2015**, *132*, 431–442. [CrossRef]
13. Peharz, G.; Siefer, G.; Bett, A.W. A Simple Method for Quantifying Spectral Impacts on Multi-Junction Solar Cells. *Sol. Energy* **2009**, *83*, 1588–1598. [CrossRef]
14. Fernández, E.F.; Almonacid, F. Spectrally Corrected Direct Normal Irradiance Based on Artificial Neural Networks for High Concentrator Photovoltaic Applications. *Energy* **2014**, *74*, 941–949. [CrossRef]

15. Sutterlueti, J.; Ransome, S.; Kravets, R.; Schreier, L. Characterising PV Modules under Outdoor Conditions: What's Most Important for Energy Yield. In Proceedings of the 26th European Photovoltaic Solar Energy Conference and Exhibition, Hamburg, Germany, 5–11 September 2011.
16. Jardine, C.N.; Betts, T.R.; Gottschalg, R.; Infield, D.G.; Lane, K. Influence of Spectral Effects on the Performance of Multi-junction Amorphous. In Proceedings of the Photovoltaic in Europe—From PV Technology to Energy Solutions, Rome, Italy, 7–11 October 2002.
17. Louwen, A.; de Waal, A.C.; van Sark, W.G. Evaluation of Different Indicators for Representing Solar Spectral Variation. In Proceedings of the 43rd IEEE Photovoltaic Specialists Conference (PVSC), Portland, OR, USA, 5–10 June 2016; pp. 133–137. [CrossRef]
18. Paudyal, B.R.; Imenes, A.G. Analysis of Spectral Irradiance Distribution for PV Applications at High Latitude. In Proceedings of the 47th IEEE Photovoltaic Specialists Conference (PVSC), Calgary, OR, Canada, 15 June–21 August 2020; pp. 1834–1841. [CrossRef]
19. Minemoto, T.; Nakada, Y.; Takahashi, H.; Takakura, H. Uniqueness Verification of Solar Spectrum Index of Average Photon Energy for Evaluating Outdoor Performance of Photovoltaic Modules. *Sol. Energy* **2009**, *83*, 1294–1299. [CrossRef]
20. IEC 60904-9. *Photovoltaic Devices—Part 9: Solar Simulator Performance Requirements*; International Electrotechnical Commission (IEC): Geneva, Switzerland, 2007.
21. Gottschalg, R.; Betts, T.R.; Infield, D.G.; Kearney, M.J. Experimental Investigation of Spectral Effects on Amorphous Silicon Solar Cells in Outdoor Operation. In Proceedings of the Conference Record of the 29th IEEE Photovoltaic Specialists Conference, New Orleans, LA, USA, 19–24 May 2002; pp. 1138–1141. [CrossRef]
22. Gottschalg, R.; Betts, T.R.; Infield, D.G.; Kearney, M.J. On the Importance of Considering the Incident Spectrum When Measuring the Outdoor Performance of Amorphous Silicon Photovoltaic Devices. *Meas. Sci. Technol.* **2004**, *15*, 460. [CrossRef]
23. Gottschalg, R.; Betts, T.R.; Infield, D.G.; Kearney, M.J. The Effect of Spectral Variations on the Performance Parameters of Single and Double Junction Amorphous Silicon Solar Cells. *Sol. Energy Mater. Sol. Cells* **2005**, *85*, 415–428. [CrossRef]
24. Takahashi, H.; Fukushige, S.; Minemoto, T.; Takakura, H. Output Estimation of Si-Based Photovoltaic Modules with Outdoor Environment and Output Map. *J. Cryst. Growth* **2009**, *311*, 749–752. [CrossRef]
25. Minemoto, T.; Takahashi, H.; Nakada, Y.; Takakura, H. Outdoor Performance Evaluation of Photovoltaic Modules Using Contour Plots. *Curr. Appl. Phys.* **2010**, *10*, S257–S260. [CrossRef]
26. Nofuentes, G.; de la Casa, J.; Torres-Ramírez, M.; Alonso-Abella, M. Solar Spectral and Module Temperature Influence on the Outdoor Performance of Thin Film PV Modules Deployed on a Sunny Inland Site. *Int. J. Photoenergy* **2013**, *2013*. [CrossRef]
27. Yoshida, S.; Ueno, S.; Kataoka, N.; Takakura, H.; Minemoto, T. Estimation of Global Tilted Irradiance and Output Energy Using Meteorological Data and Performance of Photovoltaic Modules. *Sol. Energy* **2013**, *93*, 90–99. [CrossRef]
28. Cornaro, C.; Andreotti, A. Influence of Average Photon Energy Index on Solar Irradiance Characteristics and Outdoor Performance of Photovoltaic Modules. *Prog. Photovolt. Res. Appl.* **2013**, *21*, 996–1003. [CrossRef]
29. Sirisamphanwong, C.; Sirisamphanwong, C.; Ketjoy, N. The Effect of Average Photon Energy and Module Temperature on Performance of Photovoltaic Module under Thailand's Climate Condition. *Energy Procedia* **2014**, *56*, 359–366. [CrossRef]
30. Chantana, J.; Imai, Y.; Kawano, Y.; Hishikawa, Y.; Nishioka, K.; Minemoto, T. Impact of Average Photon Energy on Spectral Gain and Loss of Various-Type PV Technologies at Different Locations. *Renew. Energy* **2020**, *145*, 1317–1324. [CrossRef]
31. Norton, M.; Amillo, A.M.G.; Galleano, R. Comparison of Solar Spectral Irradiance Measurements Using the Average Photon Energy Parameter. *Sol. Energy* **2015**, *120*, 337–344. [CrossRef]
32. Nofuentes, G.; Gueymard, C.A.; Aguilera, J.; Pérez-Godoy, M.D.; Charte, F. Is the Average Photon Energy a Unique Characteristic of the Spectral Distribution of Global Irradiance? *Sol. Energy* **2017**, *149*, 32–43. [CrossRef]
33. Tsuji, M.; Rahman, M.M.; Hishikawa, Y.; Nishioka, K.; Minemoto, T. Uniqueness Verification of Solar Spectrum Obtained from Three Sites in Japan Based on Similar Index of Average Photon Energy. *Sol. Energy* **2018**, *173*, 89–96. [CrossRef]
34. Chantana, J.; Ueno, S.; Ota, Y.; Nishioka, K.; Minemoto, T. Uniqueness Verification of Direct Solar Spectral Index for Estimating Outdoor Performance of Concentrator Photovoltaic Systems. *Renew. Energy* **2015**, *75*, 762–766. [CrossRef]
35. Gueymard, C.A. Daily Spectral Effects on Concentrating PV Solar Cells as Affected by Realistic Aerosol Optical Depth and Other Atmospheric Conditions. In Proceedings of the SPIE Optical Modeling and Measurements for Solar Energy Systems III, San Diego, CA, USA, 2–4 August 2009. [CrossRef]
36. Gueymard, C.A. The SMARTS Spectral Irradiance Model after 25 Years: New Developments and Validation of Reference Spectra. *Sol. Energy* **2019**, *187*, 233–253. [CrossRef]
37. Alonso-Abella, M.; Chenlo, F.; Nofuentes, G.; Torres-Ramírez, M. Analysis of Spectral Effects on the Energy Yield of Different PV (Photovoltaic) Technologies: The Case of Four Specific Sites. *Energy* **2014**, *67*, 435–443. [CrossRef]
38. García-Domingo, B.; Aguilera, J.; de la Casa, J.; Fuentes, M. Modelling the Influence of Atmospheric Conditions on the Outdoor Real Performance of a CPV (Concentrated Photovoltaic) Module. *Energy* **2014**, *70*, 239–250. [CrossRef]
39. García, R.; Torres-Ramírez, M.; Muñoz-Cerón, E.; de la Casa, J.; Aguilera, J. Spectral Characterization of the Solar Resource of a Sunny Inland Site for Flat Plate and Concentrating PV Systems. *Renew. Energy* **2017**, *101*, 1169–1179. [CrossRef]
40. Nofuentes, G.; García-Domingo, B.; Muñoz, J.V.; Chenlo, F. Analysis of the Dependence of the Spectral Factor of Some PV Technologies on the Solar Spectrum Distribution. *Appl. Energy* **2014**, *113*, 302–309. [CrossRef]

41. Ye, J.Y.; Reindl, T.; Aberle, A.G.; Walsh, T.M. Effect of Solar Spectrum on the Performance of Various Thin-Film PV Module Technologies in Tropical Singapore. *IEEE J. Photovolt.* **2014**, *4*, 1268–1274. [CrossRef]
42. Nofuentes, G.; de la Casa, J.; Solís-Alemán, E.M.; Fernández, E.F. Spectral Impact on PV Performance in Mid-Latitude Sunny Inland Sites: Experimental vs. Modelled Results. *Energy* **2017**, *141*, 1857–1868. [CrossRef]
43. Neves, G.; Vilela, W.; Pereira, E.; Yamasoe, M.; Nofuentes, G. Spectral Impact on PV in Low-Latitude Sites: The Case of Southeastern Brazil. *Renew. Energy* **2021**, *164*, 1306–1319. [CrossRef]
44. Polo, J.; Alonso-Abella, M.; Ruiz-Arias, J.A.; Balenzategui, J.L. Worldwide Analysis of Spectral Factors for Seven Photovoltaic Technologies. *Sol. Energy* **2017**, *142*, 194–203. [CrossRef]
45. Gueymard, C.A.; Myers, D.; Emery, K. Proposed Reference Irradiance Spectra for Solar Energy Systems Testing. *Sol. Energy* **2002**, *73*, 443–467. [CrossRef]
46. Gueymard, C.A. Interdisciplinary Applications of a Versatile Spectral Solar Irradiance Model: A Review. *Energy* **2005**, *30*, 1551–1576. [CrossRef]
47. Myers, D.R. Estimates of Uncertainty for Measured Spectra in the SERI Spectral Solar Radiation Data Base. *Sol. Energy* **1989**, *43*, 347–353. [CrossRef]
48. Schubert, F.; Klameth, K.; Darou, S.; Spinner, D. Measurement Uncertainties of a Compact Array Spectrometer. *Energy Procedia* **2015**, *77*, 179–186. [CrossRef]

Micheli, L.; Caballero, J.A.; Fernández, E.F.; Smestad, G.P.; Nofuentes, G.; Mallik, T.K. Correllating Photovoltaic Soiling Losses to Waveband and Single-Value Transmittance Measurements. Energy 2019, 180, 376-386*;*

https://doi.org/10.1016/j.energy.2019.05.097

**Estado:** Publicado

**Factor de Impacto (JCR Science Edition 2019)**: 6,082

**Categorías científicas y posición dentro de las mismas (JCR Science Edition 2019):** 3/61 (Q1) en “Thermodynamics”; 20/112 (Q1) en “Energy and fuels”.

Energy 180 (2019) 376–386

Contents lists available at ScienceDirect

Energy

journal homepage: www.elsevier.com/locate/energy

# Correlating photovoltaic soiling losses to waveband and single-value transmittance measurements

Leonardo Micheli [a, b, *], Jose A. Caballero [b], Eduardo F. Fernandez [b, **], Greg P. Smestad [c], Gustavo Nofuentes [b], Tapas K. Mallick [d], Florencia Almonacid [b]

[a] National Renewable Energy Laboratory, Golden, CO, USA
[b] Centro de Estudios Avanzados en Energía y Medio Ambiente (CEAEMA), University of Jaén, Jaén, Spain
[c] Sol Ideas Technology Development, San José, CA, USA
[d] University of Exeter, Penryn, UK

ARTICLE INFO

*Article history:*
Received 20 September 2018
Received in revised form
29 April 2019
Accepted 13 May 2019
Available online 16 May 2019

*Keywords:*
Soiling
Photovoltaic
Reliability
Spectral losses
Optical transmittance

ABSTRACT

This paper presents the results of an investigation on the spectral losses of photovoltaic (PV) soiling. The transmittance of a glass coupon exposed to natural soiling outdoors in Jaén, southern Spain, has been measured weekly and used to estimate the soiling losses that various types of photovoltaic materials would experience if installed in the same location. The results suggest that measuring the hemispherical transmittance of the soiling accumulated on a PV glass coupon can give enough information to quantify the impact of soiling on energy production. Each PV technology is found to have a preferred spectral region, or a specific single wavelength, for which the transmittance through a PV glass coupon could be used for the best estimation of soiling losses. Overall, considering the average spectral transmittance between the extreme wavelengths of the material-specific absorption band, or the transmittance of soiling at a single wavelength between 500 and 600 nm yields the best estimations for different PV technologies. The results of this work can lead to innovative approaches to detect soiling in the field and to estimate the impact of spectral changes induced by soiling on PV energy production.


## 1. Introduction

The accumulation of dust, particles, and dirt on the surface of photovoltaic (PV) modules reduces the intensity of the light transmitted through the cover glass—and, therefore, the amount of energy generated by the solar cells. This issue, known as *soiling*, affects PV systems worldwide, causing power losses as high as 70% in the worst scenarios [1]. These losses are due to the drop in optical transmittance, because soiling absorbs part of the incoming sunlight and increases the fraction of reflected light. Soiling can be mitigated by cleaning the PV modules when the energy losses are higher than the cleaning costs. This means that an accurate soiling monitoring system is required to properly address this issue, thereby increasing the energy yield while minimizing the operating and maintenance cost.

It is important to highlight that, along with the broadband reduction in irradiance, soiling also changes the spectrum of the transmitted light, causing larger transmittance drops in the blue region, meaning that PV technologies with different bandgaps can be differently affected by soiling [2–5]. Hence, measuring and analyzing soiling should not disregard the spectral effects that soiling can have on various PV technologies; but determining the spectral component of soiling on fielded PV modules is still challenging.

The current soiling monitoring technologies calculate losses by comparing the performance of a soiled device with the performance of a device that has been kept clean throughout the time period. This means that they can calculate losses occurring for only a single PV technology, unless multiple soiled devices are employed. Different and more affordable solutions are required to estimate the impact of soiling on the various PV technologies. Therefore, it is essential to investigate the correlations connected to the spectral nature of natural soiling, the irradiance spectra, and the

* Corresponding author. Centro de Estudios Avanzados en Energía y Medio Ambiente (CEAEMA), University of Jaén, Jaén, Spain.
** Corresponding author. Centro de Estudios Avanzados en Energía y Medio Ambiente (CEAEMA), University of Jaén, Jaén, Spain.
*E-mail addresses:* lmicheli@ujaen.es (L. Micheli), eduardo.fernandez@ujaen.es (E.F. Fernandez).

https://doi.org/10.1016/j.energy.2019.05.097
0360-5442/

**Abbreviations**

| | |
|---|---|
| $A_{PV}$ | active area of the photovoltaic device |
| a-Si | amorphous silicon |
| AST | average soiling transmittance |
| CdTe | cadmium telluride |
| CIGS | copper indium gallium diselenide |
| $E_G$ | spectral distribution of irradiance on the photovoltaic surface |
| Isc | short-circuit current |
| MAPE | mean absolute percentage error |
| MPE | mean percentage error |
| m-Si | monocrystalline silicon |
| NIR | near infrared |
| p-Si | polycristalline silicon |
| $R^2$ | coefficient of determination |
| $r_s$ | soiling ratio |
| SR | spectral response of the unsoiled PV module |
| UV | ultra-violet |
| VIS | visible |
| $\tau$ | hemispherical spectral transmittance |

soiling losses through extended experimental campaigns.

In light of the above, the scope of this work is to analyze the spectral components of the soiling losses, and to investigate the impact of soiling on the various wavelengths of the irradiance spectrum and on the various PV technologies. This study shows how transmittance measurements can be used to estimate the soiling losses of PV modules and also how a single wavelength measurement can be used to estimate the soiling losses of various PV technologies. The results of this work are expected to contribute identifying innovative solutions and metrics to measure the soiling ratio of any PV technology, lowering the cost of soiling monitoring and limiting its impact on the PV cost competiveness.

## 2. Background

Soiling is the result of the interaction of a number of environmental factors [6–12]. Typically, the soiling of a PV system is monitored by using soiling stations, where the electrical output of a soiled PV device (*soiled device*) is compared with the output of the PV device under clean conditions (*control device*). Generally, two PV cells or modules are employed: one of them is regularly cleaned (*control device*), whereas the second is left to soil naturally (*soiled device*) [13]. Despite the simple approach, these stations require regular cleanings, which might be expensive to perform, in order to limit the uncertainty of the measurement, as the error associated with stations that are not well maintained can be as high as the soiling loss [14].

In order to eliminate the requirement for washing a reference device and to lower the cost of soiling monitoring, new soiling detection technologies have been recently developed. A first product, called DustIQ and developed by Kipp&Zonen, uses a photodiode to measure the backward reflection of a soiled PV glass, mounted next to or within a PV array [15]. A second product, named MARS and developed by Atonometrics, uses a camera to analyze the impact of soiling on a soiled PV glass, by measuring the brightness of the pixels in the camera's field of view [16]. These two products do not require any cleaning, and measure the soiling accumulated on PV glass to estimate the soiling losses occurring on similarly mounted PV modules located nearby. In other geometries, in contrast, only one PV cell is used as both the soiled and the control device [17]. In this case, a cover glass is placed on top of the cell to collect soiling and is removed only to take the control device measurement.

Along with their dependence on the broadband irradiance, the performance of PV systems have also a dependence on the spectral content of the sunlight, as well as on the specific spectral absorption band of the technology [18]. Soiling has also an effect on the spectrum of the irradiance hitting the semi-conductive material and therefore its impact varies depending on the irradiance spectrum and on the spectral response of the PV technology. Despite that, none of the current soiling monitoring technologies is able to estimate the spectral component of the soiling losses and, therefore, to correct the soiling measurement for different PV technologies.

So far, most of the research addressing the spectral impact of soiling has been conducted by analyzing artificial soiling [2,19,20]. These studies have been crucial to understanding the effects of soiling on the performance of PV systems. But even if artificial soiling makes it possible to conduct the investigation in a controlled environment, it limits the understanding of the spectral nature of soiling in actual outdoor conditions, where types of soiling and deposition rates are different and can vary with time. The first results based on an outdoor experimental campaign on spectral soiling losses, where natural soiling was collected on glass coupons exposed for two-months in eight locations worldwide, were recently presented [3]. The results of that work confirmed the higher attenuation of soiling at lower wavelengths, as previously indicated by other studies [2,4]. Despite all these important efforts, the relation between the spectral nature of soiling and its impact on each PV technology needs to be further investigated because their different absorption bands can lead to dissimilar losses among the various PV materials even in the same conditions of soiling. In this light, the current work focuses on understanding the spectral profile of natural soiling and its impact on various PV technologies, and on identifying the correlations between the transmittance of soiling and the losses in PV. These correlations can make it possible to estimate the soiling losses of various PV technologies by measuring the transmittance of soiling within a limited waveband or even at a single wavelength, opening the possibility to innovative soiling detection mechanisms.

In order to measure the spectral transmittance of soiling and to calculate its impact on the soiling losses of PV modules, a 4 cm × 4 cm PV glass coupon has been outdoor mounted and monitored in this study. The use of glass coupons to analyze and monitor the soiling of PV modules is a standard method for the soiling community, already employed for both research and commercial purposes. Outdoor mounted PV coupons were used by Burton et al. [21] to study the composition and the size distribution of soiling deposited on PV modules. The same setup, replicated also in a second location, was used by Boyle et al. [22] to investigate the deposition of particle matter on PV systems. Similarly, the dust accumulated on PV glass coupons was used by Conceição et al. [23] to estimate the soiling loss occurring on two mono-Si PV modules nearby. A team at NREL exposed PV glass coupons for one year in five different locations to understand the effectiveness of anti-soiling coatings and to quantify the abrasion due to external agents and various cleaning methods [24,25]. Nayshevsky et al. [26] used glass coupons to investigate the use of hybrid hydrophobic-hydrophilic coatings to improve the collection of dew and so to decrease the soiling rates on PV modules. Also, as mentioned, novel maintenance-free soiling detectors quantify the soiling accumulated on a PV glass to estimate the soiling losses of PV modules [15,16]. Gostein et al. [27] demonstrated an high correlation between the soiling losses estimated by MARS and the losses

measured on a PV cell, both covered by PV glass coupons artificially deposited with three different types of dusts were placed on top of them. Korevaar et al. [28] compared the measurements of DustIQ with the soiling ratio measured by a soiling station in Morocco, showing a good correlation between the two profiles over a short period.

Despite the wide usage of coupons for PV soiling studies, further studies are already being conducted to understand the different soiling mechanisms occurring on stand-alone glass vs. PV modules [29]. The present paper uses the transmittance measured on a PV glass to estimate the soiling losses that a module exposed to the same soiling conditions would experience. Therefore, this study does not directly compare two different measurements as the transmittance of a PV glass and the power loss of a PV module. For this reason, the discussion on the different soiling deposition mechanisms occurring on glass and modules is considered out of the scope of this work.

## 3. Materials and methods

### 3.1. Soiling spectral indices

The most commonly used metric to quantify the impact of soiling is the Soiling Ratio ($r_s$), which expresses the ratio between the output of a soiled PV device and the output of the same device under clean conditions [30]. Similar to the transmittance, the higher the soiling ratio, the less the soiling deposited on the modules. The soiling ratio assumes a value of 1 in clean conditions, with no soiling, and decreases while soiling deposits. The soiling losses, expressed as the fractional loss in power due to soiling, can be estimated as: 1- $r_s$. The short-circuit current can be used as the electrical output for the calculation of the soiling ratio if soiling is uniform, whereas the maximum power point is required for a better estimate of nonuniform soiling [9,13]. In this work, the nonuniform effects of soiling are not considered: therefore, the instantaneous soiling ratio at any time *t* is calculated as follows:

$$r_s(t) = \frac{Isc_{soil}(t)}{Isc_{ref}(t)} \tag{1}$$

where $Isc_{soil}$ and $Isc_{ref}$ are the short-circuit currents of a soiled PV device and of the control device, respectively. Considering this, the soiling ratio for a specific period of time T can be obtained as the average of the measured instantaneous soiling ratios by the following expression:

$$\overline{r_s}(T) = \frac{1}{n}\sum_{i=1}^{n} r_s(t) \tag{2}$$

where n is the number of measurements over the period of time T.

The time-dependent short-circuit currents of Equation (1), $Isc_{soil}$ and $Isc_{ref}$, could be obtained either experimentally from two monitored PV devices, or, as in the present work, calculated by solving the following expressions [31]:

$$Isc_{ref}(t) = A_{PV}\int_{\lambda_1}^{\lambda_2} E_G(\lambda,t)SR(\lambda)d\lambda \tag{3}$$

$$Isc_{soil}(t) = A_{PV}\int_{\lambda 1}^{\lambda 2} E_G(\lambda,t)\tau_{soiling}(\lambda,t)SR(\lambda)d\lambda \tag{4}$$

where $\lambda_1$ and $\lambda_2$ are the lower and upper limits of the absorption band of each PV device's absorber material (i.e., m-Si, CdTe, CIGS), $A_{PV}$ is its active area, SR($\lambda$) is the spectral response, $\tau_{soil}$ ($\lambda$,t) is the hemispherical spectral transmittance of soiling accumulated on the surface of the soiled device, and $E_G(\lambda,t)$ is the actual spectral distribution of the solar irradiance on the plane of the PV panels.

At the same time, the average spectral transmittance (AST) of soiling across a specific spectral waveband can be calculated with the following relationship:

$$AST_i(t) = \frac{1}{\lambda_{2_i} - \lambda_{1_i}}\int_{\lambda_{1i}}^{\lambda_{2i}} \tau_{soiling}(\lambda,t)d\lambda \tag{5}$$

where $\lambda_{1i}$ and $\lambda_{2i}$, respectively, are the shortest and longest wavelengths in the selected waveband *i*. The various wavebands considered in this work describe either a specific spectral region or an individual PV material's absorption band and are listed in Table 1. Note that the lower and upper limits of the spectral region bands are defined by considering the absorption bands of the PV materials; the shortest and longest wavelengths selected are, respectively, 300 nm for the ultraviolet and 1240 nm for the near-infrared regions.

### 3.2. Experimental campaign

#### 3.2.1. Location

A 48-week experiment—from January 2017 to January 2018—was conducted on the roof of the A3-building at the University of Jaén, in Jaén, Spain (latitude 37°49′N, longitude 3°48′W, elev. 457 m). Jaén is a medium-size town located in southern Spain with a high annual energy resource (more than 1800 kWh/m$^2$), and extreme temperatures ranging from less than 5 °C in winter to more than 40 °C in summer [32]. Atmospheric conditions are described by low-medium values of precipitable water, turbidity, and airborne particulate matter, even if this can periodically reach unusually high values due to specific and stochastic events such as Saharan dust storms or the burning of branches from olive groves in

**Table 1**
Wavebands considered in the present study.

| Waveband | | $\lambda_1$ [nm] | $\lambda_2$ [nm] |
|---|---|---|---|
| Spectral regions | Ultraviolet (UV) | 300 | 400 |
| | Visible (VIS) | 400 | 700 |
| | Near-infrared (NIR) | 700 | 1240 |
| PV material absorption bands | Monocrystalline silicon (m-Si) | 340 | 1190 |
| | Polycrystalline silicon (p-Si) | 310 | 1180 |
| | Amorphous silicon (a-Si) | 300 | 790 |
| | Cadmium telluride (CdTe) | 310 | 880 |
| | Copper indium gallium diselenide (CIGS) | 370 | 1240 |
| | Perovskite | 300 | 820 |

the local region [33].

### 3.2.2. Transmittance

One Diamant® low-iron glass coupon 4 cm × 4 cm in size and 3 mm thick from Saint-Gobain Glass was placed horizontally outdoors to capture natural dust (*Soiled Coupon*). The same mounting configuration shown in Ref. [3] was used. The coupon was left to soil naturally, and was manually cleaned only once after 24 weeks, at the half way point of the experimental period, to check for the absence of permanent degradation on the glass. Its hemispherical transmittance was measured weekly within a wavelength range between 300 and 1240 nm, using a Lambda 950 spectrophotometer with a 60-mm-diameter integrating sphere at the Center of Scientific-Technical Instrumentation (CICT) of the University of Jaén. The general arrangement is outlined in Fig. 1. Another sample (*Control Coupon*) was stored in a dust-free box to prevent its optical transmittance characteristics from being adversely affected from accidental soiling, and it was used as the baseline for each measurement. Its transmittance also allowed us to check the quality and repeatability of weekly measurements. The soiling transmittance is obtained from the measurement as follows:

$$\tau_{soiling}(\lambda) = \frac{\tau_{soil}(\lambda)}{\tau_{ref}(\lambda)} \tag{6}$$

where $\tau_{soil}(\lambda)$ and $\tau_{ref}(\lambda)$ are the spectral transmittance of the Soiled Coupon and Control Coupon, respectively, for one of the wavelength ranges described in Table 1.

### 3.2.3. Irradiance

The global spectral irradiance between the 350-nm and 1050-nm wavelength band was measured at 5-min intervals using a weatherproof spectroradiometer (EKO® MS700) oriented south and tilted 30° above the horizontal. This angle has been selected to maximize the collected irradiation over the year [34]. This instrument presents a spectral resolution of 10 nm and a temperature dependency within ±1% for temperatures ranging from −20 °C to +50 °C. The expanded uncertainties of the instrument are ±10.90%, ±4.20%, and ±4.10%, respectively, for the 350–450-nm, 450–900-nm, and 900–1050-nm wavebands, according to the certificate of calibration provided by the manufacturer. The absorption bands of some PV devices (see Table 1 and Fig. 2) go beyond the measurement range of the spectroradiometer. This limitation has been overcome by using the methodology proposed by Martín and Ruiz [35]. The missing wavebands have been estimated by scaling the AM1.5G reference spectrum according to the ratio between the integrated actual and referenced spectral irradiance in the range of 700–1050 nm. This methodology was used and validated by Nofuentes et al. [36] to elucidate the impact of the average photon energy (APE) on the spectral mismatch factor (MM). In addition, all measurements recorded at irradiance levels below 300 W/m$^2$ have not been taken into account so as to avoid the non-linear performance of PV cells at such low irradiance values [36–38]. Nevertheless, these low irradiance levels do not play a significant role in the annual electrical output of PV systems at locations with a high-energy solar resource, such as the location considered in this study [39–41]. In addition, all the measurements with an incident angle equal to or greater than 60º have been removed to reduce the impact of the increased glass Fresnel reflection [42]. This approach also automatically excludes conditions in which the impact of soiling has been found to be strongly related to the angle of incidence [43].

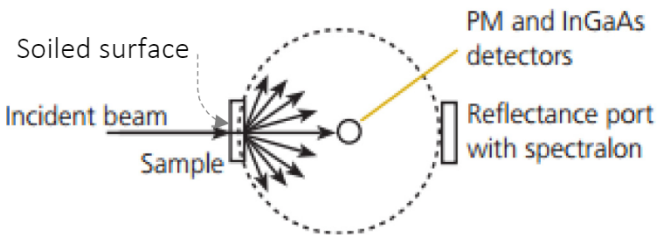


**Fig. 1.** Schematic of the hemispherical transmittance measurement using the integrating sphere. The detectors are mounted orthogonally from the beam direction on the exterior of the sphere.

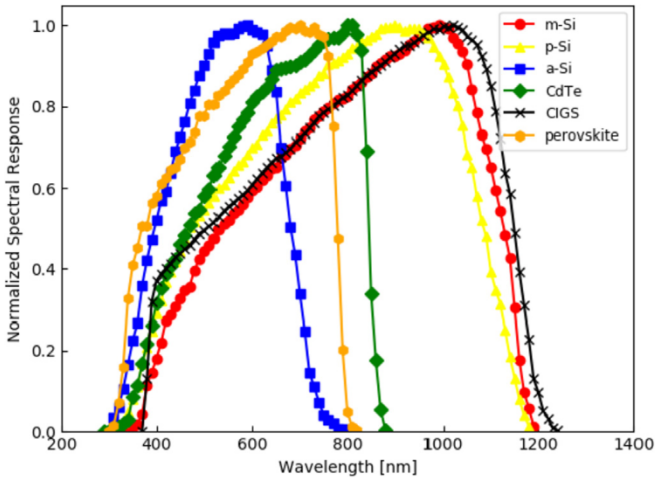


**Fig. 2.** Normalized spectral response of the six PV materials considered in this study.

### 3.3. Methodology

PV materials have different spectral absorption bands and different spectral responses, as shown in Fig. 2 for the six PV technologies investigated in this study. In addition, the transmittance of soiling has a nonuniform spectral distribution, with higher losses at shorter wavelengths, as shown in the bottom chart of Fig. 3. This means that soiling can have different impact on the various PV materials, which is a result of the product of the spectral response with the time-dependent irradiance and soiling transmittance spectra. Note that discussing the effects of soiling on the different PV technologies is outside the scope of this paper, which only focuses on the relationship between soiling losses and soiling transmittance. With this in mind, we have established the following procedure to conduct the analysis presented in this paper:

1. Measuring the spectral transmittance of soiling ($\tau_{soiling}(\lambda)$) collected on the Soiled Coupon once per week by using Equation (6).
2. Calculating the soiling ratios by using Equations (1)–(4). The SR of each PV device, the $\tau_{soiling}(\lambda)$ obtained in step 1, and the irradiance spectra recorded during the same day are used as inputs.
3. Estimating the average transmittance of soiling (AST($\lambda$)) for the regions of the spectrum and the PV devices listed in Table 1 using Equation (5) and $\tau_{soiling}(\lambda)$.
4. Comparing the soiling ratios obtained in step 2 for the different wavebands investigated in step 3 by using several standard statistical metrics.

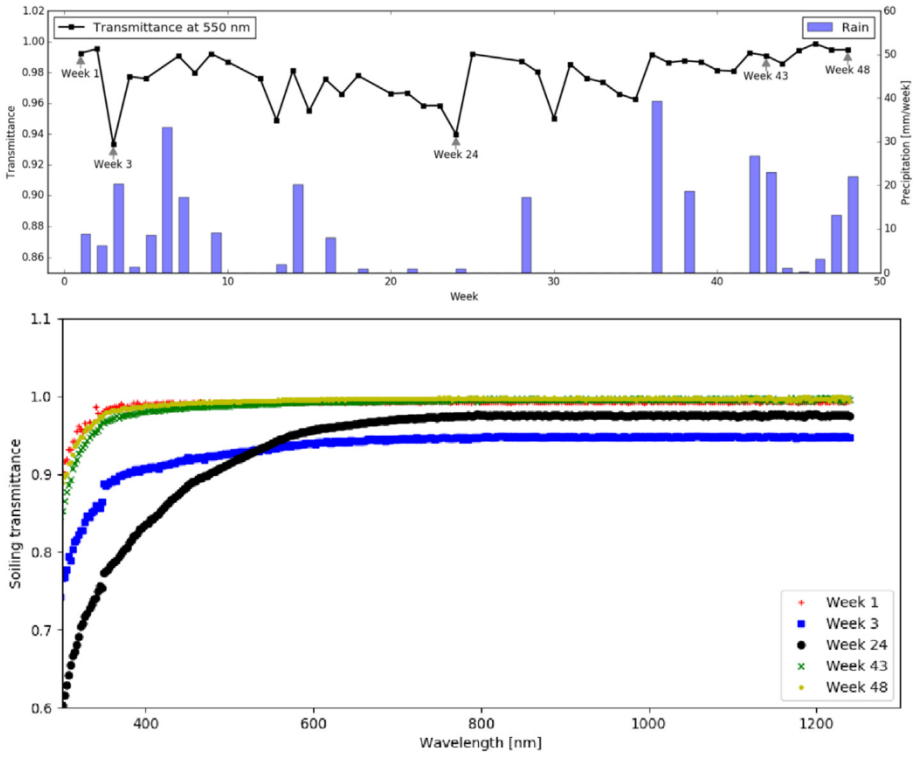


**Fig. 3.** Top: weekly transmittance of the coupon at 550 nm (left y-axis) and accumulated precipitation (right y-axis) during the investigation period. Bottom: soiling transmittance for five representative weeks of the data collection period.

### 3.4. Data collection

Soiling tends to accumulate during dry periods. However, it can be washed away by rainfall [8]. The time series of the transmittance at 550 nm of the coupon exposed for one year in Jaén is shown in Fig. 3 (top chart). Five representative weeks are labeled, and the spectral transmittance during those are shown in the lower plot. In order to prove the relations between rainfall and soiling, the weekly accumulated precipitation, recorded by an atmospheric station MTD 3000 from Geonica S.A. located on the rooftop of the one of the buildings of the University of Jaén, is also reported on the right y-axis of the top chart.

The transmittance decreases between week 1 and week 3, due to an extreme soiling event, recorded also by the local particulate matter station of the Andalucía air quality monitoring and control network located around 1 km from the experimental set-up, which recorded a $PM_{10}$ concentration of 87.5 $\mu g/m^3$, out of an annual average of 25.8 $\mu g/m^3$. The transmittance then raises in week 4 thanks to the large amount of precipitation recorded in that week that has a cleaning effect on the coupon. After few soiling and cleaning events between weeks 10 and weeks 20 that keep limited soiling on the coupon, the transmittance reaches a minimum value in week 24. After week 24, the soiled glass is manually cleaned to check for signs of degradation; as shown at the top of Fig. 3, its transmittance is restored to 1, proving no degradation due to external exposure compared to Coupon 0. A clear soiling trend can also be seen between weeks 31 and 35, during which the transmittance decreases at a rate of −0.0056 per week ($R^2 = 0.97$), down to a minimum value of 0.962. During the last weeks of the data collection, the transmittance is quite high and consistent because of the frequent rainfall events that keep the coupon clean.

This paper considers only the hemispherical transmittance of soiling. Even if less affected by soiling than the direct component [3], the hemispherical transmittance has been preferred because it is more representative of the actual effect of soiling on power conversion. Photovoltaic modules, indeed, can convert both the direct and diffuse components of the light, as well as the part that is scattered by soiling. The hemispherical transmittance measurement can capture all these components. Therefore, any transmittance mentioned in the document must be considered as hemispherical.

## 4. Results and discussion

In this section, two different analyses are carried out. First, the soiling ratio is estimated for three different spectral regions and for a region specific to the spectral response band of each PV material. Second, an estimation is made by using a single wavelength to facilitate the quantification of the spectral impact of soiling as accurately as possible with a simple single measurement. Each analysis is conducted by using different statistical indexes: the determination coefficient ($R^2$), the mean absolute percentage error (MAPE), and the mean percentage error (MPE). These magnitudes have been calculated by means of the following expressions [44]:

$$R^2 = \left( \frac{\sum_{i=1}^{n} \left(r_s - \overline{r_s}\right)\left(Z - \overline{Z}\right)}{\sqrt{\sum_{i=1}^{n} \left(r_s - \overline{r_s}\right)^2 \sum_{i=1}^{n} \left(Z - \overline{Z}\right)^2}} \right)^2 \tag{7}$$

$$MAPE\ (\%) = \frac{100}{n} \sum_{i=1}^{n} \left| \frac{Z - r_s}{r_s} \right| \tag{8}$$

$$MPE\ (\%) = \frac{100}{n}\sum_{i=1}^{n}\frac{Z - r_s}{r_s} \tag{9}$$

where n is the number of soiling ratio data points and Z represents the soiling ratio predicted through the average spectral transmittance or a single wavelength transmittance data points used to estimate the soiling ratio. The coefficient of determination measures the quality of the fit between the soiling ratios and the Z values. It has a value of 1 if the Z points predict the soiling ratios with a linear equation with no error, and it has a value of 0 if no linear correlation exists between the soiling ratios and the Z points. The MAPE measures the average value of the absolute errors between the soiling ratios and their calculated values (Z points). It has a value of 0 if the soiling ratios and the Z value are the same, and it increases depending on the number and the magnitude of the errors in the prediction. The MPE is a metric calculated similarly to MAPE, but it takes into account the actual values of the errors instead of their absolute values, and it gives information on any systematic bias in the prediction: it is positive if the predicted values tend to overestimate soiling; otherwise, it is negative.

### 4.1. Analysis of spectral waveband

In this subsection, we investigate the correlations between the average spectral transmittance across different spectral bands and the soiling ratio. In Fig. 4, the soiling ratio, calculated weekly using Eq. (2), is plotted against the average spectral transmittance of the ultraviolet, visible, and near-infrared regions, as given by Eq. (5). The best linear fits and the coefficients of determination ($R^2$) obtained for each PV technology in each region are also reported in the charts. For better readability, only three PV materials with high (a-Si), intermediate (CdTe) and low (m-Si) energy gaps are represented. Fig. 5 shows the current density of the three materials exposed to the reference AM1.5 global irradiance. The data for all technologies, inclusive of MAPE and MPE values, are reported in Table 2.

As shown, the quality of the best fit varies with both the spectral region and the PV technology. Using the UV portion of the light lowers the correlation for all the technologies, with MAPE percentages of 7% or higher. In particular, the MPE values are all found to be negative, meaning that AST returns lower values than the actual soiling ratios. This is not surprising because the UV region contributes little to the current generation in PV modules because it represents only a limited portion of the solar irradiance spectrum. Moreover, all the PV technologies have low spectral response in this region (Fig. 5), whereas soiling causes dramatic transmittance drops [2,3]. The best result for the UV is found for a-Si because this is the technology with the highest absorption at the lowest wavelengths (Fig. 5).

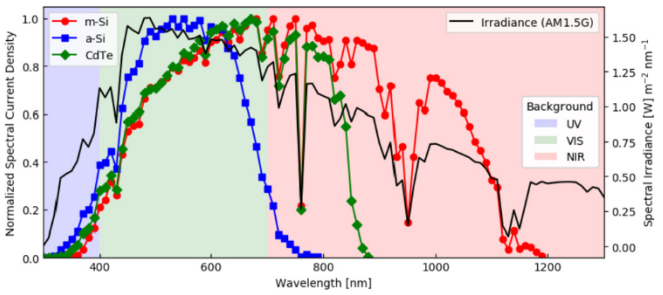


**Fig. 5.** Current density of three PV materials under the standard AM1.5 global irradiance (ASTM G173 – 03) on the left y-axis. The irradiance spectrum (black line) is plotted on the right y-axis. The colors in the background mark the three spectral regions.

Overall, the best results are obtained if the visible AST is considered, with the maximum $R^2$ achieved by a-Si, perovskite, and CdTe technologies; most of their absorption occurs in this region (Fig. 5). All the technologies have low MAPE (<1%), with a-Si reaching values lower than 0.1%. Soiling losses of a-Si technologies can be predicted with high accuracy by measuring the visible AST only.

The low-energy bandgap materials (m-Si, p-Si, CIGS) are the only technologies to have $R^2$ above 90% in both the visible and near-infrared regions. This is because the solar irradiance is high, and their spectral response is significant both in the visible and at higher wavelengths (Fig. 5). Their MAPE is lower in the NIR than in the visible. On the other hand, $R^2$ drops and the MAPE increases for a-Si in the NIR because of the very limited spectral response in this region.

The visible portion of the spectrum returns the best results if

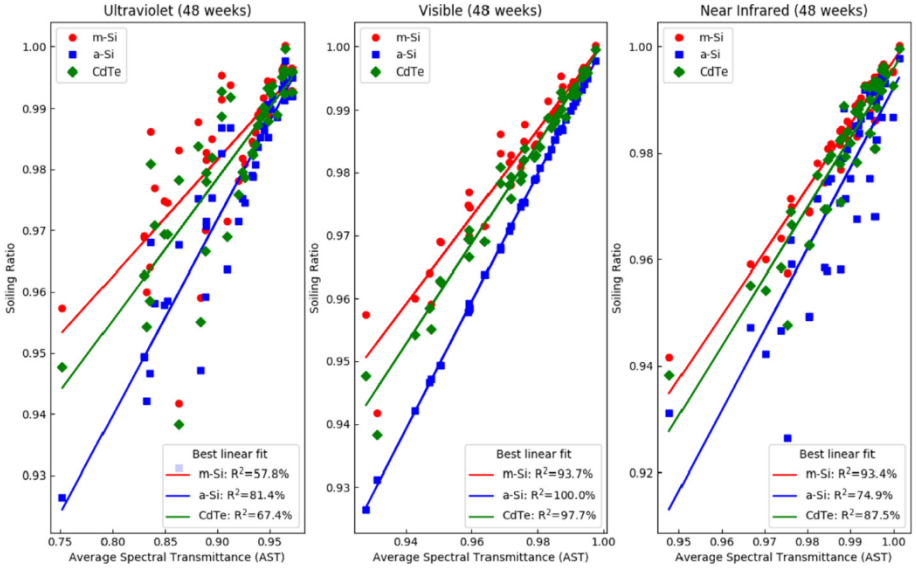


**Fig. 4.** Soiling ratio vs AST for three representative PV materials in the three spectral regions.

**Table 2**
$R^2$, MAPE, and MPE, for Jaén, Spain, between soiling ratio and transmittance in three spectral regions for the six PV materials considered.

| Material | Ultraviolet (300–400 nm) | | | Visible (400–700 nm) | | | Near-Infrared (700–1240 nm) | | |
|---|---|---|---|---|---|---|---|---|---|
| | $R^2$ (%) | MAPE (%) | MPE (%) | $R^2$ (%) | MAPE (%) | MPE (%) | $R^2$ (%) | MAPE (%) | MPE (%) |
| m-Si | 57.8 | 7.76 | −7.76 | 93.7 | 0.88 | −0.88 | 93.4 | 0.52 | 0.52 |
| p-Si | 61.3 | 7.69 | −7.69 | 95.4 | 0.80 | −0.80 | 91.5 | 0.60 | 0.60 |
| a-Si | 81.4 | 6.94 | −6.94 | 100 | 0.04 | 0.03 | 74.9 | 1.45 | 1.45 |
| CdTe | 67.4 | 7.50 | −7.50 | 97.7 | 0.59 | −0.59 | 87.5 | 0.81 | 0.81 |
| CIGS | 60.7 | 7.71 | −7.71 | 95.1 | 0.82 | −0.82 | 91.9 | 0.58 | 0.58 |
| perovskite | 77.6 | 7.15 | −7.15 | 99.8 | 0.20 | −0.20 | 79.0 | 1.21 | 1.21 |

materials from various energy bandgaps are investigated, even if it introduces a significant negative offset (MAPE $\geq$ 0.8%) for low-energy gap materials. The results for some PV technologies can be enhanced by using the specific material absorption band instead of a spectral region for calculating AST (Fig. 6). Indeed, $R^2$ of at least 98%, MAPE between 0.04% and 0.65%, and negative MPE up to −0.65% for all the materials (with the worst values for a-Si and perovskite) are the result by using the PV absorption bands in calculating AST. The negative bias is because the spectral response of each material slowly grows with the wavelength from UV to visible and/or the NIR, until it peaks and dramatically drops after that (Fig. 5). PV technologies have limited spectral response in that wide pre-peak region, and the irradiance region has the lowest intensity in UV. On the other hand, the AST is calculated as a simple average of the waveband transmittance (see Equation (8)), giving the same weight to all the wavelengths in the spectral range, independently of the spectral response and irradiance. So, the soiling-intensive short-wavelength band has a larger impact on the AST than on the actual PV modules, leading to an overestimation of the soiling (represented by lower predicted, Z, than actual soiling ratios, $r_s$).

### 4.2. Analysis of the transmittance at single wavelength

In the previous subsection, we showed how we use the average transmittance of a waveband to estimate the soiling losses occurring over the whole irradiance spectrum for different PV technologies. In this section, we investigate if the transmittance of a single wavelength can be used for the same purpose. For this reason, the same analysis presented earlier has been repeated using wavelengths at 50-nm steps between 300 nm and 1000 nm. All the results are plotted in Fig. 7. As can be seen, the maximum $R^2$ ($\geq$99%) and minimum MAPE are obtained if the hemispherical transmittance at single wavelengths between 500 and 650 nm is used to estimate the soiling losses of PV materials.

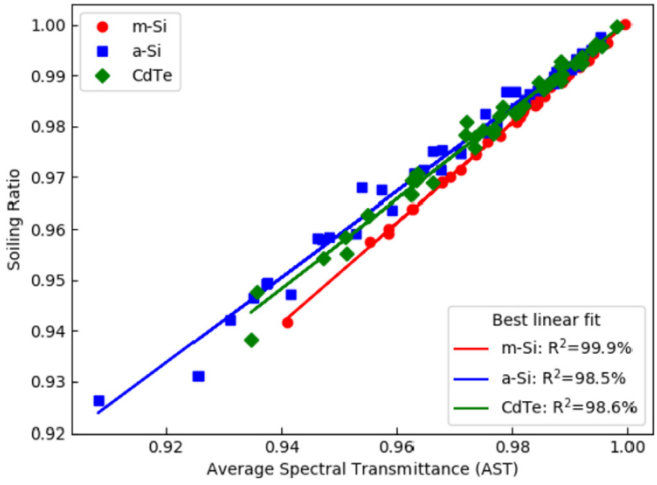


**Fig. 6.** Soiling ratio versus AST for three representative PV material absorption bands.

The best-performing wavelengths for each material are reported in Table 3. Except for CdTe, the wavelengths that maximize the $R^2$ for a material are those that minimize the MAPE, as well (CdTe's MAPE = 0.21% and $R^2$ = 98.3% at 600 nm). The results show that $R^2 \geq 99\%$ and MAPE <0.35% can be achieved for any PV technology if the transmittance of soiling at a specific wavelength is considered. This suggests that the soiling losses for each material could be ideally predicted by using a single-wavelength measurement with high accuracy. Table 3 suggests that the most appropriate wavelength of each technology can be selected by considering their energy bands: 500 nm for high (a-Si), 550 nm–600 nm for intermediate (CdTe and perovskite), and 600 nm for low (m-Si, p-Si, and CIGS) energy bandgaps. All materials, except a-Si, show lower MAPE if the transmittance of a single wavelength is used instead of the AST of any of the wavebands investigated in the previous section.

If soiling needs to be determined for more than one PV technology with the same measurement, then it is of interest to find a single wavelength that minimizes the overall error. The coefficients of determination, MAPE, and MPE for each PV technology at the most significant wavelengths found earlier (500, 550, and 600 nm) are reported in Table 4. The transmittance measured at any of the selected wavelengths achieves $R^2 \geq 90\%$ when compared to the soiling ratio of any material. Despite that, the average $R^2$ is lower at the extremes of the selected range. 500 nm favors a-Si and perovskite, but it yields worse predictions for other technology; in contrast, 600 nm maximizes low-energy-band materials, but negatively affects a-Si and perovskite. Moreover, 500 nm shows negative MPE for all the technologies (transmittance systematically lower than soiling ratio) and, in some cases, MAPE is higher than 1%. Therefore, 500 nm seems to be beneficial only if a-Si is investigated. On the other hand, 600 nm should be considered if low-energy bandgap materials are under investigation. Acceptable results are yielded at 600 nm for CdTe, even if 550 nm maximizes its results. Overall, 550 nm can be considered the most convenient if soiling losses need to be determined from one simple wavelength because $R^2$ is equal to or higher than 98% for all the materials.

The results of this work suggest that soiling detection could be performed by using average waveband or single-wavelength transmittance measurements. The time series of the soiling ratio and of the various indexes here analyzed are shown in Fig. 8 for three representative PV materials. Each material has a waveband or wavelength that maximizes the soiling loss prediction, as summarized in Table 5. This can lead to the development of innovative soiling detecting systems, based on transmittance measurements, that might be able to quantify the impact of soiling on different PV technologies.

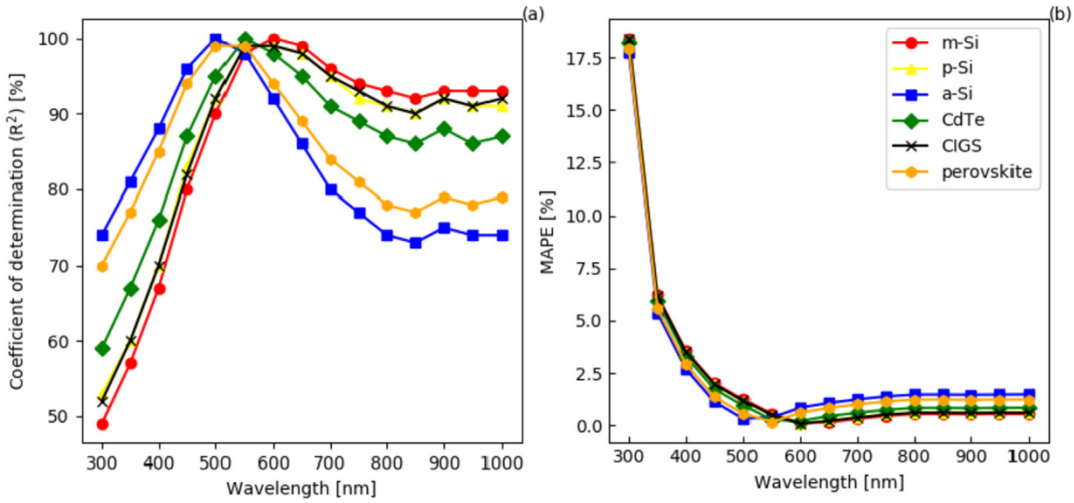


**Fig. 7.** (a) $R^2$ and (b) MAPE obtained when soiling losses for various PV technologies located in Jaén, Spain are estimated using a single hemispherical transmittance wavelength.

**Table 3**
Single wavelengths that maximize the coefficient of determination for each PV technology.

| Material | Maximum $R^2$ | | |
|---|---|---|---|
| | Wavelength [nm] | $R^2$ (%) | MAPE (%) |
| m-Si | 600 | 99.7 | 0.10 |
| p-Si | 600 | 99.4 | 0.08 |
| a-Si | 500 | 99.7 | 0.33 |
| CdTe | 550 | 99.8 | 0.25 |
| CIGS | 600 | 99.5 | 0.08 |
| perovskite | 550 | 99.0 | 0.16 |

### 4.3. Discussion

The experimental investigation here presented was based on a one-year data collection performed in Jaén in Southern Spain. In order to understand the applicability of the presented results to other regions and different soiling conditions, a preliminary analysis of the transmittance at single wavelength, similar to that shown in Section 4.2, has been conducted based on the transmittance losses measured in Golden, Colorado and in San José, California, both in the USA. The coupons are of the same materials and have same size as those used in Jaén, and were horizontally mounted for 6 weeks between January and March in Colorado and for 8 weeks between December and March in California [3]. The weekly hemispherical transmittance between 300 nm and 1100 nm of the coupons in Colorado were measured using a Cary 5000 dual-beam UV-VIS-NIR spectrophotometer equipped with a DRA-2500 integrating sphere. The weekly hemispherical transmittance of the coupons soiled in California was measured with a BWTek iSpec BWS015-Mod fiber optic spectrometer attached to a Spectralon-coated 2 inch diameter Newport integrating sphere. A tungsten lamp allowed for measurements from 410 nm to the NIR, while a phosphor-coated low pressure mercury-vapor lamp (with a peak wavelength near 365 nm) extended the measurements into the UV. The same methodology described in Section 3.3 has been employed, using, in these two cases, the reference ASTM G-173 a.m.1.5 solar spectral irradiance.

Comparing the results of Figs. 7 and 9, one sees that similar optimum wavelengths to detect soiling are obtained. Because of the limited number of data points collected at both locations, $R^2$ values (not shown) higher than 97% were found for any wavelength $\geq$ 400 nm. On the other hand, the analysis of the MAPE returned results similar to those shown earlier. Due to the low transmittance losses recorded in Golden (average transmittance between 0.976 and 1.000), CO, the MAPEs for all the wavelengths are found to be lower than 0.7% (Fig. 9a), with values lower than 0.2% for all the materials in the previously mentioned waveband 500 nm–600 nm. In general, the best wavelengths in Colorado are those between 500 and 700 nm, with a slight red-shift due to the fact that the transmittance losses in the blue spectra are not as high as in conditions of high transmittance loss. Indeed, when a location with higher soiling losses is considered (average transmittance between 0.958 and 0.986), such as San José, CA (Fig. 9b), the same correlations as for Jaén are found, with the best wavelengths ranging between 500 nm and 600 nm, where MAPE lower than 0.4% are found.

These preliminary results seem to extend and confirm the findings of the investigation conducted in Jaén: it is possible to predict the soiling ratio of different PV modules by measuring the transmittance of soiling at a single wavelength. In light of this, additional studies at different locations are recommended.

**Table 4**
$R^2$, MAPE, and MPE between soiling ratio and transmittance in three spectral regions for the five PV materials considered (for soiling in Jaén, Spain).

| Material | 500 nm | | | 550 nm | | | 600 nm | | |
|---|---|---|---|---|---|---|---|---|---|
| | $R^2$ (%) | MAPE (%) | MPE (%) | $R^2$ (%) | MAPE (%) | MPE (%) | $R^2$ (%) | MAPE (%) | MPE (%) |
| m-Si | 90.3 | 1.24 | −1.24 | 98.3 | 0.54 | −0.54 | 99.7 | 0.10 | −0.08 |
| p-Si | 92.3 | 1.16 | −1.16 | 99.1 | 0.46 | −0.46 | 99.4 | 0.08 | 0.00 |
| a-Si | 99.7 | 0.33 | −0.33 | 97.9 | 0.38 | 0.38 | 91.6 | 0.85 | 0.85 |
| CdTe | 95.4 | 0.95 | −0.95 | 99.8 | 0.25 | −0.25 | 98.3 | 0.21 | 0.21 |
| CIGS | 92.0 | 1.18 | −1.18 | 99.0 | 0.48 | −0.48 | 99.5 | 0.08 | −0.02 |
| perovskite | 98.9 | 0.57 | −0.57 | 99.0 | 0.16 | 0.14 | 94.0 | 0.61 | 0.61 |

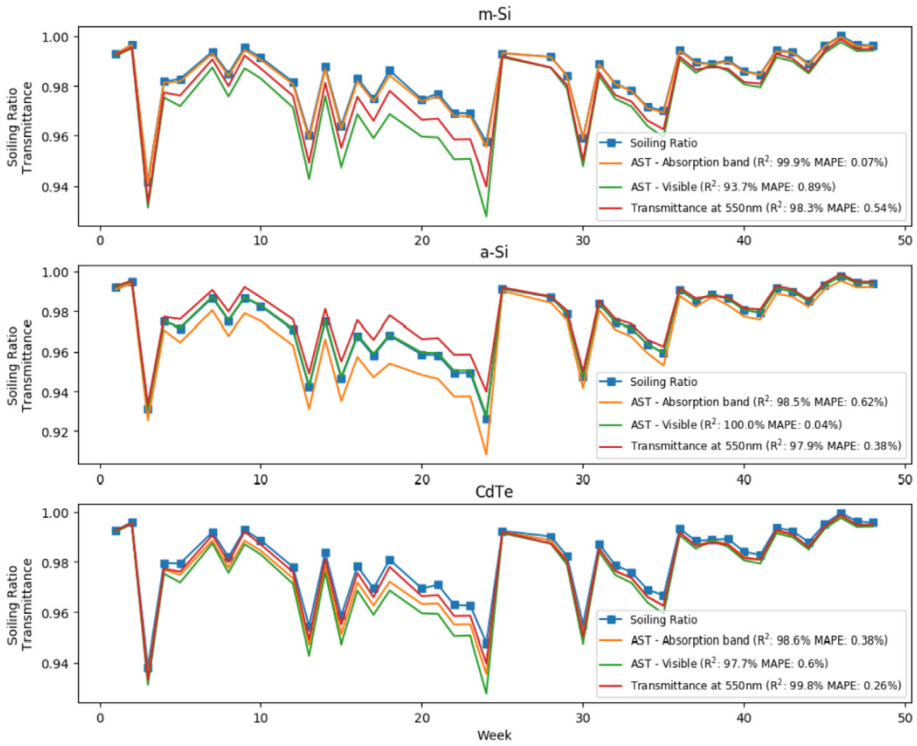


**Fig. 8.** Weekly time series of soiling ratio, AST over the specific material absorption band, and over the visible spectrum and single-wavelength transmittance at 550 nm for m-Si, CdTe, and a-Si.

**Table 5**
Summary of the best correlations obtained for each material between the soiling ratios and the various parameters investigated.

| Material | Best results |
|---|---|
| m-Si | Transmittance at 600 nm or AST at specific absorption band |
| p-Si | Transmittance at 600 nm |
| a-Si | AST in the visible |
| CdTe | Transmittance at 550 or 600 nm |
| CIGS | AST at specific absorption band, followed by transmittance at 600 nm |
| perovskite | Transmittance at 550 nm, followed by AST in the visible |

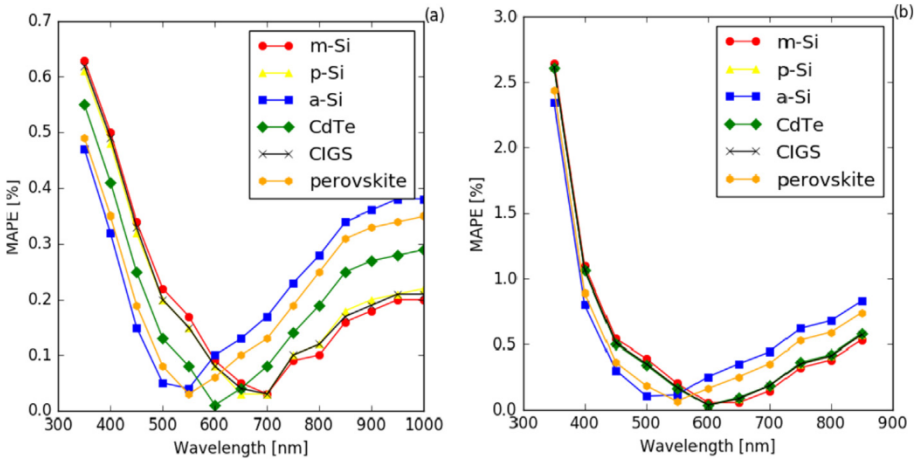


**Fig. 9.** MAPE obtained when soiling losses occurred in Golden, Colorado, (a, left chart) and in San José, California (b, right chart) for various PV technologies are estimated using a single hemispherical transmittance wavelength.

## 5. Conclusions

One PV glass coupon was exposed outdoors for 48 weeks in Jaén, a city in southern Spain. The spectral transmittance of the soiling accumulated on the coupon was measured weekly to evaluate the transmittance drop due to soiling and to estimate the losses that this would have caused on PV modules. We investigated the ability to predict soiling losses of different PV materials using only transmittance data. The results show that soiling at a location can, in principle, be estimated by using the transmittance at selected wavelength ranges—or, even at a single wavelength—with high accuracy.

In Jaén, the best estimations are obtained if the transmittance is measured at a wavelength between 500 and 600 nm. Each energy-band category shows a range in which the results are optimized: 500 nm for high (a-Si), 550 nm–600 nm for intermediate (CdTe and perovskite), and 600 nm for low (m-Si, p-Si and CIGS) energy bandgaps. Alternatively, the average spectral transmittance over the specific material absorption band returns the best soiling estimates compared to the average transmittance of the spectral regions for all materials, except for amorphous silicon and perovskite cells. Among the three regions of the solar irradiance, the best results are obtained for the visible band ($R^2 \geq 94\%$ for all the materials), even if this introduces a systematic offset in calculating the soiling ratio for low-energy-bandgap materials (as shown for the m-Si time series in Fig. 8).

The findings of this work results can lead to the development of innovative spectral soiling-detector devices. The data collection used for this analysis took place over 48 weeks at only one location that, over a one-year period, is exposed to various types of soiling (Saharan dust, olive tree pollen and smoke, and urban particulate matter). Even so, similar investigations should be replicated at different locations. Preliminary analogous investigations, conducted for 6–8 weeks at sites exhibiting different soiling conditions, confirmed that the best wavelengths for the estimation of soiling are found to range between 500 nm and 700 nm, with a slight redshift in the results for conditions of low-soiling. Since the transmittance in this study was measured at zero angle of incidence, whereas for PV modules deployed in the field, the transmittance of soiling varies daily and hourly (depending on the angle of incidence), further studies should be conducted to consider these effects and to confirm the findings of the present study.

## Acknowledgments

This work was conceived and partially funded as part of the "Global investigation on the spectral effects of soiling losses" project, financed under the EPSRC SUPERGEN SuperSolar Hub's "International and industrial engagement fund."

This research was partially funded by the Universidad de Jaén (UJA) and Caja Rural de Jaén, grant number UJA2015/07/01.

This work was authored in part by Alliance for Sustainable Energy, LLC, the manager and operator of the National Renewable Energy Laboratory for the U.S. Department of Energy (DOE) under Contract No. DE-AC36-08GO28308. Funding provided by the U.S. Department of Energy's Office of Energy Efficiency and Renewable Energy (EERE) under Solar Energy Technologies Office (SETO) Agreement Number 30311. The views expressed in the article do not necessarily represent the views of the DOE or the U.S. Government. The U.S. Government retains and the publisher, by accepting the article for publication, acknowledges that the U.S. Government retains a nonexclusive, paid-up, irrevocable, worldwide license to publish or reproduce the published form of this work, or allow others to do so, for U.S. Government purposes.

This study is partially based upon work from COST Action PEARL PV (CA16235), supported by COST (European Cooperation in Science and Technology). COST (European Cooperation in Science and Technology) is a funding agency for research and innovation networks. Our Actions help connect research initiatives across Europe and enable scientists to grow their ideas by sharing them with their peers. This boosts their research, career and innovation, see www.cost.eu.

Part of this work was funded through the European Union's Horizon 2020 research and innovation programme under the NoSoilPV project (Marie Skłodowska-Curie grant agreement No. 793120).

## References

[1] Sarver T, Al-Qaraghuli A, Kazmerski LL. A comprehensive review of the impact of dust on the use of solar energy: history, investigations, results, literature, and mitigation approaches. Renew Sustain Energy Rev 2013;22:698–733. https://doi.org/10.1016/j.rser.2012.12.065.

[2] Qasem H, Betts TR, Müllejans H, AlBusairi H, Gottschalg R. Dust-induced shading on photovoltaic modules. Prog Photovoltaics Res Appl 2014;22:218–26. https://doi.org/10.1002/pip.2230.

[3] Micheli L, Fernández EF, Smestad GP, Alrashidi H, Sarmah N, Hassan IAI, Kasry A, Nofuentes G, Sood N, Pesala B, Senthilarasu S, Almonacid F, Reddy KS, Muller M, Mallick TK. A unified global investigation on the spectral effects of soiling losses of PV glass substrates : preliminary results. In: IEEE 44th photovolt. spec. conf.; 2017. p. 3–8. IEEE, Washington, D.C.

[4] Kalogirou SA, Agathokleous R, Panayiotou G. On-site PV characterization and the effect of soiling on their performance. Energy 2013;51:439–46. https://doi.org/10.1016/j.energy.2012.12.018.

[5] Miller DC, Gedvilas LM, To B, Kennedy CE, Kurtz SR. Durability of poly ( methyl methacrylate ) lenses used in concentrating photovoltaic modules preprint. In: SPIE sol. energy + technol.; 2010.

[6] Kimber A, Mitchell L, Nogradi S, Wenger H. The effect of soiling on large grid-connected photovoltaic systems in California and the southwest region of the United States. In: Photovolt. energy conversion, conf. Rec. 2006; 2006. p. 2391–5. IEEE 4th World Conf.

[7] Kaldellis JK, Kokala a. Quantifying the decrease of the photovoltaic panels' energy yield due to phenomena of natural air pollution disposal. Energy 2010;35:4862–9. https://doi.org/10.1016/j.energy.2010.09.002.

[8] Mejia FA, Kleissl J. Soiling losses for solar photovoltaic systems in California. Sol Energy 2013;95:357–63. https://doi.org/10.1016/j.solener.2013.06.028.

[9] Micheli L, Muller M. An investigation of the key parameters for predicting PV soiling losses. Prog Photovoltaics Res Appl 2017;25:291–307. https://doi.org/10.1002/pip.2860.

[10] Micheli L, Ruth D, Muller M. Seasonal trends of soiling on photovoltaic systems. In: 2017 IEEE 44th photovolt. spec. conf.; 2017. IEEE, Washington, D.C.

[11] Javed W, Guo B, Figgis B. Modeling of photovoltaic soiling loss as a function of environmental variables. Sol Energy 2017;157:397–407. https://doi.org/10.1016/j.solener.2017.08.046.

[12] Micheli L, Deceglie MG, Muller M. Predicting photovoltaic soiling losses using environmental parameters: an update. Prog Photovolt Res Appl March 2019;27(3):210–9.

[13] Gostein M, Duster T, Thuman C. Accurately measuring PV soiling losses with soiling station employing module power measurements. In: IEEE 42nd photovolt; 2015. Spec. Conf.

[14] Muller M, Micheli L, Martinez-Morales AA. A method to extract soiling loss data from soiling stations with imperfect cleaning schedules. In: 2017 IEEE 44th photovolt. spec. Conf.; 2017. IEEE, Washington, D.C.

[15] M. Korevaar, J. Mes, P. Nepal, G. Snijders, X. van Mechelen, Novel soiling detection system for solar panels, in: 33rd Eur. photovolt. sol. energy conf. exhib., Amsterdam, The Netherlands, n.d.: pp. 2349–2351. doi:10.4229/EUPVSEC20172017-6BV.2.11.

[16] Gostein M, Faullin S, Miller K, Schneider J, Stueve B. Mars soiling sensor ™. In: 7th world conf. Photovolt. Energy convers.; 2018. IEEE, Waikoloa, HI.

[17] Curtis T, Tatapudi S, Tamizhmani G. Design and operation of a waterless PV soiling monitoring station. In: 7th world conf. Photovolt. Energy convers.; 2018. IEEE, Waikoloa, HI.

[18] Rodrigo PM, Fernández EF, Almonacid FM, Pérez-Higueras PJ. Quantification of the spectral coupling of atmosphere and photovoltaic system performance: indexes, methods and impact on energy harvesting. Sol Energy Mater Sol Cells 2017;163:73–90. https://doi.org/10.1016/j.solmat.2017.01.018.

[19] Burton PD, King BH, Riley D. Predicting the spectral effects of soils on high concentrating photovoltaic systems. Sol Energy 2015;112:469–74. https://doi.org/10.1016/j.solener.2014.11.022.

[20] Burton PD, King BH. Spectral sensitivity of simulated photovoltaic module soiling for a variety of synthesized soil types. IEEE J. Photovoltaics. 2014;4:890–8. https://doi.org/10.1109/JPHOTOV.2014.2301895.

[21] Burton PD, Boyle L, Griego JJM, King BH. Quantification of a minimum detectable soiling level to affect photovoltaic devices by natural and simulated

soils. IEEE J. Photovoltaics. 2015;5:1143–9. https://doi.org/10.1109/JPHOTOV.2015.2432459.
[22] Boyle L, Flinchpaugh H, Hannigan M. Assessment of PM dry deposition on solar energy harvesting systems: measurement–model comparison. Aerosol Sci Technol 2016;50:380–91. https://doi.org/10.1080/02786826.2016.1153797.
[23] Conceição R, Silva HG, Mirão J, Gostein M, Fialho L, Narvarte L, Collares-Pereira M. Saharan dust transport to Europe and its impact on photovoltaic performance: a case study of soiling in Portugal. Sol Energy 2018;160:94–102. https://doi.org/10.1016/j.solener.2017.11.059.
[24] Toth Sarah, Muller Matthew, Miller David C, Moutinho Helio, To Bobby, Micheli Leonardo, Linger Jeffrey, Engtrakul Chaiwat, Einhorn Asher, Simpson Lin. Soiling and cleaning: initial observations from 5-year photovoltaic glass coating durability study. Sol Energy Mater Sol Cells 2018;185:375–84. https://doi.org/10.1016/j.solmat.2018.05.039. ISSN 0927-0248.
[25] Einhorn A, Micheli L, Miller DC, Simpson LJ, Muller M, Toth S, John JJ, Kottantharayil A, Engtrakul C. Optical microscopy study of soiling on PV glass: evaluation of possible mitigation strategies. In: 7th world conf. Photovolt. energy convers; 2018. Waikoloa, HI.
[26] Nayshevsky I, Xu Q, Lyons AM. Hydrophobic-hydrophilic surfaces exhibiting dropwise condensation for anti-soiling applications. IEEE J. Photovoltaics 2019;9:302–7. https://doi.org/10.1109/JPHOTOV.2018.2882636.
[27] Gostein M, Faullin S, Miller K, Schneider J, Stueve B. MARS soiling sensor. In: 36th Eur. Photovolt. Sol. Energy conf. Exhib.; 2018. Bruxelles, Belgium.
[28] Korevaar M, Mes J, Merrouni AA, Bergmans T, Van Mechelen X. Unique soiling detection system for PV modules. In: 35th Eur. photovolt. sol. energy conf. exhib.; 2018. p. 1988–90.
[29] Smestad GP, Moriarty T, Micheli L, Simpson L, Hamadani B, Germer TA, TamizhMani G, Oh J. EQE soiling ratio and transmission losses. In: 2018 int. PV soiling work.; 2018. Denver (CO), www.solideas.com/projects/pvquality/assets/workshop_Smestad_Nov2018c.pdf.
[30] International Electrotechnical Commission. Photovoltaic system performance – Part 1: Monitoring. 2017 (IEC 61724-1, Edition 1.0, 2017-03).
[31] Fernández EF, Loureiro AJG, Smestad GP. Multijunction concentrator solar cells: analysis and fundamentals. In: Pérez-Higueras P, Fernández EF, editors. High conc. photovoltaics fundam. eng. power plants. Springer International Publishing; 2015. https://doi.org/10.1007/978-3-319-15039-0.
[32] Fernández EF, Pérez-Higueras P, Garcia Loureiro AJ, Vidal PG. Outdoor evaluation of concentrator photovoltaic systems modules from different manufacturers: first results and steps. Prog Photovoltaics Res Appl 2012;21:693–701. https://doi.org/10.1002/pip.1262.
[33] Fernández EF, Soria-Moya A, Almonacid F, Aguilera J. Comparative assessment of the spectral impact on the energy yield of high concentrator and conventional photovoltaic technology. Sol Energy Mater Sol Cells 2016;147:185–97. https://doi.org/10.1016/j.solmat.2015.12.003.
[34] Deutsche Gesellschaft Für Sonnenenergie (Dgs). Planning and installing photovoltaic systems: a guide for installers, architects and engineers. third ed. Gosport: Routledge; 2013.
[35] Martin N, Ruiz JM. A new method for the spectral characterisation of PV modules. Prog Photovoltaics Res Appl 1999;7:299–310.
[36] Nofuentes G, García-domingo B, Muñoz JV, Chenlo F. Analysis of the dependence of the spectral factor of some PV technologies on the solar spectrum distribution. Appl Energy 2014;113:302–9. https://doi.org/10.1016/j.apenergy.2013.07.044.
[37] Gueymard CA, Myers DR. Evaluation of conventional and high-performance routine solar radiation measurements for improved solar resource, climatological trends, and radiative modeling. Sol Energy 2009;83:171–85. https://doi.org/10.1016/j.solener.2008.07.015.
[38] Ishii T, Otani K, Takashima T, Xue Y. Solar spectral influence on the performance of photovoltaic (PV) modules under fine weather and cloudy weather conditions. Prog Photovoltaics Res Appl 2011;15. n/a-n/a. doi:10.1002/pip.1210.
[39] Luque A, Hegedus S. Handbook of photovoltaic science and engineering. Chichester, UK: John Wiley & Sons, Ltd; 2003. https://doi.org/10.1002/0470014008.
[40] Torres-Ramírez M, Nofuentes G, Silva JP, Silvestre S, Muñoz JV. Study on analytical modelling approaches to the performance of thin film PV modules in sunny inland climates. Energy 2014;73:731–40. https://doi.org/10.1016/j.energy.2014.06.077.
[41] Nofuentes G, Gueymard CA, Aguilera J, Pérez-Godoy MD, Charte F. Is the average photon energy a unique characteristic of the spectral distribution of global irradiance? Sol Energy 2017;149:32–43. https://doi.org/10.1016/j.solener.2017.03.086.
[42] Dirnberger D, Blackburn G, Müller B, Reise C. On the impact of solar spectral irradiance on the yield of different PV technologies. Sol Energy Mater Sol Cells 2014;132:431–42. https://doi.org/10.1016/j.solmat.2014.09.034.
[43] Zorrilla-Casanova J, Piliougine M. Analysis of dust losses in photovoltaic modules. In: World Renew. Energy congr.; 2011. p. 2985–92. https://doi.org/10.3384/ecp110572985. Linköping (Sweden).
[44] Fernández EF, Ferrer-Rodríguez JP, Almonacid F, Pérez-Higueras P. Current-voltage dynamics of multi-junction CPV modules under different irradiance levels. Sol Energy 2017;155:39–50. https://doi.org/10.1016/j.solener.2017.06.012.

Caballero, J.A.; Fernández, E.F.; Theristis, M.; Almonacid, F; Nofuentes, G. Spectral Corrections Based on Air Mass, Aerosol Optical Depth, and Precipitable Water for PV Performance Modeling. IEEE Journal of Photovoltaics 2018, 8(2), 552-558;

https://doi.org/10.1109/jphotov.2017.2787019

**Estado:** Publicado

**Factor de Impacto (JCR Science Edition 2018):** 3,398

**Categorías científicas y posición dentro de las mismas (JCR Science Edition 2018):** 42/103(Q2) en “Energy and fuels”; 86/293 (Q2) en “Materials science, multidisciplinary”; 35/148 (Q1) en “Physics, applied”.

# Spectral Corrections Based on Air Mass, Aerosol Optical Depth, and Precipitable Water for PV Performance Modeling

J. A. Caballero, E. F. Fernández, M. Theristis, F. Almonacid, and G. Nofuentes

***Abstract*—Broadband incident global irradiance must be corrected when modeling the performance of a photovoltaic (PV) module to account for the impact of spectrum. However, most existing correction methods exhibit both climate and site dependencies. This paper presents a new set of analytical equations aimed at modeling the spectral effects exhibited by six PV single-junction materials under all operating conditions. Thus, the equations proposed here involve the three parameters that mostly influence the spectrum shape: air mass (AM), aerosol optical depth, and precipitable water. The extraction of the equations and their coefficients is then presented. Next, the method is empirically validated over the course of a 12-mo experimental campaign. Thus, coefficients of determination ranging from 0.87 (multicrystalline silicon) to 0.92 (amorphous silicon) prove that modeled values of the spectral mismatch factor (MM) are well aligned with experimental ones. In addition to the values of mean bias error that are virtually equal to zero, this new procedure also yields values of root mean square error that stay below 0.85% when modeling MM for all the technologies under investigation. Such figures are far better than those achieved by using the popular Sandia Labs method, based solely on AM.**

***Index Terms*—Aerosol optical depth (AOD), air mass (AM), analytical equations, photovoltaic (PV) performance, precipitable water (PW), spectral effects.**

## I. Introduction

PHOTOVOLTAIC (PV) developers need to model the impact of varying spectra on solar cells as the latter are sensitive to the composition of the solar spectrum. Thus, spectral effects take place when the actual spectral distribution of the incident irradiance (spectral irradiance) that impinges on the PV device differs from the specific reference solar spectrum AM1.5G used for rating purposes [1]. Cloud cover influences spectral irradiance, but in clear-sky situations—this is when the highest PV output is achieved—it is mainly affected by other parameters, such as the air mass (AM), aerosol optical depth (AOD), and precipitable water (PW) [2], [3].

Spectral measurements are not common and in general only broadband irradiance data, measured by pyranometers or derived from other irradiance measurements, are available [4]. Therefore, broadband irradiance must be adjusted to an effective irradiance, which actually contributes to generate the photogenerated current of the PV device [5]. Thus, ignoring the impact of the angle of incidence and/or the distribution of the spectrum may lead to unrealistic yield predictions. Specifically, if spectral issues are neglected, errors of up to 10% may be incurred when modeling some parameters, such as the short-circuit current of a PV specimen under extreme conditions, especially when dealing with single-junction large band gap materials [6].

As mentioned above, ground-based measurements of the solar spectrum are scarce due to the cost and care required to take spectrally resolved irradiance measurements by using a spectroradiometer on a temporally continuous basis. Moreover, spectral measurements consist of two-dimensional (2-D) data that are not always easy to manage and introduce in PV designs [7], [8]. Satellite-based solar radiation modeled data have been used to generate maps of the annual average influence of the spectrum over very large areas [9], but the simulation techniques used may need further experimental validation. The same objection also applies to a recent paper aimed at carrying out a worldwide analysis of the annual spectral impact on seven PV technologies [3]. Spectral effects have also been explored by means of simulation in promising developments, such as dye-sensitized and perovskite solar cells [10].

The characterization of the spectral irradiance and its influence on PV materials using a single index approach has been repeatedly attempted [11]. Originally proposed by Jardine *et al.* [12], the average photon energy (APE) has probably become the most popular of these indices, as it has been hypothesized to be a unique characteristic of the solar spectrum [13], [14]. Doubtless, this one-to-one relationship would greatly simplify modeling the spectral impact on PV. However, recent research has called this purported bijective relationship into question [8], [15].

Spectral corrections based on available PV device and atmospheric parameters have been proposed by many authors. Thus,

Manuscript received September 28, 2017; revised November 26, 2017; accepted December 15, 2017. This work was supported in part by the Spanish Science and Innovation Ministry within the frame of the Project with reference code ENE2008-05098/ALT and in part by the CEAEMA within the frame of the project 'Caracterización y modelado de las irradiancias espectrales global sobre plano inclinado y directa normal mediante técnicas estadísticas y de inteligencia artificial'. The work of J. A. Caballero was supported by the Plan de Apoyo a la Investigación de la Universidad de Jaén y la Caja Rural de Jaén under the project UJA2015/07/01. *(Corresponding author: E. F. Fernández.)*

J. A. Caballero, E. F. Fernández, F. Almonacid, and G. Nofuentes are with the Centre for Advanced Studies in Energy and Environment, University of Jaén, Jaén 23071, Spain (e-mail: vicinv@ujaen.es; fenandez@ujaen.es; facruz@ujaen.es; gnofuen@ujaen.es).

M. Theristis is with the PV Technology Laboratory, FOSS Research Centre for Sustainable Energy, Department of Electrical and Computer Engineering, University of Cyprus, Nicosia 1678, Cyprus (e-mail: theristis.marios@ucy.ac.cy).

Color versions of one or more of the figures in this paper are available online at http://ieeexplore.ieee.org.

Digital Object Identifier 10.1109/JPHOTOV.2017.2787019

spectral gains exhibited by crystalline silicon (c-Si) and amorphous silicon (a-Si) have been modeled by Martín and Ruiz [16] as a function of AM and the clearness index. In this direction, a model proposed by Gottschalg *et al.* [17] uses AM and a modified clearness index to account for the effect of the spectrum on c-Si and a-Si. However, recent research has shown how this model fails to fully capture seasonal variations of experimental data [18]. An improved version of this model that includes the influence of PW has also been proposed, although this enhanced model seems not to be completely site-independent [19]. Promising results have recently been achieved by Lee *et al.* [20] by proposing an analytical equation that relates the spectral mismatch to AM and PW. However, the experimental validation of this equation conducted by the authors is limited to monocrystalline silicon (mono-Si) and cadmium telluride (CdTe).

A fourth-order polynomial function based on AM is the most commonly used expression to approximate $f_s(E(\lambda))$, the function that accounts for the impact of the spectral global irradiance of the actual solar spectrum ($E(\lambda)$, in$\mathrm{W{\cdot}m^{-2}{\cdot}nm^{-1}}$)

$$f_s\left(E\left(\lambda\right)\right) \approx f\left(\mathrm{AM}\right) = \alpha_4 \cdot \mathrm{AM}^4 + \alpha_3 \cdot \mathrm{AM}^3 + \alpha_2 \cdot \mathrm{AM}^2 + \alpha_1 \cdot \mathrm{AM} + \alpha_0 \quad (1)$$

where $f$(AM) is known as the AM modifier and the $\alpha$-coefficients are empirically obtained. Originally proposed by Sandia Labs [21], this spectral correction will hereafter be referred to as Sandia Labs method or simply Sandia Labs'. Convenient and straightforward, this equation is widely used since AM may be computed from the position of the sun. However, evidence suggests that unlike c-Si, spectral effects in thin film technologies are not primarily driven by AM [4], [22]. This single-parameter correction exhibits climatic and seasonal dependency, as the shape of the spectrum in clear-sky conditions is also influenced by AOD and PW.

This paper introduces a simple set of analytical equations involving AM, AOD, and PW aimed at correcting the solar spectrum on six single-junction PV technologies: a-Si, perovskite, CdTe, multicrystalline silicon (multi-Si), mono-Si, and Copper Indium Gallium Selenide (CIGS). This method is an attempt to improve PV spectral modeling, based on already well-known concepts. Indeed, databases such as AERONET [23] offer high quality ground-based observations of AOD and PW worldwide.

## II. Theory

Using reference devices with a flat spectral response such as pyranometers simplifies the definition of the spectral mismatch factor (MM), or simply spectral factor (SF), according to the IEC 60904-7 standard [24]

$$\mathrm{MM} = \frac{\int_{\lambda_1}^{\lambda_2} E\left(\lambda\right) \mathrm{SR}\left(\lambda\right) d\lambda \int_{\lambda_3}^{\lambda_4} E^*\left(\lambda\right) d\lambda}{\int_{\lambda_1}^{\lambda_2} E^*\left(\lambda\right) \mathrm{SR}\left(\lambda\right) d\lambda \int_{\lambda_3}^{\lambda_4} E\left(\lambda\right) d\lambda} \quad (2)$$

where $\lambda_1$ (nm) and $\lambda_2$ (nm) are the lower and upper limits within which the absorption takes place in the PV device, $\lambda_3$ (nm) and $\lambda_4$ (nm) are the wavelength limits within which the reference device is spectrally sensitive, SR($\lambda$) ($\mathrm{A{\cdot}W^{-1}}$) is the spectral response of the PV device, and $E^*$ ($\lambda$) ($\mathrm{W{\cdot}m^{-2}{\cdot}nm^{-1}}$) is the spectral irradiance of the reference spectrum AM1.5G, as stated in the IEC 60904-3 standard [1].

MM accounts for the influence of the spectrum on PV performance as the effective irradiance ($G_{\mathrm{eff}}$, in $\mathrm{W{\cdot}m^{-2}}$) that actually contributes to generate the short circuit current density of the device may be written as

$$G_{\mathrm{eff}} = G \cdot f_s\left(E\left(\lambda\right)\right) \cdot f\left(\mathrm{AOI}\right) = G \cdot \mathrm{MM} \cdot f\left(\mathrm{AOI}\right) \quad (3)$$

where $f$(AOI) is a function that accounts for the impact of the angle of incidence. The nonlinearity of PV performance at low illumination is assumed to be negligible in (2). Thus, if only spectral issues are taken into account, values of MM greater than 1 mean spectral gains, whilst values of this parameter less than 1 mean spectral losses.

It is worth noting that (2) may be simplified if we assume that $G$ ($\mathrm{W{\cdot}m^{-2}}$) is the incident broadband global irradiance calculated by integrating $E$ ($\lambda$) between $\lambda_3$ and $\lambda_4$—accounting only for spectral effects; $G^*$ [($\mathrm{W{\cdot}m^{-2}}$)] is the incident global irradiance at standard test conditions (STC); $J_{\mathrm{sc}}$ ($\mathrm{A{\cdot}m^{-2}}$) is the short-circuit current density of the PV device under $E$ ($\lambda$)—leaving aside AOI effects—and $J_{\mathrm{sc}}^*$ [A] is the short-circuit current density of the PV device at STC. MM may, thus, be given by

$$\mathrm{MM} = \frac{G^* J_{\mathrm{sc}}}{G\, J_{\mathrm{sc}}^*}. \quad (4)$$

## III. Methodology

A set of analytical equations intended to model the spectral correction of single-junction PV devices as a function of AM, AOD, and PW is proposed here. The methodology that has been followed to obtain such equations is similar to that used by Theristis *et al.* [25] to model the spectral impact on the performance of a CPV lattice-matched triple junction (LM 3J) solar cell. This procedure is summarized in what follows and consequently the reader is referred to these studies for further details.

Six PV technologies have been considered in this paper: a-Si, perovskite, CdTe, multi-Si, mono-Si, and CIGS. Perovskite solar material has also been studied due to the high potential it is likely to achieve in the PV market within the coming years. Typical relative spectral responses ($\mathrm{SR_r}$, in which measured SR is scaled so that maximum values of SR equals 1) assumed in this study for these materials have been sourced from [7], [8], [26] and are depicted in Fig. 1. Then, the influence each atmospheric parameter exerts on the spectral behavior of such materials was obtained by combining the SR of each technology with synthetic spectra generated by means of the simple model of the Atmosphere Radiative Transfer of Sunshine, version 2 (SMARTS2) [27]. Specifically, the following relatively realistic ranges were used to build the modeled spectra:

1) $1 \leq \mathrm{AM} \leq 5$, step 0.25;
2) $0.05 \leq \mathrm{AOD} \leq 0.6$, step 0.05;
3) $0.25 \leq \mathrm{PW} \leq 4$ cm, step 0.25 cm.

For each PV material considered, the values of MM under the resulting 3264 spectra were derived by means of (2). As MM for each material under scrutiny ($\mathrm{MM_{PVmaterial}}$) is assumed to

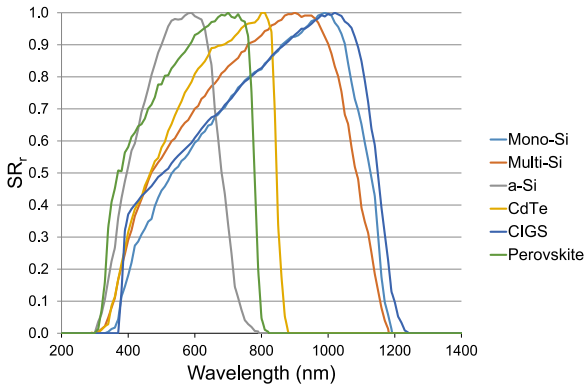


Fig. 1. Relative spectral responses for the single-junction PV materials under investigation.

be a function of AM, AOD, and PW, it may be written as

$$\begin{aligned} \mathrm{MM}_{\mathrm{PVmaterial}} &= f(\mathrm{AM},\mathrm{AOD},\mathrm{PW})_{\mathrm{PVmaterial}} \\ &= f(\mathrm{AM})_{\mathrm{PVmaterial}} + f\,(\mathrm{AOD})\,_{\mathrm{PVmaterial}} \\ &\quad + f(\mathrm{PW})_{\mathrm{PVmaterial}} \end{aligned} \tag{5}$$

$f(\mathrm{AM})_{\mathrm{PVmaterial}}$ coincides with (1), while $f(\mathrm{AOD})_{\mathrm{PVmaterial}}$ and $f(\mathrm{PW})_{\mathrm{PVmaterial}}$ are given by

$$\begin{aligned} f(\mathrm{AOD})_{\mathrm{PVmaterial}} &= f(\mathrm{AOD_{coeff}})_{\mathrm{PVmaterial}} \\ &\quad \cdot (\mathrm{AOD} - \mathrm{AOD_{ref}})) \end{aligned} \tag{6}$$

$$\begin{aligned} f(\mathrm{PW})_{\mathrm{PVmaterial}} &= f(\mathrm{PW_{coeff}})_{\mathrm{PVmaterial}} \\ &\quad \cdot (\mathrm{PW} - \mathrm{PW_{ref}}) \end{aligned} \tag{7}$$

where $\mathrm{AOD_{ref}} = 0.084$ and $\mathrm{PW_{ref}} = 1.4164$ cm. Such values correspond to the reference spectrum AM1.5G. Regarding $f(\mathrm{AOD})_{\mathrm{PVmaterial}}$, if PW is kept constant and MM is plotted versus AOD at various values of AM, these data series may be fitted linearly at each value of AM considered. Then, the coefficients (or slopes) of these fits are obtained and plotted versus AM. Next, these coefficients are fitted using different functions of AM according to the material under investigation. Thus, for a-Si and perovskite a second-order polynomial is used as

$$f(\mathrm{AOD_{coeff}})_{\mathrm{a-Si,perovskite}} = \alpha_7 \cdot \mathrm{AM}^2 + \alpha_6 \cdot \mathrm{AM} + \alpha_5 \tag{8}$$

while a linear function is used for multi-Si, mono-Si, and CIGS that may be written as follows:

$$f(\mathrm{AOD_{coeff}})_{\mathrm{mono-Si,multi-Si,CIGS}} = \alpha_6 \cdot \mathrm{AM} + \alpha_5. \tag{9}$$

Finally, CdTe coefficients are fitted logarithmically

$$f(\mathrm{AOD_{coeff}})_{\mathrm{CdTe}} = \alpha_6 \cdot \ln(\mathrm{AM}) + \alpha_5. \tag{10}$$

The values of the coefficient of determination ($R^2$) of (8)–(10) for all the materials studied range from 0.97 to 1. The same procedure is applied to obtain the equations relative to $f(\mathrm{PW})_{\mathrm{PVmaterial}}$. Likewise, values of $R^2$ for such spectral corrections stay above 0.98. Table I gathers all the equations obtained as a function of AM, according to the material and the atmospheric parameter involved.

The $\alpha$-coefficients of the Equations listed in Table I are estimated by carrying out a multiple linear regression analysis on measurements taken outdoors.

## IV. Analysis of Proposed Procedures

### A. Experimental Validation

The experimental campaign lasted from March 2016 to February 2017, inclusive, and data were logged at 5-min intervals. This 12-mo experiment was conducted in its entirety in the outdoor research facilities of the University of Jaén (Jaén, Spain, latitude 37.8°N, longitude 3.8°W, with a Mediterranean–Continental climate and an average annual horizontal irradiation of 1790 kWh·m$^{-2}$).

When computing experimental values of MM, $E$ ($\lambda$) was measured with a spectroradiometer—and then extrapolated, as explained hereafter–whilst $G$ came from measurements taken by a pyranometer [8]. The experimental spectral global tilted irradiance (GTI) data used in this paper were recorded in the outdoor research facilities located at the High Technical School building of the University of Jaén. These data were recorded by means of a weatherproof EKO MS-700 grating spectroradiometer. This instrument was mounted on an equator-facing plane with a 30° tilt angle being intended to maximize the collection of irradiation over the year [28]. Spectral measurements provided by the spectroradiometer are limited to the wavelength range from 350 to 1050 nm. Thus, according to the certificate of calibration issued by its manufacturer, the expanded uncertainties for the spectral measurements are the following: ±10.89%, ±4.13%, and ±4.06% for the 350–450 nm, 450–900 nm, and 900–1050 nm wavebands, respectively. The incident broadband GTI measurements were taken by means of a Kipp & Zonnen CMP 21 pyranometer coplanar with the spectroradiometer. Likewise, the estimated expanded uncertainty of the pyranometer equals ±1.5%, as reported by the calibration certificate provided by an accredited independent laboratory.

As commented above, the measurement range of the spectroradiometer is limited to 350–1050 nm. However, the relative spectral responses of the PV materials under scrutiny are not confined within this waveband, as depicted in Fig. 1. Therefore, calculations of MM by means of (2) detailed in what follows requires the extrapolation of each measured spectral GTI. To this end, the method proposed by Martín and Ruiz [16] was adopted. Assuming the AM1.5G solar spectral distribution as a reference, each measured spectrum was extrapolated outside the 350–1050 nm waveband by scaling this reference spectrum according to the ratio between the integrated measured spectral irradiance in the range 700–1050 nm and the integrated AM1.5G spectrum along this wavelength range. Nofuentes *et al.* [29] also used this method to look into the dependence of MM on the APE.

Spectral GTI data taken at values of incident global irradiance less than 300 Wm$^{-2}$ were disregarded, since these low irradiance levels are irrelevant in practical terms regarding the annual PV output produced in sunny sites such as Jaén [15], [30]– [34]. Moreover, dropping measurements at these low irradiance levels reduces the uncertainty introduced in the results

TABLE I
PROPOSED SPECTRAL CORRECTIONS FOR EACH PV MATERIAL

| Material | f(AM) | $f(\mathrm{AOD}_{\mathrm{coeff}})$ | $f(\mathrm{PW}_{\mathrm{coeff}})$ |
|---|---|---|---|
| a-Si | $\alpha_4x^4+\alpha_3x^3+\alpha_2x^2+\alpha_1x+\alpha_0$ | $\alpha_7x^2+\alpha_6x+\alpha_5$ | $\alpha_9\ln(x)+\alpha_8$ |
| Perovskite | $\alpha_4x^4+\alpha_3x^3+\alpha_2x^2+\alpha_1x+\alpha_0$ | $\alpha_7x^2+\alpha_6x+\alpha_5$ | $\alpha_9\ln(x)+\alpha_8$ |
| CdTe | $\alpha_4x^4+\alpha_3x^3+\alpha_2x^2+\alpha_1x+\alpha_0$ | $\alpha_6\ln(x)+\alpha_5$ | $\alpha_9\ln(x)+\alpha_8$ |
| Multi-Si | $\alpha_4x^4+\alpha_3x^3+\alpha_2x^2+\alpha_1x+\alpha_0$ | $\alpha_6x+\alpha_5$ | $\alpha_9\ln(x)+\alpha_8$ |
| Mono-Si | $\alpha_4x^4+\alpha_3x^3+\alpha_2x^2+\alpha_1x+\alpha_0$ | $\alpha_6x+\alpha_5$ | $\alpha_9\ln(x)+\alpha_8$ |
| CIGS | $\alpha_4x^4+\alpha_3x^3+\alpha_2x^2+\alpha_1x+\alpha_0$ | $\alpha_6x+\alpha_5$ | $\alpha_9\ln(x)+\alpha_8$ |

Where $x = \mathrm{AM}$.

to be presented hereafter [35], partly because the influence of the nonlinear PV performance at low light levels is minimized [29], [36]. Additionally, spectral measurements taken with an incident angle greater than 60° were discarded, thus, reducing the impact of the cosine response of the measuring instruments.

The atmospheric parameters involved in the equations proposed—namely, AOD at 500 nm and PW—were measured by means of a solar spectral irradiance meter (SolarSIM-D2) from Spectrafy Inc. [37], [38]. Tests conducted in the National Renewable Energy Laboratory [38] provide the high level of accuracy of this device. The AM was computed by using the sun's zenith angle ($z$) [39]

$$\mathrm{AM} = \frac{1}{\cos(z) + 0.50572 \cdot (96.07995 - z)^{-1.6364}}. \quad (11)$$

The SolarSIM-D2 was mounted on a BSQ Solar two-axis solar tracker, located on the rooftop of the CEAEMA (Centro de Estudios Avanzados en Energía y Medio Ambiente) building of the University of Jaén. This building is around 500 m away from that on which the spectroradiometer was placed. Direct normal irradiance (in $\mathrm{W{\cdot}m^{-2}}$) and atmospheric data were also recorded every 5 min through Ethernet connection.

To avoid the impact of moving clouds on the measurements and to ensure realistic values and to discard physically false values for the specific location, the experimental spectral GTI and atmospheric parameters were filtered according to the criteria used by Theristis *et al.* [25].

The spectral GTI data recorded—and then extrapolated—were used to compute the experimental values of MM for each PV material so as to be compared against those values of the latter parameter modeled by means of the analytical equations proposed. Due to space constraints, only four scattering diagrams comprising 5398 points each are depicted in Figs. 2–5, corresponding to a-Si, CdTe, multi-Si, and CIGS. In these figures, the diagonal line with unitary slope represents the ideal relationship between experimental and modeled values. For the six PV materials under study, the determination coefficient ($R^2$) ranges from 0.87 (multi-Si) to 0.92 (a-Si). Such values clearly indicate the high quality of the proposed relationships.

### B. Comparative Analysis

A comparative analysis has been performed to assess the accuracy of the proposed method against Sandia Labs', in which only AM is involved. The regression coefficients obtained for the relationship presented here are gathered in Table II.

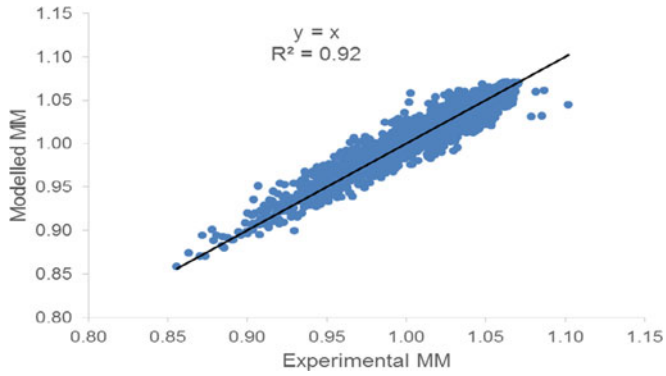


Fig. 2. Modeled versus experimental values of MM for a-Si (highest value of $R^2$ achieved).

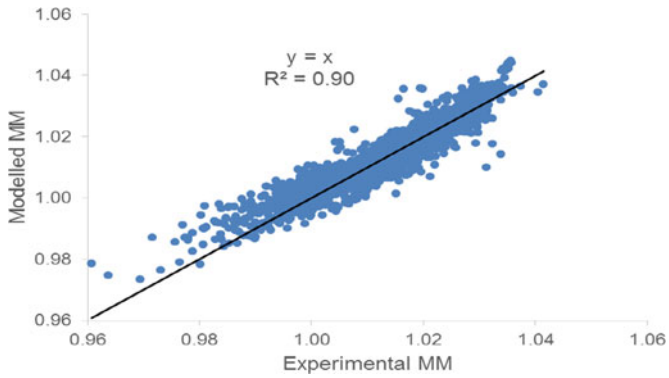


Fig. 3. Modeled vs experimental values of MM for CdTe.

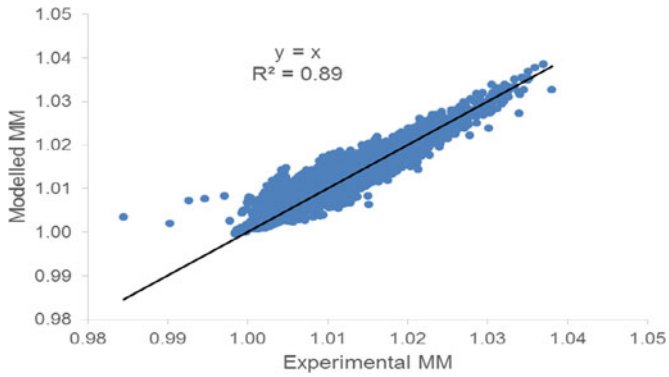


Fig. 4. Modeled versus experimental values of MM for CIGS.

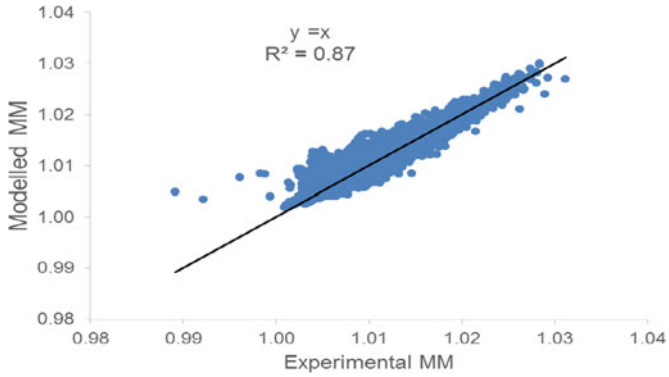


Fig. 5. Modeled versus experimental values of MM for multi-Si (lowest value of $R^2$ achieved).

TABLE II
TABLE OF REGRESSION COEFFICIENTS FOR THE PROPOSED METHOD

| | Coeff. | $SF_{a\text{-}Si}$ | $SF_{perovskite}$ | $SF_{CdTe}$ | $SF_{multi\text{-}Si}$ | $SF_{mono\text{-}Si}$ | $SF_{CIGS}$ |
|---|---|---|---|---|---|---|---|
| AM | $\alpha_0$ | 1.1060 | 1.0637 | 1.0044 | 0.9836 | 0.9706 | 0.9801 |
| | $\alpha_1$ | -0.0848 | -0.0491 | 0.0095 | 0.0254 | 0.0377 | 0.0283 |
| | $\alpha_2$ | 0.0302 | 0.0180 | -0.0037 | -0.0085 | -0.0123 | -0.0092 |
| | $\alpha_3$ | -0.0076 | -0.0047 | 0.0002 | 0.0016 | 0.0025 | 0.0019 |
| | $\alpha_4$ | 0.0006 | 0.0004 | 0.0000 | -0.0001 | -0.0002 | -0.0001 |
| AOD | $\alpha_5$ | -0.1283 | -0.0773 | -0.0046 | 0.0094 | 0.0159 | 0.0117 |
| | $\alpha_6$ | 0.0986 | 0.0583 | -0.0182 | -0.0132 | -0.0165 | -0.0126 |
| | $\alpha_7$ | -0.0254 | -0.0159 | None | None | None | None |
| PW | $\alpha_8$ | 0.0156 | 0.01251 | 0.0095 | -0.0002 | -0.0016 | -0.0011 |
| | $\alpha_9$ | 0.0146 | 0.0109 | 0.0068 | -0.0011 | -0.0027 | -0.0019 |

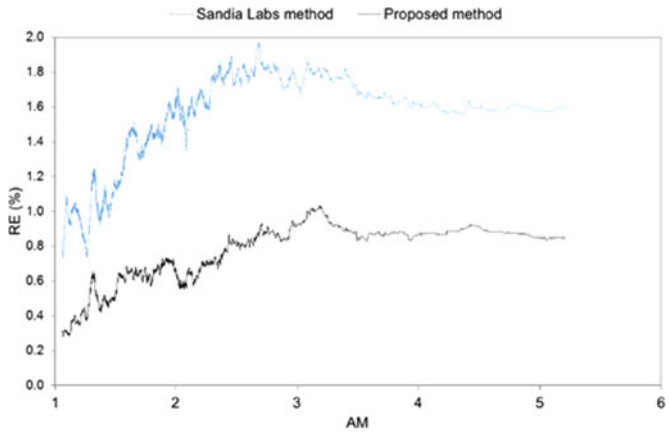


Fig. 6. RE (absolute value) between experimental and modeled values of MM for a-Si calculated by the two methods that are compared against AM.

The absolute value of the relative error (RE) in both methods against the experimental MM for a-Si has been plotted for all AM, AOD, and PW values recorded over the experimental campaign in Figs. 6–8, respectively. Fig. 6 shows how the RE (absolute value) of the proposed method stays lower than that incurred by Sandia Labs'. Indeed, a nearly constant offset of some 1% between both trends exists for values of AM greater than 2. A somewhat similar pattern between the RE (absolute value) of both methods against AOD is noticed in Fig. 7. When plotted versus PW (see Fig. 8), the RE (absolute value) of the proposed method remains relatively constant in clear contrast with the "U-shaped" trend of Sandia Labs'.

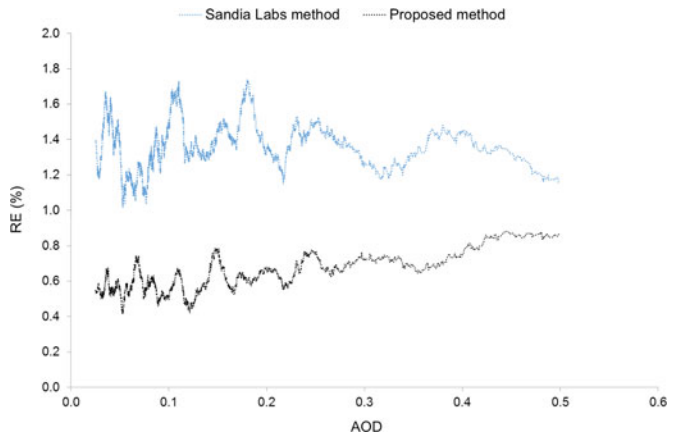


Fig. 7. RE (absolute value) between experimental and modeled values of MM for a-Si calculated by the two methods that are compared against AOD.

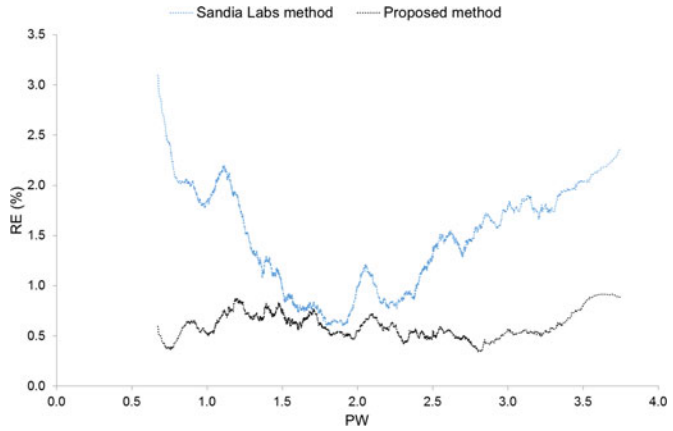


Fig. 8. RE (absolute value) between experimental and modeled values of MM for a-Si calculated by the two methods that are compared against PW.

Space limitations constrain the possibility of plotting the trend of the absolute value of RE versus AM, AOD, and PW for the remaining five technologies under investigation. The fact is that a very similar pattern to that described in the preceding paragraph is identified for perovskite, CdTe, and CIGS. Thus, Sandia Labs' shows larger and more pronounced discrepancies between modeled and experimental values of MM for these materials than those achieved by using the equations proposed in this paper. Absolute values of RE incurred by the proposed method for mono-Si and multi-Si are slightly lower than those of Sandia Labs'.

In order to gain a better understanding of the results, the root mean square error (RMSE) and mean bias error (MBE) are bar plotted in Fig. 9 for the two methods that are compared. As mentioned above, the spectral correction described here largely outperforms that provided by the equations of Sandia Labs for all the PV materials included, save mono-Si, and multi-Si. The differences between errors incurred for the latter materials with

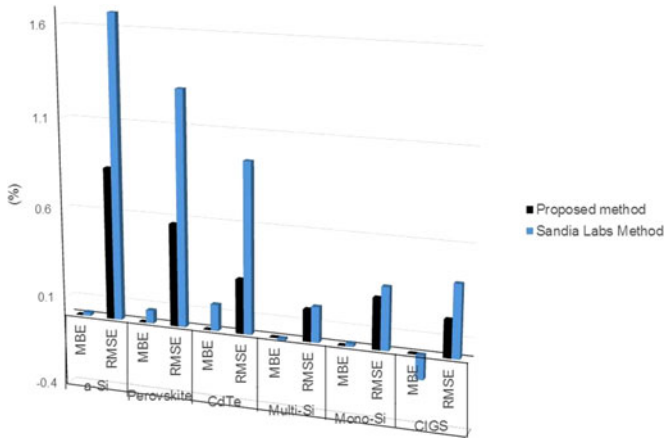


Fig. 9. Bar plot showing values of errors MBE and RMSE of the two methods that are compared for the six PV technologies studied. A 3-D bar chart has been selected to let the reader note that MBE values incurred by the proposed method are extremely low but obviously not equal to zero.

both methods are not so pronounced, although Sandia Labs' performs slightly worse. It is worth noting that the proposed method yields values of MBE very close to zero for all the PV materials under scrutiny. This indicates that MM is neither overestimated nor underestimated over a whole year. Values of RMSE of the proposed method remain below 0.85% in all cases, being slightly less than that achieved by means of Sandia Labs' for mono-Si and multi-Si.

Overall, the proposed method performs better when compared with Sandia Labs'. As the comparison was conducted in Jaén (Spain) in which low AOD and PW values prevail, it is expected that the proposed method would also outperform Sandia Labs in sites with extreme atmospheric characteristics such as locations with high AOD (e.g., Kuwait, Kanpur [40]) and PW (e.g., Tenosique, Kaashidhoo [40]). This should be dealt with further in future research, trying to validate the equations proposed here with real PV module measurements.

## V. Conclusion

A new method has been proposed for modeling the spectral effects of single junction solar cells based on AM, AOD, and PW, suitable for PV performance modeling. The most innovative aspect of this method lies in the fact that it accounts for the main parameters that shape global spectral irradiance in clear sky conditions. Accordingly, the spectral corrections presented here may lend themselves to be transferrable between sites with different climates for the PV materials studied.

The procedure to obtain the analytical equations for the six PV materials under scrutiny (a-si, perovskite, CdTE, multi-Si, mono-Si, and CIGS) is based on a previous paper in which similar expressions were proposed for a CPV LM 3J solar cell. The empirical validation was performed using outdoor measurements collected in Jaén, Spain. Computing experimental values of MM were based on the measured outdoor spectral GTI, broadband GTI, and the relative spectral responses of different PV technologies. Modeled data are well aligned with experimental ones as the values of the determination coefficients obtained range from 0.87 (multi-Si, worst fit) to 0.92 (a-Si, best fit).

The spectral correction of Sandia Labs—calculated only as a function of AM—is outperformed by the proposed method, inasmuch as the equations presented here involve the main atmospheric parameters that mostly affect the GTI spectrum. Thus, absolute values of the RE of the proposed method are lower than those of Sandia Labs' for the six PV technologies studied. Such better performance is highly noticeable for a-Si, perovskite, CdTe, and CIGS, especially as values of AM and AOD increase. Moreover, MBE virtually equals zero while RMSE stays below 0.85% for every technology considered. It was found that the values of these metrics calculated for each PV material by using the AM-based spectral correction proposed by Sandia labs are greater than those obtained by means of the proposed method.

Due to the low average AOD and PW values that occur in Jaén, it is believed that the proposed method will suitably capture the spectral performance of PV materials in sites with extreme atmospheric conditions. Further research on this issue will be the object of future work involving real PV module measurements, so that a general and universal method might be obtained.

## References

[1] 2008. Photovoltaic Devices—Part 3. Measurement Principles for Terrestrial Photovoltaic (PV) Solar Devices With Reference Spectral Irradiance Data. Geneva, IEC 60904-3 (ed. 3.0).

[2] B. Marion, "Influence of atmospheric variations on photovoltaic performance and modeling their effects for days with clear skies," in *Proc. 38th IEEE Photovolt. Spec. Conf.*, 2012, pp. 003402–003407.

[3] J. Polo, M. Alonso-Abella, J. A. Ruiz-Arias, and J. L. Balenzategui, "Worldwide analysis of spectral factors for seven photovoltaic technologies," *Solar Energy*, vol. 142, pp. 194–203, 2017.

[4] C. R. Osterwald, K. A. Emery, and M. Muller, "Photovoltaic module calibration value versus optical air mass: The air mass function," *Progress Photovolt., Res. Appl.*, vol. 22, pp. 560–573, 2014.

[5] J. Y. Ye, T. Reindl, A. G. Aberle, and T. M. Walsh, "Effect of solar spectrum on the performance of various thin-film PV module technologies in tropical Singapore," *IEEE J. Photovolt.*, vol. 4, no. 5, pp. 1268–1274, Sep. 2014.

[6] R. Gottschalg, T. R. Betts, D. G. Infield, and M. J. Kearney, "The effect of spectral variations on the performance parameters of single and double junction amorphous silicon solar cells," *Solar Energy Mater. Solar Cells*, vol. 85, pp. 415–428, 2005.

[7] M. Alonso-Abella, F. Chenlo, G. Nofuentes, and M. Torres-Ramírez, "Analysis of spectral effects on the energy yield of different PV (photovoltaic) technologies: The case of four specific sites," *Energy*, vol. 67, pp. 435–443, 2014.

[8] D. Dirnberger *et al.*, "On the impact of solar spectral irradiance on the yield of different PV technologies," *Solar Energy Mater. Solar Cells*, vol. 132, pp. 431–442, 2015.

[9] A. M. G. Amillo, T. Huld, P. Vourlioti, R. Müller, and M. Norton, "Application of satellite-based spectrally-resolved solar radiation data to PV performance studies," *Energies*, vol. 8, pp. 3455–3488, 2015.

[10] E. F. Fernández, F. A. Cruz, T. K. Mallick, and S. Sundaram, "Effect of spectral irradiance variations on the performance of highly efficient," *IEEE J. Photovolt.*, vol. 5, no. 4, pp. 1150–1157, Jul. 2015.

[11] P. M. Rodrigo, E. F. Fernández, F. A. Almonacid, and P. J. Pérez, "Quantification of the spectral coupling of atmosphere and photovoltaic system performance indexes, methods and impact on energy harvesting," *Solar Energy Mater. Solar Cells*, vol. 163, pp. 73–90, 2017.

[12] C. Jardine, T. R. Betts, R. Gottschalg, D. G. Infield, and K. Lane, "Influence of spectral effects on the performance of multijunction amorphous silicon cells," in *Proc. 17th Eur. Photovolt. Solar Energy Conf.*, 2002, pp. 1756–1759.

[13] T. Minemoto, Y. Nakada, H. Takahashi, and H. Takakura, "Uniqueness verification of solar spectrum index of average photon energy for evaluating outdoor performance of photovoltaic modules," *Solar Energy*, vol. 83, no. 8, pp. 1294–99, 2009.

[14] M. Norton, A. M. Gracia Amillo, and R. Galleano, "Comparison of solar spectral irradiance measurements using the average photon energy parameter," *Solar Energy*. vol. 120, pp. 337–44, 2015.
[15] G. Nofuentes, C. A. Gueymard, J. Aguilera, M. D. Prez-Godoy, and F. Charte, "Is the average photon energy a unique characteristic of the spectral distribution of global irradiance?" *Solar Energy*, vol. 149, pp. 32–43, 2017.
[16] N. Martin and J. M. Ruiz, "A new method for the spectral characterisation of PV modules," *Progress Photovolt. Res. Appl.*, vol. 7, pp. 299–310, 1999.
[17] R. Gottschalg, T. R. Betts, D. G. Infield, and M. J. Kearney, "On the importance of considering the incident spectrum when measuring the outdoor performance of amorphous silicon photovoltaic devices," *Meas. Sci. Technol.*, vol. 15, pp. 460–466, 2004.
[18] B. C. Duck and C. J. Fell, "Comparison of methods for estimating the impact of spectrum on PV output," in *Proc. IEEE 42nd Photovolt. Spec. Conf.*, 2015, pp. 1–6.
[19] B. C. Duck and C. J. Fell, "Improving the spectral correction function," in *Proc. IEEE 43rd Photovolt. Spec. Conf.*, 2016, pp. 2647–2652.
[20] M. Lee, A. F. Panchula, F. Solar, and S. Francisco, "Variation in spectral correction of PV module performance based on different precipitable water estimates," in *Proc. 43rd IEEE Photovolt. Spec. Conf.*, 2016, pp. 2692–2697.
[21] D. L. King, W. E. Boyson, and J. A. Kratochvil, "Photovoltaic array performance model," *Sandia Rep. SAND 2004-3535*, 2004.
[22] B. Marion, M. G. Deceglie, and T. J. Silverman, "Analysis of measured photovoltaic module performance for Florida, Oregon, and Colorado locations," *Solar Energy*, vol. 110, pp. 736–744, 2014.
[23] B. N. Holben *et al.*, "AERONET—A federated instrument network and data archive for aerosol characterization," *Remote Sens. Environ.*, vol. 66, pp. 1–16, 1998.
[24] Photovoltaic devices—Part 7: Computation of the Spectral Mismatch Correction for Measurements of Photovoltaic Devices," Geneva, Switzerland, IEC 60904-7 (Ed. 3.0), 2008.
[25] M. Theristis, E. F. Fernández, F. Almonacid, and P. J. Pérez, "Spectral corrections based on air mass, aerosol optical depth, and precipitable water for CPV performance modeling," *IEEE J. Photovolt.*, vol. 6, no. 6, pp. 1598–1604, Nov. 2016.
[26] S. Senthilarasu, E. F. Fernández, F. Almonacid, and T. K. Mallick, "Solar energy materials & solar cells effects of spectral coupling on perovskite solar cells under diverse climatic conditions," *Solar Energy Mater. Solar Cells*, vol. 133, pp. 92–98, 2015.
[27] C. A. Gueymard, "Simple model of the atmospheric radiative transfer of sunshine, version 2 (SMARTS2): Algorithms description and performance assessment," Florida Solar Energy Center, Cocoa, FL, USA, Rep. FSEC-PF-270-95, 1995.
[28] Deutsche Gesellschaft for Sonnenenergie, *Planning and Installing Photovoltaic Systems: A Guide for Installers*, 3.0 ed. London, U.K.: Earthscan, 2011.
[29] G. Nofuentes, B. García-Domingo, J. V. Munoz, and F. Chenlo, "Analysis of the dependence of the spectral factor of some PV technologies on the solar spectrum distribution," *Appl. Energy*, vol. 113, pp. 302–309, 2014.
[30] H. Wilk, "Electricity yield of PV systems in different climates and dependence of module efficiency as a function of irradiance and other factors," in *Proc. EUPVSEC Barcelona*, vol. 1997, pp. 297–300, 1997.
[31] G. Nofuentes and G. Almonacid, "An approach to the selection of the inverter for architecturally integrated photovoltaic grid-connected systems," *Renew. Energy*, vol. 15, pp. 487–490, 1998.
[32] A. Luque and S. Hegedus, *Handbook of Photovoltaic Science and Engineering*, 2.0 ed. Hoboken, NJ, USA: Wiley, 2011.
[33] G. Nofuentes, M. Fuentes, J. Aguilera, and J. V. Muñoz, "An assessment on simple modeling approaches to the electric behavior of two CIS PV modules in a sunny climate," *J. Solar Energy Eng.*, vol. 131, 2009, Art. no. 031013.
[34] M. Torres-Ramírez, G. Nofuentes, J. P. Silva, S. Silvestre, and J. V. Muñoz, "Study on analytical modelling approaches to the performance of thin film PV modules in sunny inland climates," *Energy*, vol. 73, pp. 731–740, 2014.
[35] C. A. Gueymard and D. R. Myers, "Evaluation of conventional and high-performance routine solar radiation measurements for improved solar resource, climatological trends, and radiative modeling," *Solar Energy*, vol. 83, pp. 171–185, 2009.
[36] T. Ishii, K. Otani, T. Takashima, and Y. Xue, "Solar spectral influence on the performance of photovoltaic (PV) modules under fine weather and cloudy weather conditions," *Progress Photovolt. Res. Appl.*, vol. 21, pp. 481–489, 2013.
[37] V. Tatsiankou, K. Hinzer, H. Schriemer, J. Haysom, and R. Beal, "A novel instrument for cost-effective and reliable measurement of solar spectral irradiance," in *Proc. 42nd IEEE Photovolt. Spec. Conf.*, New Orleans, LA, USA, 2015, pp. 1–4.
[38] V. Tatsiankou *et al.*, "Design principles and field performance of a solar spectral irradiance meter," *Solar Energy*, vol. 133, pp. 94–102, 2016.
[39] F. Kasten and A. T. Young, "Revised optical air mass tables and approximation formula," *Appl. Opt.*, vol. 28, pp. 4735–4738, Nov. 15, 1989.
[40] C. A. Gueymard, "Daily spectral effects on concentrating PV solar cells as affected by realistic aerosol optical depth and other atmospheric conditions," *Proc. SPIE*, vol. 7410, 2009, Art. no. 741007.

Authors' photographs and biographies not available at the time of publication.